The University of Southern Mississippi

The Aquila Digital Community

Spring 5-1-2018

Functional Emulsions via Thiol-Ene Chemistry

Douglas Amato
University of Southern Mississippi

Follow this and additional works at: https://aquila.usm.edu/dissertations

 Part of the Polymer Chemistry Commons

FUNCTIONAL EMULSIONS VIA THIOL-ENE CHEMISTRY

by

DOUGLAS AMATO

A Dissertation
Submitted to the Graduate School,
the College of Science and Technology
and the Department/ School of Polymer Science and Engineering
at The University of Southern Mississippi
in Partial Fulfillment of the Requirements
for the Degree of Doctor of Philosophy

Approved by:

Dr. Derek L.Patton, Committee Chair
Dr. Robson F. Storey
Dr. Sarah E. Morgan
Dr. Charles L. McCormick
Dr. Yoan C. Simon

_____	_____	_____
Dr. Derek L. Patton	Dr. Jeffrey S. Wiggins	Dr. Karen S. Coats
Committee Chair	Department Chair	Dean of the Graduate School

ABSTRACT

Polymer particles (micro to nano) with tunable functionality have emerged as a promising and viable technology platform for applications including coatings, cosmetics, nanomedicine, and imaging. Unfortunately, the lengthy polymerization time and lack of intrinsic functionality in the monomers used to fabricate particles is an industrial challenge. Thiol-ene chemistry cirmcumvents these limitations with very rapid polymerization kinetics, high reaction yields, with supressed side reactions and inherent functionality. This dissertation demonstrates the utility of thiol-ene/yne polymerization in miniemulsion and microfluidics to generate functional materials in a one-pot-method. The functionality is typically generated via off-stoichiometry thiol-ene (OSTE) resins which allow for either excess SH or alkene/yne functionality to be present throughout the material. The accessability of these functional groups are proven via infrared spectroscopy, confocal and optical microscopy.

The first chapter focuses on the burgeoning field of thiol-ene/yne chemistry within multiphase emulsions and introduces innovative methods to generate functional particles/materials. Chapter II describes the first thiol-ene miniemulsion process where surfactant concentration, ultrasonication time/amplitude, and OSTE resins are explored. Chapter III expands the miniemulsion process to include thiol-yne resins in addition to the ability to encapsulate hydrophobic materials such as modified silver nanoparticles. Chapter IV highlights the utility of thiol-ene resins within microfluidics to generate unique multiphase particles that can outperform traditional acrylate-based resins. The application of thiol-ene chemistry in emulsions introduces a new class of functional materials which can be easily translated into exicisting technologies.

ACKNOWLEDGMENTS

I must begin chronologically, by thanking both my parents, whose love and support has served as a safety net for me to fall back on throughout my life. I am grateful for the multiple trips to National Parks, museums, aquariums, etc. – as it created an atmosphere of curiosity which translated well into my career as a scientist. As educators, my parents helped with the retention and dissemination of knowledge – skills which have helped me immensely. Thank you Mom, Dad, and Kyah for teaching me how to learn and teach.

While my family instilled the importance of education in me, the U.S. Department of Energy (DOE) National Science Bowl sharpened my thirst for science. It is empowering to buzz in with an answer to a question confidently. I will be indebted to the volunteers of this wonderful program and I will continue to be engaged in volunteering to support local teams and competitions.

My most direct influence must go to my first advisor Phil Costanzo. As a pre-dental sophomore taking organic chemistry, Phil was the first to show me that if you work hard – your knowledge can be limitless. Your constant effort to raise the bar and demand the most out of us – made us all better organic chemists. I thank Phil tremendously for sparing me a terribly monotonous dental career, allowing me to join his research group, and assigning me a lab partner named Dahlia in the polymer synthesis class.

While my family and professors helped give me thirst as a scientist, Dahlia rounded me as a human being. She taught me that to get things, you must earn them through hard work. Importantly, she exposed me to the other side of humanity, in which

things like food, or even love, are not to be taken for granted. As a scientist, Dahlia has challenged me the most. She has pushed me to create the most out of a little – and in a short amount of time. The speed at which projects were completed during my PhD can be soley attributed to her ambition. She has been a fantastic lab partner, person to carpool to work with, and life partner – and I am grateful for her opinions, advice, friendship, and love.

I must thank my advisor, Derek Patton, for giving me the opportunity to continue to grow as a scientist and a mentor. Derek provides a research environment that has allowed me to persue any research interest – down any path. While frustrating at times, the lack of direction forced me to learn, create, and discover on my own, which is the sole goal of a PhD. I leave USM prepared to explore new solutions to problems in science. Derek has also been a great mentor – professionally. Whether it is crafting an email to a new acquaintance or responding to a reviewer's question – clarity, succinctness, and respect are requirements, not options.

The members of Patton research group from 2014-18 have been helpful throughout my PhD. The Taco Thursday crew helped encourage time away from lab for more important things (mexican food, alcohol, and laughter). Emily Hoff, Brian Donovan, Jananee Narayanan, Li Xiong, Wei Guo, Yidan Guan, Cassandra Reese, Will Walker, and Shelly Vekasy helped through graduate school, with comments, questions, and revisions at every step during the doctoral process. My undergraduates, Susan Walley, William Martin, Sarah Swilley, and Michael Sandoz have all been excitable students with a desire to grow as scientists and people. This PhD was made easier by their desire to get results.

Technology has made research faster, so thank you developers and publishers for supporting/providing open access to journals as not every institution can afford access to every journal.

I would like to thank, a now former teacher and friend from Oak Grove High School, Mark Holcomb. Thank you for having an excellent attitude when working with me on summer projects. Thank you for trusting me with starting up a Science Bowl team. I am immensely proud of our team placing 2nd and 1st in the state of Mississippi and Louisiana, respectively.

Music provided an escape from the frustrations of the lab. Kanye West, Kendrick Lamar, 2 Chainz, Big Sean, Interpol, and Modest Mouse – thank you for that beautiful music.

Lastly, I would like to thank the department for making an inclusive community that looks out for each other. Every person in the department has loaned me a chemical, trained me on an instrument, or given advice on a reaction. This type of culture can only expedite progress and I feel it is worthy of recognition and acknowledgement.

DEDICATION

To Dahlia,

for teaching me how to bring the abstract into reality

To Mom and Dad,

for constant love and support through my mistakes and triumphs

To Bali,

for making dark days brighter

TABLE OF CONTENTS

LIST OF TABLES

LIST OF ILLUSTRATIONS

LIST OF SCHEMES

LIST OF ABBREVIATIONS

USM	The University of Southern Mississippi
AFM	atomic force microscope
AIBN	azobisisobutyronitrile
$CDCl_3$	deuterated chloroform
DI	deionized
DMSO	Dimethyl sulfoxide
Ene	alkene
Et_3N	triethylamine
FTIR	fourier transform infrared spectroscopy
GCMF	glass capillary microfluidics
H_2O	water
mW	milliwatts
N_2	nitrogen
NH_2	amine
OCH_3	methoxy
OH	hydroxy
OSTE	Off-stoichiometry thiol-ene
pH	potential hydrogen
r.t.	room temperature
SEM	scanning electron microscopy
SH	thiol
THF	tetrahydrofuran

TMS	trimethylsilane
X	halogen or functional group
Yne	alkyne

CHAPTER I - UTILIZATION OF THIOL-ENE CHEMISTRY IN EMULSIONS

1.1 Thiol-ene "click" coupling/polymerization reactions in heterogenous mixtures

In the last decade, thiol-ene polymerization has been widely utilized in emulsions for the rapid fabrication of functional particles (nano-micro), capsules, and drug delivery platforms.[1-5] Thiol-ene reactions are uniquely attractive for heterogenous oil-in-water (o/w) systems owing to their high efficiency/yields, rapid kinetics, facile reaction conditions (oxygen, water, room temperature), absence of expensive or potentially toxic catalysts, and tolerance towards a wide range of functional groups.[4] In this introduction chapter, we will provide an overview of recent thiol-ene reactions within emulsions – covering topics such as encapsulation, crosslinked/linear thiol-ene particle formation, and unique applications of these new materials.

1.2 Heterogeneous polymerization

Suspension polymerization, miniemulsion polymerization, dispersion polymerization, and microfluidics have emerged as industrially viable methods to generate functional particles/capsules for coatings, cosmetics, nanomedicine, bioimaging, and delivery applications.[6] In general, each technique relies on the dispersion and stabilization of monomer/polymer droplets into a continuous phase through the addition of surfactants and/or costabilizers;, however, the techniques differ in initial state of the polymerization mixture and rate/mechanism of particle nucleation/formation. In a suspension polymerization, a water insoluble initiator and monomer are mechanically stirred to form polydisperse droplets in the aqueous continuous phase. Upon initiation, the droplets are converted into beads of approximately the same size (no growth in droplet size) ranging from 1-1000 μm.[7]

In contrast to suspension polymerization, miniemulsion polymerization requires both a high energy mixer (ultrasonicator or homogenizer) to emulsify and a hydrophobic molecule to stabilize the nano-sized droplets (50-500 nm) against Ostwald ripening.[8] Alternatively, in dispersion polymerization the monomer and initiator are both soluble in the continuous phase prior to polymerization. Upon polymerization, the medium becomes a poor solvent for the polymer, leading to nucleation and particle growth with sizes ranging from 1-10 µm.[7] Unfortunately, suspension, miniemulsion, and dispersion polymerization, cannot produce truly monodisperse droplets. The ultimate control in dispersity can only be achieved through microfluidics where the linear flow of organic and aqueous phases is precisely controlled through geometric constriction and flow rates within a device to finely tune droplet size (1-1000 µm).[9] In general, the emulsification technique, monomer hydropathy, and concentration of surfactant/costabilizer need to be carefully considered when choosing a desired application, as they will impact both particle size and long-term stability.

Apart from the polymerization/nucleation mechanism for particle formation, the emulsification technique also dictates the order of the resulting emulsion (o/w, w/o/w, o/w/o/w, etc.). For instance, suspension and miniemulsion polymerizations result in oil-in-water (o/w) heterogeneous solutions, while techniques like microfluidics allow for the precise control over multiple order emulsions such as water-in-oil-in-water (w/o/w) emulsions or higher orders.[10]

Although emulsion polymerization has mainly been used for chain growth polymerization, several examples recently have highlighted the utility of step-growth polymerization for the generation of nano-sized particles.[11-12] Within the past two

decades, multiple step-growth reactions have been demonstrated in heterogenous polymerizations, such as diamine/epoxide[13], diisocyanates/diols[14-15], diazides/dialkynes via copper-mediated and copper-free azide-alkyne 1,3-dipolar cycloaddition (CuAAC)[16-17], thiol/isocyanate[18-19], dichlorophenylphosphate/diols[20], thiol/alkene[21-24], and thiol/alkyne[25]. Of these techniques, thiol-Michael and radical mediated thiol-ene/yne additions are uniquely suited for emulsion polymerization owing to their rapid polymerization kinetics, high yields, functional group tolerance, and limited side reactions.[26-28]
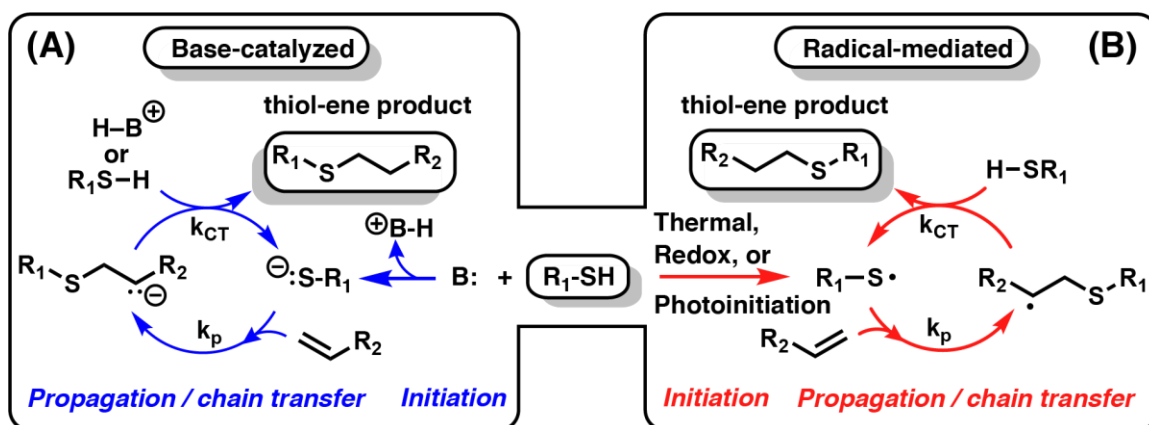
Figure 1.1 (A) Base-catalyzed (thiol-Michael) addition. (B) Radical-mediated thiol-ene addition.

Generally, the base-catalyzed thiol-Michael addition begins with proton abstraction from a thiol by a base (e.g. triethylamine) to generate a thiolate which adds across an electrophilic alkene to produce a carbon centered anion (Figure 1.1A). The subsequent anion can either abstract a proton from the conjugate acid to regenerate the base or abstract a proton from another thiol to regenerate a new thiolate. Alternatively, the radical-mediated thiol-ene reaction begins with the initiation of a thermal, redox, or photo-initiator upon exposure to a stimulus which generates a radical (Figure 1.1B). The

3

generated radical abstracts the hydrogen attached to a thiol to generate a thiol-centered

radical. The thiol radical then adds across a carbon-carbon double bond to generate a new

carbon-centered radical. Chain transfer to a new thiol can occur, and the process of

addition and chain transfer continues until various termination events.
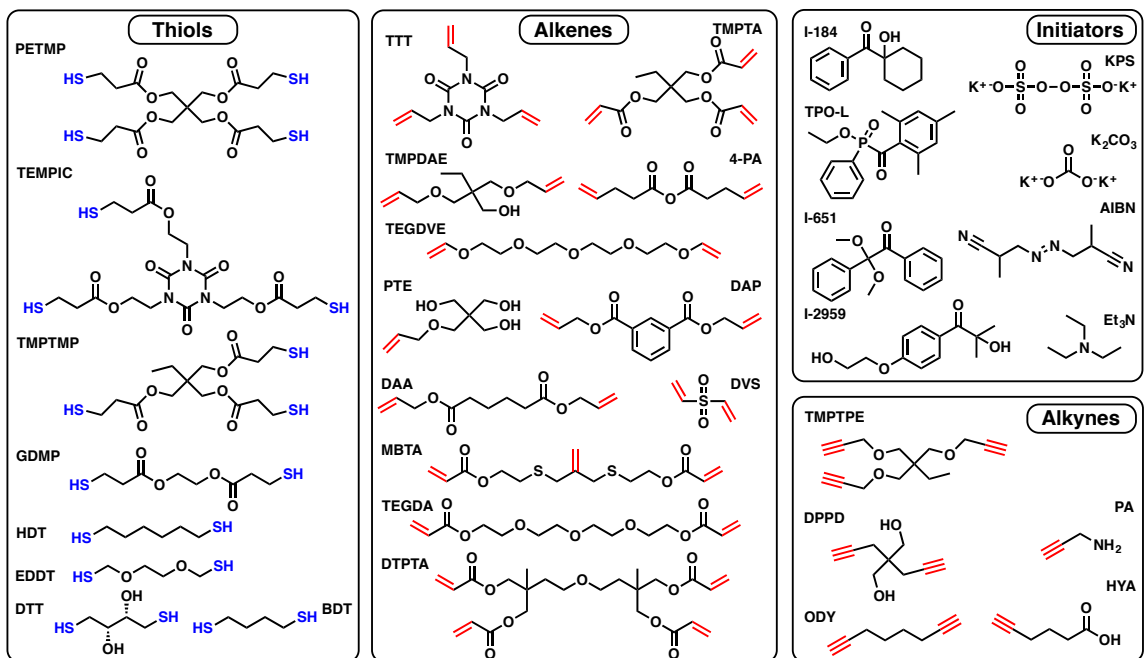
Figure 1.2 Thiols, alkenes/ynes, and initiators previously used in heterogenous thiol-ene polymerizations.

In recent years, both thiol-Michael and radical mediated thiol-ene/yne

polymerizations have been successfully highlighted in multiple emulsification platforms

(Table 1.1) with various thiols and alkene/ynes used to tune their thermal and mechanical

properties (Figure 1.2). Typically, multifunctional thiols, when paired with

multifunctional alkenes/ynes, generate homogenous crosslinked polythioether networks.

4

Table 1.1 Reported examples of polythioether emulsions.

Technique	Continuous Phase[S]	Monomers[M]	Initiator[I]	Size	Dispersity	REF
Suspension	H$_2$O + SDS	PETMP:TTT	I-184	100-400 nm	Broad	29
Suspension	H$_2$O + Tween 20, 40, 60, 80; SDS, Lutensol XL 70, XP 70; Pluronic PE6400, F108; SDBS; DTAB; or HTAB	PETMP:TTT	I-184	80-500 µm	Broad	30
Suspension	H$_2$O + SDS, DTAB, Tween 20	HDT, EGDT, PEMTP: TTT, HYA, ODY,	I-184	5-200 µm	Broad	31
Suspension	H$_2$O + GA, GG, XG, SDS	PETMP:TTT	I-184	100-600 nm	Broad	32
Suspension	H$_2$O + chitosan	PETMP, TMPTMP : TTT, APE, TMPDE	I-651	3-10 µm	Narrow	33
Suspension	Glycerol	PETMP:TTT	TPO-L	40-400 µm	Broad	34
Suspension	H$_2$O + SDS	PETMP:TTT	I-184	200-400 µm	Broad	35
Dispersion	MeOH + PVP	PETMP,TMPTMP, TEMPIC, HDT : TTT, TMPDAE, HYA, ODY	I-184	190-740 nm	Broad	36
Dispersion	MeOH + PVP	PETMP: TMPTMA	TEA	1-6 µm	Very narrow	37
Dispersion	MeOH + PVP	PETMP, TMPTMP, GDMP:TMPTA, DTPTA, DVS	Hexyl-amine	1-10 µm	Narrow	38
Dispersion	MeOH + PVP	PETMP: TEGDA, MBTA	TEA	3 µm	Narrow	39
Dispersion	MeOH + PVP	TMPTMP:DVS	TeA	2 µm	Narrow	40
Dispersion	MeOH + THF + PVP	PETMP:TMPTA Tetrazole-acrylate	TEA	4 µm	Narrow	41
Miniemulsion	H$_2$O + SDS	EGDT:DAA	I-2959	90-300 nm	Broad	21
Miniemulsion	H$_2$O + SDS	PETMP, GDMP:NDA,TMPTA	TEMPO or I-2959	200 nm	Broad	42
Miniemulsion	H$_2$O + SDS	EDDT:DAP, DAA	I-2959; I-651	155-190 nm	Broad	43
Miniemulsion	H$_2$O + SDS	PETMP:TTT	I-184	50-160 nm	Broad	44
Miniemulsion	H$_2$O + SDS	PETMP:HY, ODY, TMPTPE	I-184	45-200 nm	Broad	45
Miniemulsion	H$_2$O + Hitenol BC-20	GDMP, PETMP: DAP	I-184	150-180 nm	Broad	46
Miniemulsion	H$_2$O + Lutensol AT80	DGU: BDT	AIBN	200-300 nm	Broad	47
Miniemulsion	H$_2$O + SDS, Lutensol AT80 or AT50	DGU: BDT	AIBN or KPS	180-220 nm	Broad	48
Miniemulsion	H$_2$O + SDS or Lutensol AT80	MEE, BDT:PDU	AIBN	115-140 µm	Broad	49

Table 1.1 (Continued)

Miniemulsion + interfacial	H₂O + SDS	TMPTMP: allyl-lignin	AIBN	40-170 nm	Broad	50
Emulsion	H₂O + Hypermer B246 or Span 80	PETMP:TTT	TPO-L	1-1.4 µm	Broad	51
Emulsion	H₂O + SDS	TMPDAE, TTT : HDT, TEGDT, PETMP	KPS	73-355 nm	Broad	52
Microfluidics	H₂O + PVA	TMPTMP:TEGDVE, 4-PA, TTT	I-1173	150-300 µm	Monodisperse	53
Microfluidics	H₂O + SDS or mineral oil + ABIL EM-90	PETMP:DAP, TTT, ODY, PTE, DPPD, PA	DMPA	210-580 µm	Monodisperse	54
Acoustic excitation coaxial flow	H₂O + SDS	TTT or APE : TMPTMP	I-819	2.5-183 µm	Narrow	55
Pickering emulsion	H₂O + Thiol-ene particles	TMPTMP:TTT	I-2959	100 µm	Broad	56
Interfacial	H₂O + PVA	DTT:TMPTA, PETA, DiPEPA, DiPEHA	K₂CO₃	500 nm - 100 µm	Broad	57
Solvent evaportaion	H₂O + PVA, PVP, SDS, DTAB	PETMP, HDT, EDDT: 4-PA	I-184	200-300 nm	Broad	58

[S] SDS: sodium dodecyl sulphate; SDBS: sodium dodecylbenzene sulfonate; DTAB: dodecyltrimethylammonium bromide; TTAB: tetradecyltrimethylammonium bromide; HTAB: hexadecyltrimethylammonium bromide; PVP: poly(vinylpyrrolidone); GA: Gum Arabic; GG: while guar gum; XG: while guar gum

[M] PETMP: pentaerythritol tetrakis (3-mercaptopropionate); TMPTMP: trimethylolpropane tris(3-mercaptopropionate); GDMP: glycol di(3-mercaptopropionate); BDT: butanedithiol; HDT: 1,6-hexanedithiol; MEE: 2-mercaptoethyl ether; EDDT: 2,2-(ethylenedioxy)diethanethiol; TTT: 1,3,5-triallyl-1,3,5-triazine-2,4,6(1H,3H,5H)-trione; TMPDAE: trimethylolpropane diallyl ether; PETA: pentaerythritol tetraacrylate; DiPEPA: Dipentaerythritol pentaacrylate; DiPEHA: dipentaerythritol hexaacrylate; TMPTA: trimethylolpropane triacrylate; PDU: 1,3-propylene diundec-10-enoate; DAP: diallyl phthalate; DAA: diallyl adipate; TEMPIC: tris[2-(3-mercaptopropionyloxy) ethyl] isocyanurate; MBTA: 2-methylene-propane1,3-bis(thioethyl acrylate); TEGDA: tetra(ethylene glycol) diacrylate; DGE: dianhydro-D-glucityl diundec-10-enoate; DVS: divinyl sulfone; TEGDVE: tri(ethylene glycol) divinyl ether; 4-PA: 4-pentenoic anhydride; PTE: pentaerythritol allyl ether; DPPD: 2,2-di(prop-2-ynyl)propane-1,3-diol; HYA: 5-hexynoic acid; HY: 1-hexyne; ODY: 1,7-octadiyne; PA: propragyl amine; TMPTPE: trimethylolpropane tripropargyl ether.

[I] I2959: 2-hydroxy-4′-(2-hydroxyethoxy)-2-methylpropiophenone; I651: 2,2dimethoxy-2-phenylacetophenone; I-184: 1-Hydroxycyclohexyl phenyl ketone; TEA: triethylamine; TPO-L: ethyl (2,4,6-trimethylbenzoyl) phenylphosphinate; K2CO3: potassium carbonate; AIBN: azobisisobutyronitrile; KPS: potassium persulfate.

1.2.2 Thiol-ene/yne suspension polymerization

Durham and coworkers[29] were among the first to synthesize crosslinked polythioether microparticles via thiol-ene suspension photopolymerization where water

6

insoluble monomers (TTT and PETMP) and photoinitiator (I-184) were sonicated in a

surfactant [sodium dodecyl sulfate (SDS)] solution in the presence of cosolvent

(chloroform or toluene). Durham highlighted that particle size was directly related to

sonication time with higher energy input resulting in smaller sized particles with a broad

distribution of sizes. Similarly, Zhang et al. used ultrasonication followed by UV

irradiation for 2 minutes to synthesize large (>200 µm) porous microparticles using

PMMA as a porogen.[59] These initial studies highlighted the utility of thiol-ene

polymerization for the generation of particles with rapid polymerization kinetics and high

monomer conversions; however, these methods relied on the use of ultrasonication for

the particle fabrication.

Aside from sonication – homogenizers and high-speed mixers have proven

equally effective at generating thiol-ene microparticles in a facile manner. For instance,

Barker used a homogenizer at 16,000 rpm with an off stoichiometry thiol-ene (OSTE)

resin to generate excess thiol functionalized particles (from 1–100 µm in diameter).[33] The

excess thiol particles were subsequently reacted with C60 fullerene to serve as a

heterogenous photocatalyst.[33] Additionally, Hoffmann et al. used glycerol instead of

water as a dispersing medium in order to form OSTE particles under shear mixing (1000-

3500 rpm) without the addition of surfactants or organic cosolvents.[34] Excess thiol

particles had sizes ranging from 50–400 µm and were surface functionalized with a large

library of alkenes. Epoxide functionalized particles were subsequently used to

immobilize horseradish peroxidase with no effect on enymatic activity upon ligation.

To understand the role of surfactant in droplet stabilization, Durham and

coworkers studied the effect of surfactant concentration and surfactant type (anionic,

cationic, or neutral) on particle size and distribution.[30] In general, the study found that increasing surfactant concentration regardless of surfactant type led to smaller particles from sizes of 500 µm (0.1 wt.% surfactant) to 80 µm (5 wt.% surfactant). No particular surfactant type resulted in narrower distributions as the sonication process inherently leads to polydisperse particles. Interestingly, aside from traditional omniphilic surfactants/emulsifiers, viscosity thickening agents can also stabilize particles by limiting droplet diffusion. A small library of natural gum stabilizers was found to readily stabilize micron-sized crosslinked thiol-ene particles in the complete absence of any traditional surfactants upon ultrasonication.[32]

1.2.3 Thiol-ene/yne dispersion polymerization

Thiol-ene dispersion polymerization has been widely utilized as a facile particle synthesis method, due to several advantages including: (1) rapid nucleation of multiple droplets; (2) fabrication in the absence of water; (3) mild reaction conditions (room temperature); (4) rapid kinetics; (5) complete monomer conversion; and (6) narrow polydispersity of droplets. Thiol-ene dispersion polymerizations have successfully produced particles via either base or radical initiated mechanisms with most common initiating species being amines (primary or tertiary).

In a traditional thiol-ene dispersion polymerization, alkenes/thiols, and stabilizers are first homogenously dissolved in a solvent. Then a catalyst (typically triethylamine) is added to initiate the crosslinking process. As the molecular weight increases during polymerization, the oligomers/polymers/gels become insoluble in the solvent leading to nucleation for particle growth. If particle nucleation is slow – relative to particle growth – a broader distribution of particles is produced. Alternatively, if particle nucleation is fast,

a narrower distribution of particles is produced. The general dispersion polymerization of thiol-ene monomers is depicted in Figure 1.3.
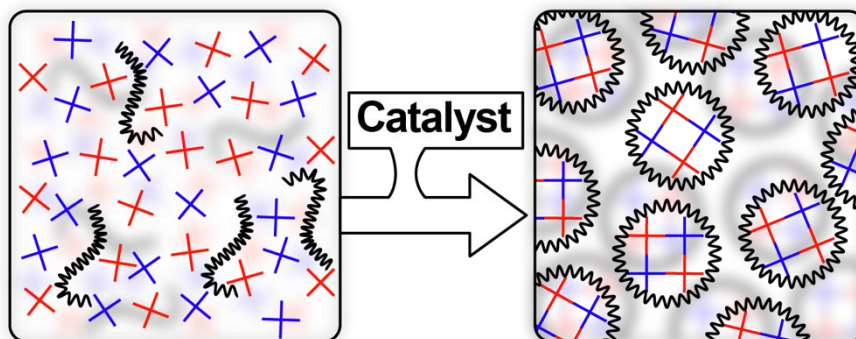
Figure 1.3 Mechanism for dispersion polymerization. Left: miscible monomer, stabilizing agent and solvent. Right: After the addition of catalyst, the crosslinked monomers are no longer soluble in the solvent and crash out to form stabilized particles.

The most critical factors in controlling the dispersity and size of particles via dispersion polymerization are the initiating species, initiator/catalyst concentration, monomer concentration, stabilizer concentration, and solvent polarity. To probe the effect of initiating species on particle size, Alimohammadi et al. compared dispersion polymerization obtained via thermal, redox, and photo initiation.[36] The study showed that the rapid initiation via photoinitiation led to narrower particle size distributions as compared to either the thermal or redox initiators. Additionally, the polymerization time required for complete conversion was less than 5 minutes via photoinitiation and ~3h for either redox or thermal initiation. Importantly, the study found that regardless of the initiation source, increasing the initiator concentration resulted in smaller particle sizes which suggests an increase in the number nucleation sites during polymerization. In terms of monomer conversion, at least 10 wt.% of a redox initiator was required to reach full monomer conversion whereas less than 1 wt.% photoinitiator or thermal initiator was sufficient to fully polymerize the particles. Additionally, Alimohammadi and coworkers[36]

varied the monomer crosslink density (from linear to very crosslinked polymers) and found that an increase in monomer functionality resulted in smaller sized particles. Interestingly, they found that for linear polythioethers, thermal properties such as the polymer glass transition or melting temperature dictated colloidal stability.[36] In general, an increase in monomer concentration led to larger particle sizes, while an increase in stabilizer or initiator concentration led to smaller sizes.[36] In the design of thiol-ene-based dispersion polymerizations, multiple variables need to be carefully considered in order to control particle size and emulsion stability.

In 2014, Wang et al. reported the first thiol-ene dispersion polymerization via Michael addition reactions between multifunctional thiols and electron deficient alkenes.[38] The initial monomers were dissolved in methanol along with poly(vinyl pyrrolidone), then upon stirring, the base-catalyst – hexylamine was added to initiate the polymerization. Crosslinked polythioether microparticles of low dispersity (3.7% coefficient of variation) were obtained with sizes ranging from 1-10 µm. OSTE was also employed to generate excess thiol or acrylate microparticles which were subsequently tagged with fluorescent dyes.

The introduction of the Michael addition as a step-growth polymerization mechanism allows for the installation of unique radical sensitive compounds into the backbone of the polymer. For example, Cox et al. also utilized Michael addition dispersion polymerization to generate a crosslinked thiol-ene network with 2-methylene-propane1,3-bis(thioethyl acrylate) (MBTA). The particles were formulated with MBTA, PETMP, I-651, and were crosslinked using triethylamine as catalyst. Upon exposure to UV light, the encapsulated photoinitiators would add across the internal alkenes of

MBTA and allow for the crosslink junction to fragment to release mechanical strains. Upon dual application of stress and UV light, permanent shape reconfiguration of microparticles was observed. This strategy provides a solution to the high radical-based reactivity of alkenes to thiols so that polymer networks could be fabricated using one specific alkene functionality at a time. Michael addition (thiol-ene dispersion polymerization) was recently used for the installation of a UV sensitive tetrazole-containing acrylate which can undergo a UV-triggered nitrile imine-mediated tetrazoleene cycloaddition.[41] The tetrazole functionality remained intact throughout the thiol-Michael reaction and the tetrazoles underwent a cycloaddition to generate fluorescent microparticles in a single step.

For drug delivery applications, successful drug encapsulation within particles has also been achieved through thiol-ene dispersion polymerization. Wang et al.[60] recently synthesized a poly(thioether orthoester) degradable network by mixing an orthoester-diacrylamide with PETMP in acrylonitrile followed by the addition of triethylamine. The resulting crosslinked polymer nanoparticles (50-800 nm) could be subsequently swollen in the presence of DMSO and doxorubicin as an encapsulant. The presence of the orthoester-diacrylamide coupled with the step-growth nature of the thiol-ene polymerization allowed for every crosslink junction to degrade upon exposure to an acidic aqueous solution. The advantage to dispersion/precipitation of the nanoparticles into an organic solvent was that it allowed for the water-sensitive orthoesters to remain intact during polymerization.

1.2.4 Miniemulsion polymerization for functional polydisperse nanoparticles

Miniemulsions are kinetically trapped and thermodynamically unstable heterophase systems created under high shear processing with polydisperse nano-sized droplets.[61] Kinetic stabilization of the droplets if conferred by the addition of a hydrophobic molecule such hexadecane or cetyl alcohol. The hydrophobic compound prevents Ostwald ripening (emulsion breakdown occurring to a difference in Laplace pressure between droplets of different sizes) by preventing the diffusion of other additives between droplets through the continuous phase via formation of concentration gradients.[62] Unique to miniemulsion polymerization, both initiation and particle nucleation occur in discrete dispersed droplets, or nanoreactors, which enables constant size and composition of each droplet during the miniemulsion polymerization as shown in Figure 1.4.[63]
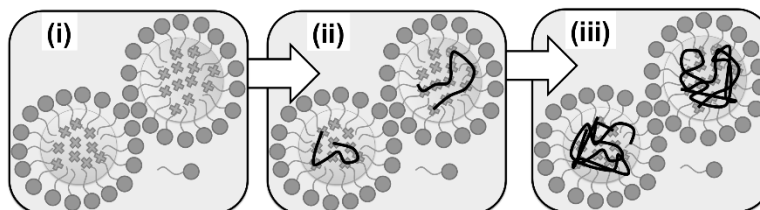
Figure 1.4 Polymerization steps within a miniemulsion: (i) initiation within a droplet, (ii) propagation within a droplet, and (iii) fully polymerized droplet.

In order to form a nano-sized emulsion, high energy input through either homogenization or ultrasonication is required. In homogenization, plates with tailored geometries and hole spacing allow for oil droplets to break down in size as they are pumped through multiple times. Homogenizers have greater throughput compared to ultrasonicators, however, they require expensive equipment and require large volumes of reagents. Alternatively, ultrasonicators offer simple setup, but are limited to relatively

small volumes for processing. Additionally, the ultrasonic process generates excess heat

which can be problematic for emulsion stability and premature polymerization. It is well

documented that ultrasonication can break weak covalent bonds[64], generate radicals

which can initiate polymerization[65], and rapidly heat solutions.

Within emulsions, the reaction volumes are so low that almost quantitative

conversion can occur within seconds of exposure to a stimulus (e.g. UV light). To this

end, Jasinski and coworkers showed that linear thiol-ene polymers (derived from

ethyleneglycol dithiol and diallyl phthalate) can be synthesized in molecular weights up

to 20 kDa in less than 15 seconds via miniemulsion photopolymerization.[43] Interestingly,

when either a water soluble or oil soluble photoinitiator was used, near quantitative

conversion was observed with no significant difference in particle size.[43] Additionally,

the average particle size of the emulsified droplets (150 nm) did not change significantly

after photopolymerization (130 nm) and scaled with an increase in reactor size (up to 150

mL).[21] The resulting linear polythioether nanoparticles were used to make clear,

chemically resistant, and semicrystalline (55% crystallinity) elastomeric films. Moreover,

Wang et al. also demonstrated that OSTE polymerization between multi-functional thiols

and acrylates could result in functional nanoparticles.[42] Particles synthesized with excess

thiols were successfully functionalized with 11-azido-1-undecene and excess acrylate.

Additionally, when OSTE particles were cast as a film and subsequently irradiated to

further crosslink the acylate groups present in the latex a T_g increase from -1 ± 2 °C to 69

± 2 °C was observed.

Amato et al. have published multiple papers on thiol-ene/yne miniemulsions for

the fabrication of functional polythioether nanoparticles.[44-46] Amato demonstrated that the

inclusion of a radical inhibitor should be added to prevent the sonochemical generation of hydroxyl radicals which can initiate the polymerization as droplets are being sheared.[44] Additionally, Amato found that increasing the ultrasonication time or amplitude leads to smaller size nanoparticles (from 80 to 35 nm).[44] OSTE reactions were employed to generate either excess SH or alkene/yne functional nanoparticles. These OSTE nanoparticles were subsequently functionalized via reactive fluorescent probes and imaged via confocal microscopy.[44-45] Importantly, the thiol-yne nanoparticles can be ligated through the copper(I)-catalyzed alkyne-azide cycloaddition to a library of commercially available azides.[45]

Although a hydrophobic solvent is typically added to the monomer phase to reduce viscosity during the emulsification process, Amato showed that a "functional" solvent such as antimicrobial terpenes like carvacrol or thymol could be incorporated during the emulsification process to create a drug-delivery platform.[46] These carvacrol and thymol-loaded nanoparticles exhibited potent antimicrobial activity against a broad range of pathogenic bacteria. While terpenes were used as a model antimicrobial delivery platform, the concept applies to other hydrophobic drugs or hydrophobically modified nanoparticles as previously demonstrated in traditional chain growth miniemulsions.[66]

Similarly, de Meneses[47] encapsulated clove oil (<25 wt.%) during the miniemulsion polymerization of a new bio-based dialkene to generate nanoparticles for antioxidant delivery. A follow up study showed that these polymers had up to 19% crystallinity, biocompatibility, and high encapsulation efficiency of coumarin (up to 98%).[49] Miniemulsion polymerization was also used to synthesize linear degradable

poly(thioether esters) with molecular weights ranging from 5-20 kDa.[49] The linear

poly(thioether ester) nanoparticles were shown to be biocompatible towards murine

fibroblast, HeLa, and red blood cells and are being developed for a new controlled

delivery platform.

Finally, thiol-ene miniemulsion have also been explored as a viable method for

rapid production of capsules. Chen and coworkers synthesized allyl-functionalized lignin,

emulsified it with hexadecane, butyl acetate, and a coumarin dye, and then added a

dithiothreitol (a water soluble dithiol) to induce interfacial polymerization.[50] The allyl

functionalized lignin cannot homopolymerize which ensures that a capsule is formed

upon polymerization (confirmed via transmission electron microscopy). The unique size

obtained with miniemulsions coupled with the rapid polymerization kinetics introduced

via thiol-ene chemistry could lead to higher throughput latexes for paints, cosmetics, and

agriculture.

1.2.5 Other heterogenous thiol-ene techniques

Aside from emulsification techniques mentioned above, the rapid production of

functional particles via thiol-ene/yne polymerization can also be achieved through other

methods such as microfluidics, acoustically-induced droplet breakup, and Pickering

emulsions. Amato[53] and Prasath[54] have utilized microfluidics to generate functional

monodisperse microcapsules via glass capillary microfluidics (GCMF) and a t-junction,

respectively. GCMF utilizes the alignment of tapered and machine-cut glass capillaries to

create inlets and nozzles. The glass capillaries can be surface functionalized via silane

chemistry to promote the wetting or dewetting of fluids. Figure 1.5 depicts a typical

GCMF w/o/w device in which water is first emulsified by coxial flow of the middle fluid.

The resulting w/o emulsion is immediately flow-focused by the outer fluid to induce droplet breakup. This two-step process allows for fine control over shell (oil) thickness and droplet size, while forming monodisperse w/o/w droplets. Typically, photocurable acrylates are polymerized to solidify the oil phase upon exposure to light, however, recent work by Lee and coworkers have highlighted difficulties of this platform in encapsulating omniphilic cargo.[67-68] Specifically, Lee showed that within 24 h, 100% of fluorescein (an omniphilic dye) was released from these encapsulated particles. To solve this problem, Lee demonstrated that water/fluorocarbon oil/resin/water or oil/water/resin/water triple emulsions were necessary to retain omniphilic molecules.

Recently, Amato[53] utilized a GCMF device to fabricate monodisperse w/o/w emulsions to highlight the importance of monomer curing and structure on the retention of encapsulated additives. Low monomer conversion resulted in immediate leaking of the inner fluid from through the oil shell, whereas high conversion resulted in long term (>30 day) encapsulation. Additionally, Prasath and coworkers used a simple o/w t-junction device to generate large (200-600 µm) monodisperse porous beads via thiol-ene/yne photopolymerization.[54] Polymerization of monomers, such as propargyl amine, allowed for the incorporation of amine functionality into the polymerized beads which has direct application as a support bead within the peptide coupling industry.
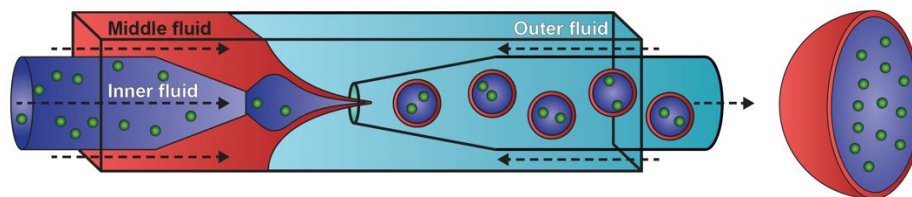
Figure 1.5 Typical glass-capillary microfluidic device to produce o/w/o droplets.

Aside from microfluidics, acoustic excitation coaxial flow has also been studied by Windham and coworkers in which acoustically driven mechanical perturbations breakup a thiol-ene liquid jet, resulting in micron-sized thiol-ene droplets that can be photochemically polymerized to yield thiol-ene microspheres.[55] The particle size could be controlled by adjusting the amplitude, frequency, flow rate, and resin viscosity while maintaining a relatively narrow size dispersity.

Control over where initiation occurs (e.g. in oil or water) can be utilized to control particle morphology through various interfacial polymerization techniques. Li et al.[56] were able to encapsulate isophorone diisocyanate (IPDI) within a photocured thiol-ene shell made up of TTT and TMPTMP via a Pickering emulsion. To achieve this, an aqueous solution of photoinitiator (I-2959) and poly(gylcidyl methacrylate) particles was emulsified with the resin (TTT, TMPTMP, and IPDI), shaken, and then irradiated. The particles adsorbed to the o/w interface and the UV irradiation only allowed for interfacial polymerization leading to the formation of a hollow capsule (observed via fracture scanning electron microscopy). Similarly, Liao and coworkers[57] demonstrated that interfacial polymerization can occur if a water soluble thiol was copolymerized with an oil soluble alkene for the encapsulation of fragrance oil. First, an emulsion of fragrance oil and a library of acrylates, water and surfactant were prepared – followed by the dropwise addition of dithiothreitol (water soluble thiol) and K_2CO_3 (aqueous initiator). Upon complete addition of the thiol, stable spherical capsules were obtained. The capsules could be ruptured either by application of force or by heating to pressurize the capsules. These examples highlight the ability to employ parameters such as the

solubility of the initiating species or monomer to yield different particle morphologies upon polymerization.

Preformed polythioether linear polymers can also be subjected to nanoprecipitation to generate nanoparticles. For example, Durham and coworkers highlighted that linear poly(thioether anhydride) copolymers can undergo nanoprecipitation to generate nano-sized-crosslinked particles.[58] First a small library of linear polyanhydrides were synthesized, dissolved into dichloromethane (DCM) and combined with I-184 (photoinitiator) and PETMP (tetra-thiol). The monomer/polymer resin was then added to an aqueous-surfactant solution, sonicated, and then irradiated with UV light to cure the particles. After heating to remove DCM, particles with sizes ranging from 250-400 nm were generated. These semi-crosslinked networks had degradation rates that were dependent on the amount of PETMP (crosslinker) added to the formulation.

1.3 Conclusion

Remarkable progress has been made in the design and characterization of particles prepared via thiol-ene/yne chemistry with various emulsification techniques. Many examples presented have shown great promise in the encapsulation and delivery of model hydrophobic cargo (drug, fragrance, or dye), and these systems provide a facile and scalable method moving forward. Unfortunately, multiple opportunities to tailor drug release within well-defined thiol-ene networks remain unexplored, such as monomer design and functionality, crosslink density, hydrophobicity, and thermal mechanical properties. Additionally, precise control over the release of hydrophobic cargo from thiol-ene matrices remains a constant challenge that needs to be addressed. Lastly, the

remarkable functional group tolerance and plug-in-play nature of the thiol-ene monomers

can lead to new fundamental network structure-drug release relationships within

functional thiol-ene particles.

CHAPTER II - FUNCTIONAL, SUB-100 NM POLYMER NANOPARTICLES VIA
THIOL-ENE MINIEMULSION PHOTOPOLYMERIZATION

2.1 Abstract

In this work, sub-100 nm crosslinked polythioether nanoparticles were synthesized *via* thiol-ene photopolymerization in miniemulsion using high-energy homogenization. The effects of the miniemulsion formulation and homogenization parameters – including inhibitor concentration, surfactant concentration, organic weight fraction, ultrasonication time and amplitude – on nanoparticle size and size distribution were investigated. Thiol-ene nanoparticles with a mean particle diameter of 46 nm were obtained under optimized conditions for the current system at 2.5 wt. % organic fraction and 20 mM surfactant concentration. In an effort to demonstrate potential utility of thiol-ene nanoparticles, we exploit the step-growth radical mechanism of thiol-ene photopolymerization under non-stoichiometric conditions to fabricate functional nanoparticles that express excess thiol or alkene at the particle surface. We show that these excess functional groups can be utilized as reactive handles in thiol-Michael and radical-mediated thiol-ene reactions for immobilization of fluorescent moieties *via* postpolymerization modification.

2.2 Introduction

Polymer nanoparticles with tunable functionality have emerged as a promising

and viable technology platform for applications including coatings, cosmetics,

nanomedicine, and imaging. The prospects of advancing these and other technologies

have provided great impetus for the development of rapid, low-cost methodologies for

the synthesis of functional polymer nanoparticles – particularly with sizes less than

100 nm. Polymer nanoparticles have been prepared by two general routes: 1)

postpolymerization processing, including nanoprecipitation, dialysis, and supercritical

fluid expansion, and 2) direct polymerization of monomers or crosslinking of macromers

in dispersed heterophase systems, including microfluidics, microemulsion, and

miniemulsions.[69] Miniemulsions – with droplet sizes typically in the range of 20-200 nm

– are particularly well-suited for the synthesis of small polymer nanoparticles.[63, 70]

Miniemulsions are non-equilibrium systems created under high shear conditions (i.e.

ultrasonication or high-pressure homogenization) yielding small, narrowly distributed

droplets stabilized by a surfactant and costabilizer (or hydrophobe) in a continuous

phase.[61] Unlike conventional emulsion polymerization, initiation and particle nucleation

occur predominately in droplets, which serve as discrete nanoreactors, enabling the

preservation of size and composition of each droplet during polymer synthesis.[63]

While miniemulsion polymerizations have predominately been conducted using

radical chain growth mechanisms, several examples have highlighted the utility of

various step-growth mechanisms – particularly step-growth polyaddition

polymerizations.[11-12] The earliest work focused on classic polyaddition reactions in

miniemulsion, such as diamine/epoxide[13] and diisocyanates/diols.[15] More recently, the

focus has shifted to "click" polyaddition reactions in miniemulsions for the synthesis of polymer microparticles, nanoparticles, and nanocapsules. Landfester et al.[16] employed miniemulsion copper-mediated and copper-free azide-alkyne 1,3-dipolar cycloaddition (CuAAC) interfacial polymerization for the synthesis of polytriazole nanocapsules. Similarly, Bernard et al.[17] reported interfacial CuAAC miniemulsion polymerization of diazides and dialkynes under microwave irradiation to achieve glyconanocapsules with high conversion (>98%) in under 30 min.

In addition to CuAAC, thiol-mediated chemistries (i.e. thiol-ene/yne, thiol-Michael) represent an attractive family of "click" polyaddition reactions for rapid fabrication of microparticles and nanoparticles in dispersed heterophase systems, as these reactions generally proceed under mild conditions with high efficiency and rapid reaction kinetics.[26-28] For radical-mediated thiol-ene reactions, the thioether product forms *via* a free-radical step-growth process facilitated by a rapid, highly efficient chain transfer reaction between multifunctional alkenes and thiols, which provides insensitivity to oxygen and water. The earliest examples of thiol-ene related miniemulsions involved surface functionalization of residual alkenes with PEG-thiol on styrene/divinylbenzene composite nanoparticles,[71] and crosslinked biodegradable nanoparticles composed of allyl-functionalized polylactide with a difunctional thiol.[72] Regarding direct polymerization of thiol-ene in disperse heterophase systems, Shipp and coworkers[73] recently reported the first example of crosslinked polythioether microparticles synthesized via thiol-ene suspension photopolymerization. Shipp's initial work focused on the effects of surfactant concentration, cosolvent, and mixing on microparticle formation, while subsequent work explored the dependence of microparticle size and

stability on surfactant structure.[30] These initial examples clearly illustrated the utility of thiol-ene photopolymerization for creating microparticles with rapid reaction rates, high monomer conversion and homogeneous network structure in dispersed systems; however, Shipp's work focused minimally on the use of high-energy ultrasonication for the preparation of small thiol-ene nanoparticles. Similarly, Zhang *et al.*[59] reported thiol-ene suspension photopolymerization for the synthesis of large (>200 μm) porous microparticles using PMMA as a porogen. In 2014, Jasinski *et al.*[74] reported thiol-ene photopolymerization in miniemulsion using a difunctional thiol and a difunctional alkene yielding linear poly(thioether ester) nanolatex particles with 130 nm diameter and 55% crystallinity. The authors demonstrated the formation of clear, chemically resistant, and elastomeric films upon evaporation of water from the cured dispersions. It is also noteworthy to mention recent work by Bowman *et al.*[75] that utilized thiol-Michael polyaddition reactions in dispersion polymerization to fabricate monodisperse microspheres (>1 μm) from multifunctional thiols and Michael acceptors. Bowman importantly showed the ease by which fluorescent microspheres could be prepared *via* postpolymerization modification using off-stoichiometric conditions. Considering the relatively few examples of thiol-mediated polyadditions in dispersed systems, and the primary focus of these works on either microparticles or linear nanolatex particles, a significant opportunity remains to exploit thiol-mediated polyadditions in miniemulsion for the fabrication of crosslinked, functional polymer nanoparticles.

Herein, we report the synthesis of small, sub-100 nm polythioether nanoparticles using miniemulsion thiol-ene photopolymerization. We specifically focus on tailoring the miniemulsion formulation (inhibitor, surfactant concentration, monomer weight fraction)

and processing parameters (ultrasonication time and amplitude) to achieve nanoparticles

with diameters in the sub-100 nm range with relatively narrow size distributions. In

contrast to previous work by Shipp[73] and Jasinski,[74] we found the inclusion of a radical

inhibitor in the thiol-ene formulation to be critically important in preventing premature

polymerization during ultrasonic emulsification – prior to exposure to UV light. In an

effort to demonstrate potential utility of thiol-ene nanoparticles, we exploit the step-

growth radical mechanism of thiol-ene photopolymerization under non-stoichiometric

conditions to fabricate functional nanoparticles that express excess thiol or alkene at the

particle surface. We show that these excess functional groups can be utilized as reactive

handles in thiol-Michael and radical-mediated thiol-ene reactions for immobilization of

fluorescent moieties *via* postpolymerization modification.

2.3 Experimental

2.3.1 Materials

Hexadecane, 1,3,5-triallyl-1,3,5-triazine-2,4,6 (1H, 3H, 5H) trione (TTT), 4-p-methoxy

phenol (MEHQ), sodium dodecyl sulfate (SDS), 2,2-dimethoxy-2-phenylacetophenone

(DMPA), tetrahydrofuran (THF), 7-mercapto-4-methylcoumarin and butyl acetate

(Sigma-Aldrich), pentaerythritol tetra(3-mercaptopropionate) (PETMP, BrunoBock), 1-

hydroxycyclohexyl phenyl ketone (Irgacure 184, CIBA), and Texas Red® C2 maleimide

(Invitrogen) were obtained at the highest purity available and used without further

purification unless otherwise specified.

2.3.2 General Sample Preparation

Each sample was prepared in a 20 mL scintillation vial with a total volume 10 mL. The

organic stock solution shown in Table 1 was added into the vial containing a stock

solution of SDS and deionized water. The samples were then placed into an ice bath and

sonicated using a Q-700A-110 probe ultrasonicator at 5-25% amplitude for 5-45 minutes.

The miniemulsions were then cured using an Omnicure S1000-1B with a 100W mercury

lamp (λ_{max}=365 nm, 320-500 nm filter) and an intensity of 185 mW cm^{-2} for 10 minutes

unless noted otherwise. All samples were made in triplicate to ensure reproducible data.

To optimize the formulation for small nanoparticles, the organic fraction was varied with

a constant SDS concentration of 20 mM. The SDS stock formulation and tabulated

samples prepared are listed in Table A1 and A2.

Table 2.1 General formulation of organic stock solution for thiol-ene

photopolymerization in miniemulsion.

Organic Fraction	Mass (g)	Wt. %
Hexadecane	0.439 (1.94 mmol)	4.72
TTT	1.52 (6.10 mmol)	16.3
PETMP	2.22 (4.53 mmol)	23.8
Irgacure 184®	0.100 (0.49 mmol)	1.07
4-p-methoxy phenol	0.030 (0.24 mmol)	0.322
Butyl acetate	5.00 (43.04 mmol)	53.7

2.3.3 *Preparation of nanoparticles with excess thiol and excess alkene*

Nanoparticles with excess thiol were prepared using a 1.5:1 thiol to alkene stoichiometry,

for example, PETMP (2.8 g, 5.73 mmol) and TTT (0.95 g, 3.81 mmol). The remaining

constituents in the organic formulation from Table 1 were held constant. To the

scintillation vial, 250 µL of organic solution was pipetted into 9.75 mL of 20 mM SDS in

25

DI water. The sample was then ultrasonicated for 20 minutes at 10% amplitude and cured under UV light for 10 minutes. Nanoparticles containing excess alkene were similarly synthesized using a 2:1 alkene to thiol ratio, i.e. TTT (2.15 g, 8.63 mmol) and PETMP (1.58 g, 3.23 mmol).

2.3.4 Fluorescent tagging of excess thiol nanoparticles

From the nanoparticle suspension (10 mL) with excess thiol prepared in 2.3, 2 mL were removed and placed into a 20 mL scintillation vial wrapped in aluminum foil with a stir bar. A stock solution of Texas Red® C2 maleimide was made by addition 10 µL of Texas Red® C2 maleimide to 100 µL of DMSO. 50 µL of the Texas Red® C2 maleimide stock solution was added to the nanoparticles and stirred overnight. The nanoparticle were purified by centrifugation (5 minutes at 13,300 rpm, Fisher Scientific™ accuSpin™ Micro 17 centrifuge) to remove unreacted Texas Red® C2 maleimide. The supernatant was removed and the nanoparticle pellet was re-suspended in 1 mL DI water. The nanoparticle suspension was then cast onto a glass slide and allowed to dry at room temperature. The resulting slide was analyzed using a Zeiss LSM 510 confocal laser scanning microscope (λ_{ex}=543 nm).

2.3.5 Fluorescent tagging of excess alkene nanoparticles

From the nanoparticle suspension (10 mL) with excess ene prepared in 2.3, 1 mL was removed and centrifuged for 18 min at 13,300 rpm. The supernatant was removed and the nanoparticle pellet was re-suspended in 1 mL of THF. A solution was prepared containing 80 mg of 7-Mercapto-4-methylcoumarin, 30 mg of DMPA and 1 mL of THF was added. The solutions were combined and exposed to UV light for 5 minutes to induce the radical thiol-ene reaction. The solution was centrifuged for 10 minutes,

26

supernatant removed, the pellet re-suspended in THF. The coumarin-functionalized nanoparticles were then cast onto a glass slide with a coverslip for analysis by confocal laser scanning microscopy (λ_{ex}=405 nm).

2.3.6 Characterization

The size and distribution of the nanoparticles were measured by dynamic light scattering (DLS) using a Microtrac Nanotrac Ultra NPA150. Particle size and distribution were obtained using the Microtrac Flex software (v.10.6.1), which employs non-negatively constrained least-squares (NNLS) and cumulants analysis to obtain the intensity-weighted "z-average" mean particle size as the first cumulant, and the polydispersity index from the second cumulant.[76] Transmission electron micrographs (Digital Imaging with Gatan Model 785 ES1000W Erlangshen CCD Camera) were taken with a Zeiss 900 TEM operating at 50kV. Samples were applied to 200 mesh copper grids (3.05 mm, 200 lines/inch square mesh, EMS Cat. #G200-Cu) coated with Formvar (5% polyvinyl formal resin). The samples were then stained using OsO_4. Atomic force microscopy (AFM) was performed using a Bruker Icon in tapping mode. The samples were imaged with T300R-25 probes (Bruker AFM Probes) with a spring constant of 40 Nm^{-1}. ^{1}H NMR was recorded on a Varian Mercury Plus 300 MHz NMR in D_2O. FTIR was conducted using a Nicolet 8700 spectrometer with a KBr beam splitter and a liquid nitrogen cooled MCT/A detector.

2.4 Results and Discussion

Thiol-ene polymer nanoparticles were synthesized *via* ultrasonication of a dispersed organic phase into an aqueous solution of surfactant, as shown in Figure 2.1. The horn was inserted into a glass vial and the organic phase was emulsified into the

aqueous phase while a secondary ice bath was placed around the vial to prevent

overheating. Samples prepared without ice resulted in larger particles and coagulum

formation on the horn tip.
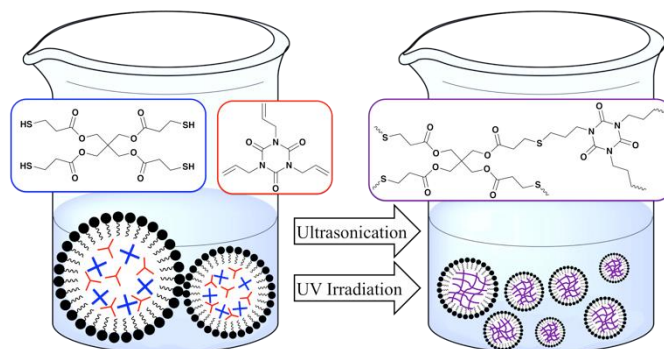
Figure 2.1 Thiol-ene precursors and miniemulsion process for preparing sub-100 nm polythioether nanoparticle *via* photopolymerization.

Thiol-ene miniemulsions were prepared by adding an organic phase containing

monomers (TTT and PETMP), photoinitiator, hydrophobe, inhibitor, and solvent to an

aqueous phase consisting of water and surfactant (SDS). Butyl acetate was chosen as the

solvent because it is close to being isorefractive with water which could lower the final

turbidity of the miniemulsion.[77] Hexadecane was chosen, as it is known to help prevent

Ostwald ripening and increase the lifetime of the miniemulsion. The organic phase once

mixed was then emulsified in the aqueous phase *via* ultrasonication to create

nanodroplets.

MEHQ (mM)*	Solids Present
111.2	No
55.68	No
27.93	Yes
13.66	Yes
7.16	Yes
0	Yes

*concentration relative to 5 grams of butyl acetate.
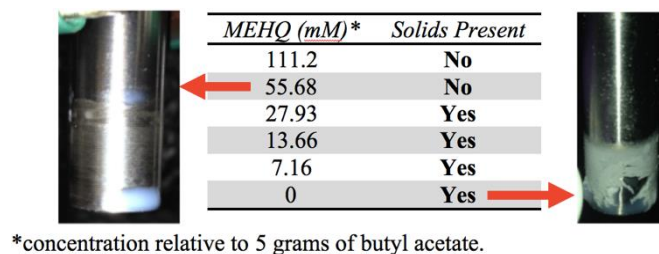
Figure 2.2 Influence of inhibitor concentration (MEHQ) on preventing polymerization during ultrasonic homogenization.

Our initial attempts to synthesize sub-100 nm thiol-ene nanoparticles using probe ultrasonication under conditions described in the literature (i.e. in the absence of radical inhibitor as reported by Shipp *et al.*[73]) resulted in the formation of solids in solution and on the surface of the horn during ultrasonication, prior to exposure to UV light, presumably due to thermally-induced polymerization. As a result of these observations, we introduced a radical inhibitor – MEHQ – into the organic phase and investigated the effect of inhibitor concentration on the miniemulsion process. MEHQ was chosen because it is a commonly used stabilizer for alkene containing monomers. The MEHQ concentration in the organic phase was varied according to values shown in Figure 2.2, where the minimum concentration that inhibited latex formation was found to be 55.7 mM. MEHQ concentrations below this minimum threshold resulted in the formation of solids on the surface of the ultrasonic horn, as shown in Figure 2.2.

To further probe the ability of the inhibitor to prevent premature polymerization during the emulsification process, thiol-ene miniemulsions with and without inhibitor were prepared using a deuterium oxide/SDS solution as the continuous phase. Upon ultrasonication, an aliquot of sample was removed and analyzed *via* ^{1}H NMR, while the remaining fraction of the sample was photopolymerized under UV light prior to collecting a second aliquot for analysis. Figure 2.3 shows the NMR spectra of thiol-ene miniemulsions with and without MEHQ prior to UV exposure. The sample with MEHQ showed the typical proton resonances for the unreacted alkene of TTT at 4.92–5.15 ppm and 5.58–5.75 ppm, and a resonance for an unreacted mercaptopropionate ($-CH_2CH_2-SH$) at 2.51 ppm. Devoid of MEHQ, the miniemulsion shows complete disappearance of the alkene and thiol monomer peaks, and exhibits peak broadening indicative of

polymerization. These results provide evidence that the uninhibited sample undergoes polymerization through the sonochemical cavitation process, and that MEHQ is required to prevent premature polymerization. These observations are supported by the work of Skinner et al.,[78] which quantified room temperature sonochemical initiation in thiol-ene systems using a radical trap (2,2-diphenyl-1-picryhydrazyl), and showed a radical generation at a rate of 0.62×10^{-4} mol dm^{-3} s^{-1} led to successful thiol-ene reactions even in the absence of a radical initiator. Therefore, MEHQ plays a critical role in the current thiol-ene miniemulsion system to prevent simultaneous occurrence of monomer droplet formation and polymerization – a process that could lead to broad particle size distributions and uncontrolled process parameters. It is also important to note that the inhibitor has a minimal effect on the thiol-ene photopolymerization process. Exposure of the inhibited thiol-ene miniemulsions to UV light results in high monomer conversion (>99%), as indicated by complete disappearance of the peaks associated with the thiol (2567 cm^{-1}) and alkene (3082 cm^{-1}) functional groups in FTIR of the cured samples (see Figure A.1).
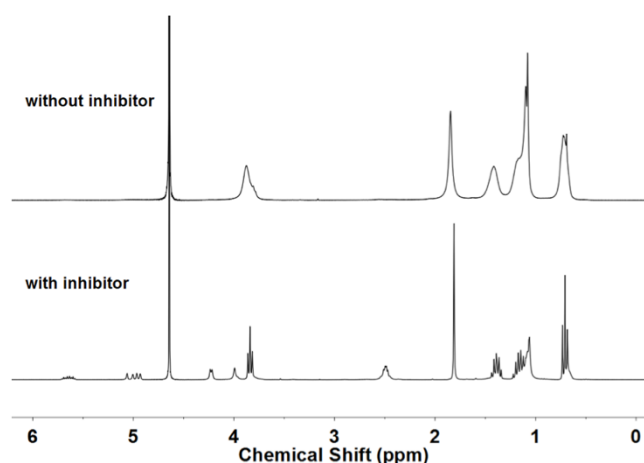
Figure 2.3 Typical ^{1}H NMR spectra of ultrasonicated samples with and without inhibitor.

The stability and size of monomer droplets, and ultimately polymer nanoparticles, obtained from heterogeneous miniemulsion polymerizations are strongly influenced by several process parameters, including surfactant structure and concentration, organic phase volume fraction, and the presence of a costabilizer. To explore the effect of SDS concentration on nanoparticle size, the concentration of SDS was varied from 0 to 40 mM, while keeping the organic fraction and composition constant. As shown in Figure 2.4a, thiol-ene miniemulsions carried out in the absence of SDS provided a mean particle size of 145 nm and a broad, multimodal particle size distribution (PDI: 0.338). With increasing SDS concentration, the mean particle size systematically decreased due to an increase in surfactant interfacial area and a decrease in interfacial tension enabling stabilization of smaller nanodroplets. 20 – 40 mM SDS provided thiol-ene nanoparticles with a mean particle size of 55 nm and relatively narrow particle size distributions (PDI: 0.255). A significant difference in particle size between 20 mM and 40 mM SDS was not observed, thus 20 mM SDS was used in all other formulations. Figure 2.4b shows a representative tapping mode AFM image of thiol-ene nanoparticles obtained by evaporation of a droplet of the photocured miniemulsion (20 mM SDS). As expected, the nanoparticles are spherical in shape and exhibit a ranges of particle sizes that agree with the DLS results.
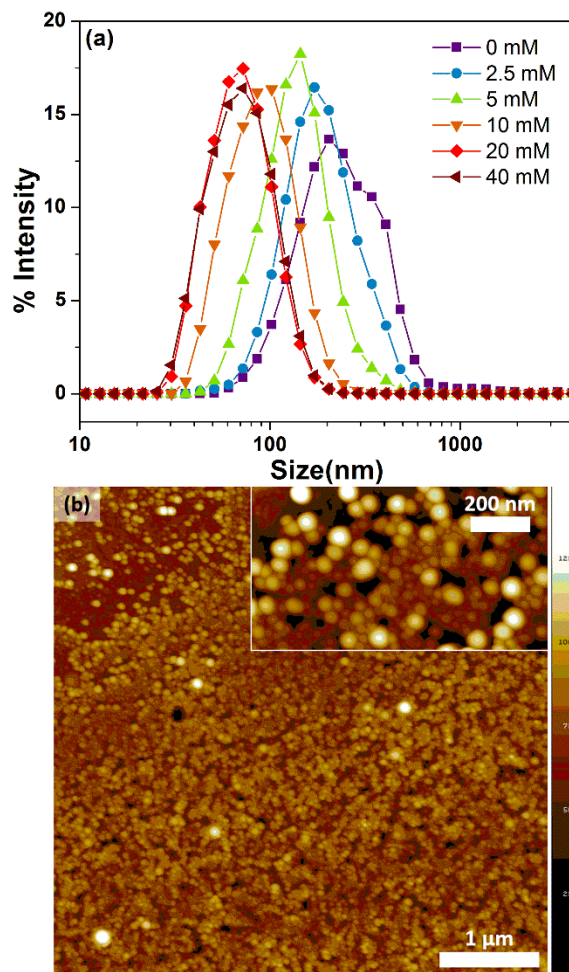
Figure 2.4 (a) Effect of SDS concentration on nanoparticle size distribution. (b) Representative tapping mode AFM image of thiol-ene nanoparticles obtained at 20 mM SDS by evaporation of a droplet of the photocured miniemulsion (Synthetic conditions: 2.5 wt.% organic, 20 min ultrasonication at 10% amplitude, 10 min UV exposure).

The effect of organic weight fraction on the particle size was examined next. For these experiments, the concentration of SDS was kept constant (20 mM), while the organic weight fraction was varied from 0.5 – 5 wt. % relative to the aqueous phase. These conditions also correlate to a varying *SDS:organic* weight ratio from 0.12 – 1.22. The results from these experiments are shown in Figures 2.5a and 2.5b, which relate mean particle size to the organic weight fraction and *SDS:organic* ratio, respectively. Percent transmission and photographs of the minemulsions described above are shown in

Figure A.3. The smallest mean particle size (46 nm) was obtained from a system containing 2.5wt. % organic phase. The corresponding TEM image for the 2.5 wt. % sample shows well-defined thiol-ene nanoparticles with sizes that are in good agreement with values obtained by DLS (see Figure A.2 for lower magnification TEM image). Increasing the organic weight fraction from 2.5 wt. % resulted in an increase in the mean particle size, as shown in Figure 5a. A larger particle size with increasing organic fraction is likely due to depletion of free SDS required to stabilize the smaller nanodroplets.[79] With overall SDS concentration held constant at 20 mM, the SDS:organic ratio, as shown in Figure 5b, decreases with increasing organic fraction enabling droplet coalescence and ultimately larger nanoparticles. Likewise, decreasing the organic weight fraction from 2.5 wt. % resulted in an increase in nanoparticle size (up to 155 nm at 0.5 wt. %). In this case, the *SDS:organic* ratio increases from 0.24 at 2.5 wt. % organic to 1.22 at 0.5 wt. % organic representing an excess of SDS, as shown in Figure 2.5b. Consequently, destabilization and coalescence of small droplets may be caused by attractive forces between multiple nanodroplets in the presence of excess surfactant – a phenomenon that follows a similar mechanism as described in depletion flocculation.[80-81]
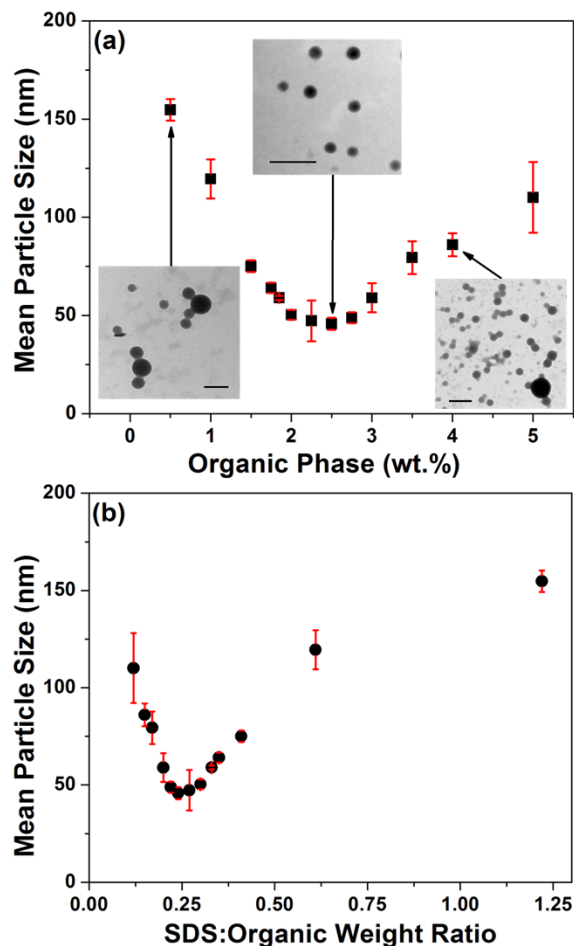
Figure 2.5 Dependence of the nanoparticle size on (a) organic weight fraction and (b) SDS:organic ratio. The (a) insets show representative TEM images of UV cured miniemulsions at various organic weight fractions (scale bar length = 200 nm). (Synthetic conditions: 20 min ultrasonication at 10% amplitude, 10 min UV exposure).

Additionally, excess surfactant can facilitate Ostwald ripening via the diffusion of organic soluble constituents from smaller droplets, across the aqueous phase, into larger droplets. Interestingly, thiol-ene miniemulsions prepared at various organic weight fractions (0.5 – 2.5 wt. %) with constant surfactant to organic ratios also exhibited a decrease in nanoparticle size with increasing organic weight fraction, as shown in Figure 2.6. Such behavior is indicative of a τ_1 mechanism, or an osmotically controlled steady-state droplet size driven by Ostwald ripening – as opposed to a steady-state controlled by

34

collision rates and colloidal stability (τ_2 mechanism).[82] The apparent τ_1 mechanism

observed here may be attributable to the choice of butyl acetate as a solvent for the thiol-

ene monomer phase. The relatively high solubility of butyl acetate in water may promote

exchange of monomers through the aqueous phase *via* Ostwald ripening. This interesting

behavior will require additional investigation; however, we note that interest in such low

(i.e. < 2.5 wt. %) solids content is likely minimal – particularly from nanoparticle yield

viewpoint.
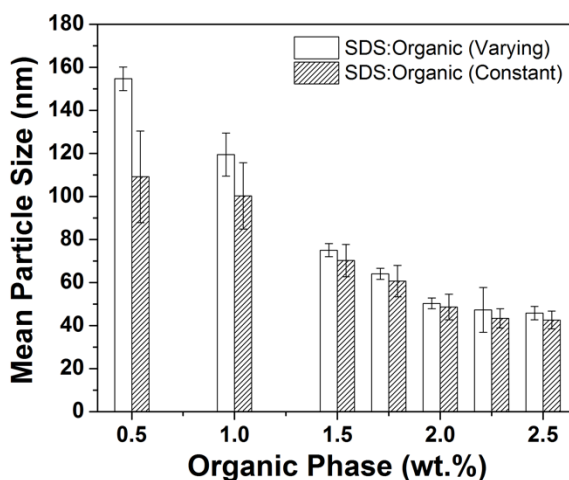
Figure 2.6 Effect of SDS:Organic ratio on mean nanoparticle size. (Synthetic conditions: 20 min ultrasonication at 10% amplitude, 10 min UV exposure).

Figure 2.7 illustrates the importance of the costabilizer – hexadecane – on droplet

stabilization directly following the formation of the miniemulsion *via* ultrasonication,

particularly when employing butyl acetate as a solvent for the monomer phase. Thiol-ene

miniemulsions prepared with and without hexadecane as a costabilizer were allowed to

equilibrate for various times prior to photopolymerization. As shown in Figure 2.7,

samples prepared with hexadecane exhibited a relatively stable mean particle size over a

72 h period, and provided thiol-ene miniemulsions with translucent optical properties

(Figure 2.7, inset). In the absence of hexadecane, the miniemulsions were highly

unstable and resulted in the formation of precipitants that settled to the bottom of the vial

upon cure. For this reason, DLS measurements for samples without hexadecane were not

representative of the full particle distribution and were not included in Figure 2.7. The

"no HD" vial in the Figure 2.7 inset image clearly shows an opaque suspension of thiol-

ene particles. Hexadecane functions to prevent Ostwald ripening by retarding monomer

and solvent diffusion from small droplets to large droplets.
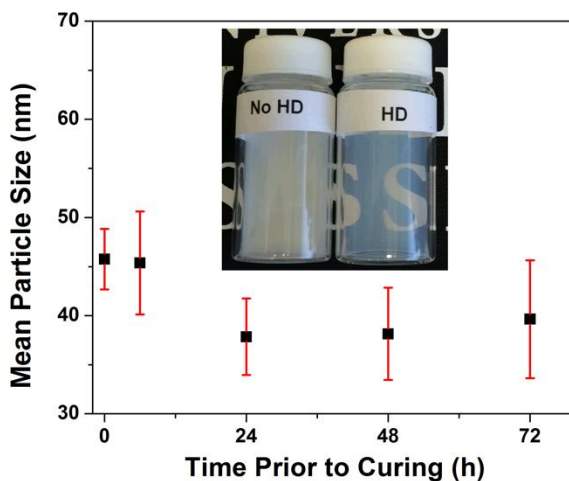
Figure 2.7 Effect on the presence of hexadecane for samples that were ultrasonicated and
then cured after three hours (Synthetic conditions: 20 mM SDS, 2.5 wt.% organic, 20 min
ultrasonication at 10% amplitude, 10 min UV exposure).

In addition to the effect of formulation parameters (i.e. surfactant concentration,

organic fraction, etc.) on nanoparticle size, we also elucidated the evolution of particle

size as a function of processing parameters, such as ultrasonication time and amplitude.

Ultrasonication experiments were carried out on samples with a constant formulation,

namely samples containing 2.5 wt. % organic phase and a constant *SDS:organic* ratio of

0.25. Figure 2.8a shows the evolution of nanoparticle size with ultrasonication time at

10% amplitude for processing times ranging from 5 – 45 minutes. As sonication time

was increased, the particle size decreased from 82 nm at 5 min to 36 nm at 45 min.

Homogenization times beyond 45 min, at constant composition and amplitude, resulted in no further decreases in particle size. It is important to note here that an ice bath was employed to keep the samples cool during the ultrasonication process. For example, the bulk temperature of the reaction media typically showed a 10 °C increase after 20 min of ultrasonication at 10% amplitude. Allowing the miniemulsions to further increase in temperature with extended sonication times resulted in reduced control over particle size and poor repeatability. Figure 2.8b shows the progression of mean particle size after 20 min of ultrasonication at various sonication powers (% amplitude). Similarly to increasing the duration of ultrasonication, it was found that a particle size of 35 nm could be obtained at 20% amplitude in half the time observed for experiments conducted at 10% amplitude. Similar trends were reported by Delamas *et al.*[83] for ultrasonic processing of small miniemulsions, where the equilibrated particle size was found to be dictated only by the total energy input with all other variables held constant. For the current thiol-ene samples, increasing the percent amplitude simultaneously increased the sample temperature (even in an ice bath), which led to larger particle sizes for amplitudes greater than 20%. Thus, for the current sample volume and compositions, 10% amplitude and 20 minutes were chosen as the standard operating conditions to provide less variation between samples.
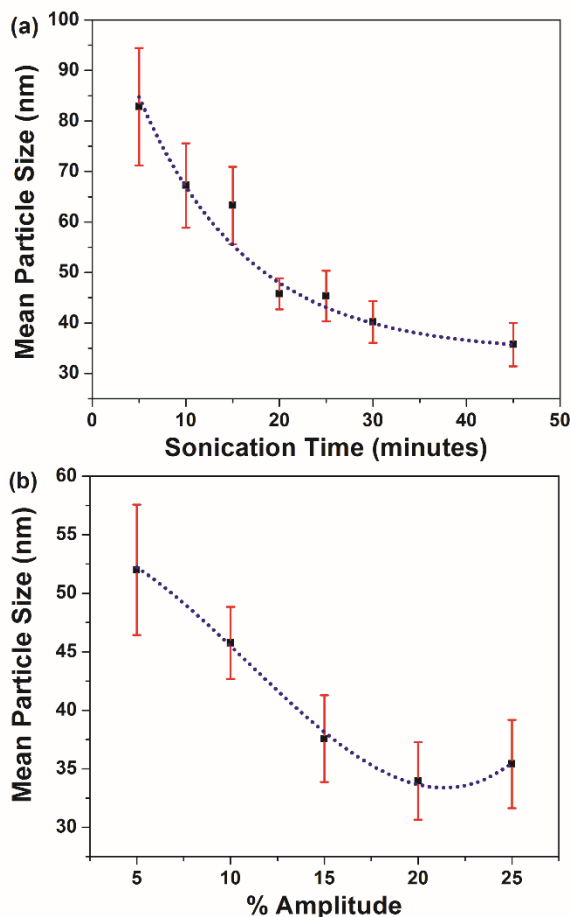
Figure 2.8 Effect of (a) sonication time (at 10% amplitude) and (b) percent amplitude (20 min ultrasonication time) on particle size. The blue dotted lines are not fits to the data and are inserted to guide the reader's eye. (Synthetic conditions: 20 mM SDS, 2.5 wt.% organic, 10 min UV exposure).

A salient feature that arises from the step-growth radical mechanism of thiol-ene photopolymerization is the ability to alter the reaction stoichiometry to achieve thiol-ene networks containing either excess thiol or alkene. The excess functional groups arising from non-stoichiometric photopolymerization conditions are then readily available for subsequent functionalization – an approach that was recently employed by Carlborg *et al.*[84] to fabricate thiol-ene microfluidic devices with functional surfaces. Likewise, Storha *et al.*[85] and Wang *et al.*[75] employed non-stoichiometric thiol-ene conditions to prepare

particles with excess thiol and/or alkene on the surface, which were subsequently

functionalized with fluorescent tags using various thiol-mediated modifications. Here,

we exploit non-stoichiometric ratios of PETMP and TTT – neither of which readily

undergo homopolymerization – to synthesize sub-100 nm thiol-ene nanoparticles with

thiol or alkene functional surfaces in a simple, one-step process (Figure 2.9). Using

similar formulations as previously described, the ratio of thiol to alkene was adjusted to

either 2:1 for thiol functionalized nanoparticles, or 1:2 for alkene functionalized

nanoparticles. These formulations were ultrasonicated to create the miniemulsion and

cured with UV light, as previously described for stoichiometric samples (TEM of non-

stoichiometric nanoparticles shown in Figure A.4). Thiol and alkene functionalized

nanoparticles were analyzed by solution ^{1}H NMR in D_2O to confirm the presence of

excess thiol and alkene available prior to functionalization (see Figure A.5 and Figure

A.6). Likewise, the excess thiol and alkene functional groups were observed by FTIR

(Figure A.1).
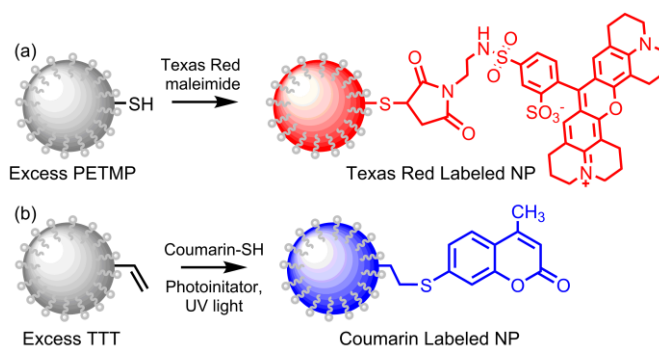
Figure 2.9 Postpolymerization modification of polythioether nanoparticles prepared with stoichiometric excess thiol or excess alkene *via* (a) thiol-Michael addition with Texas Red maleimide and (b) radical-mediated thiol-ene addition with 7-mercapto-4-methylcoumarin.

To demonstrate the simplicity of ligating pendent functional groups to the

nanoparticle surface, nanoparticles presenting excess thiol on the surface were reacted

with Texas Red C2 maleimide *via* thiol-Michael addition, while alkene functionalized

nanoparticles were reacted with 7-mercapto-4-methylcoumarin *via* radical-mediated

thiol-ene addition under UV light (10 min exposure). Nanoparticle dispersions were

purified by multiple centrifugation wash steps following functionalization.
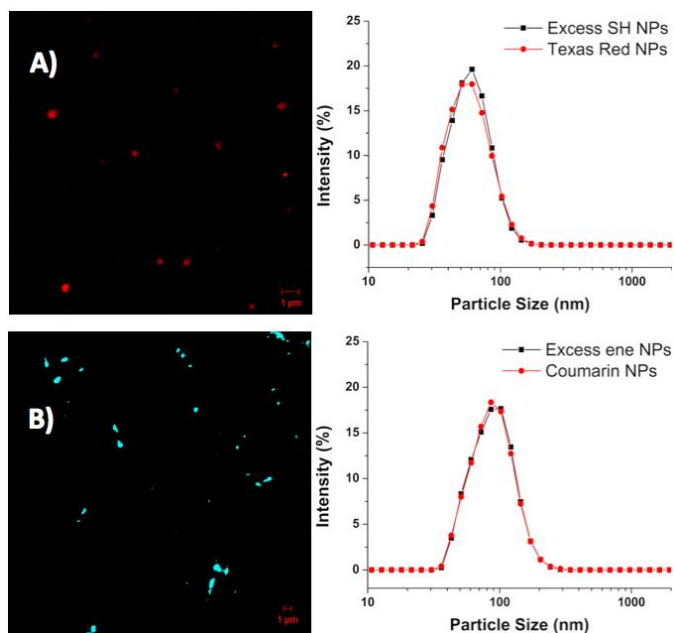
Figure 2.10 Fluorescence microscopy and particle size distributions of post-
functionalized nanoparticles: a) 2:1 thiol:ene functionalized with Texas Red C2
maleimide b) 2:1 ene:thiol functionalized with 7-mercapto-4-methylcoumarin. DLS size
distributions are shown before and after surface functionalization to illustrate the absence
of particle agglomeration during the postmodification step. (Synthetic conditions: 20
mM SDS, 2.5 wt.% organic, 20 min ultrasonication at 10% amplitude, 10 min UV
exposure).

Successful immobilization of both Texas Red and coumarin was confirmed by

fluorescence microscopy, as shown in Figure 2.10A. Importantly, DLS measurements

collected before and after surface functionalization of the nanoparticles showed no

change in particle size or evidence of nanoparticle agglomeration as a result of post-polymerization modification (Figure 2.10B).

2.5 Conclusions

In summary, crosslinked polythioether nanoparticles were prepared by radical-mediated thiol–ene miniemulsion photopolymerization. The effects of formulation (inhibitor, surfactant concentration, monomer weight fraction) and processing parameters (ultrasonication time and amplitude) on nanoparticle size were elucidated, enabling the facile synthesis of thiol-ene nanoparticles with mean particle sizes less than 100 nm. The step-growth nature of thiol-ene photopolymerization was exploited to prepare nanoparticles with thiol or alkene functional surfaces using non-stoichiometric monomer feeds. These thiol and alkene decorated nanoparticles provided a versatile platform for ligation of different functional moieties using thiol-Michael addition and thiol-ene addition, respectively, as simple, one-step postpolymerization modifications. We envision that thiol-ene miniemulsion polymerization can be exploited as a general method for the synthesis of functional polymer nanoparticles for a range of imaging, delivery, analysis, and coatings applications. Our current efforts are focused on extending this synthetic approach to high solid content miniemulsions for more practical nanoparticle yields.

CHAPTER III - FUNCTIONAL, HYBRID POLYTHIOETHER NANOPARTICLES VIA THIOL-ALKYNE PHOTOPOLYMERIZATION IN MINIEMULSION

3.1 Abstract

Thiol-yne photopolymerization in miniemulsion is demonstrated as a simple, rapid, and one-pot synthetic approach to polythioether nanoparticles with tuneable particle size and clickable functionality. The strategy is also useful in the synthesis of composite polymer-inorganic nanoparticles.

3.2 Introduction

Engineered polymer nanoparticles – with sizes ranging from 20-500 nm – are playing an increasingly important role in the advancement of emerging technologies for industrial, agricultural, pharmaceutical, and biological sectors. Exemplary applications of engineered nanoparticles in these areas include improved agricultural production and crop protection,[86] delivery of advanced therapeutics, and bioimaging/biosensing platforms.[87] Emulsion-based processes – such as miniemulsion polymerizations – provide well-studied synthetic routes to polymer nanomaterials. Miniemulsions polymerizations are characterized as aqueous dispersions of small, narrowly distributed monomer droplets stabilized against Ostwald ripening and collisional degradation by

addition of an appropriate surfactant and costabilizer.[63]   Monomer droplets ranging in size from 50-500 nm are achieved by application of high shear mixing – typically either ultrasonic processing or high-pressure homogenization – and subsequently serve as discrete nanoreactors for the formation of polymer nanoparticles.[70]

Recent miniemulsion literature has focused on "click" polyaddition reactions – such as copper-free or copper-catalysed azide-alkyne 1,3-dipolar cycloaddition (CuAAC)[16-17] and thiol-mediated chemistries (i.e. thiol-ene[30, 59, 71-74, 88] and thiol-Michael[89]) – as robust synthetic routes to nanoparticles. Recently, we reported the synthesis of crosslinked polythioether nanoparticles with sub-100 nm diameters *via* thiol-ene photopolymerization in miniemulsion.[88] Additionally, we demonstrated the preparation of nanoparticles with thiol and alkene functional surfaces by exploiting the thiol-ene step polyaddition mechanism under non-stoichiometric monomer feed conditions. The excess thiol and alkene moieties on the nanoparticle surface provided reactive handles for postpolymerization modifications *via* thiol-Michael and thiol-ene ligation reactions, respectively, to yield fluorescent nanoparticles. However, thiol-ene photopolymerization fails to provide direct access to polymer nanoparticles with one of the most commonly exploited functional groups in the "click" chemistry toolbox – i.e. the alkyne moiety.

Thiol-alkyne photopolymerization provides one such platform to access polymer materials exhibiting alkyne functionality.[90-92] Thiol-alkyne proceeds *via* a radical-mediated step-growth mechanism involving the addition of two thiols across the alkyne; the first addition yields a vinyl sulfide intermediate that subsequently reacts with a second equivalent of thiol to give the dithioether adduct (Scheme 1). Thiol-alkyne

photopolymerization proceeds at room temperature, in the presence of oxygen, with rapid reaction kinetics, and yields inherently thiol or alkyne functional materials resulting from the step-growth process – particularly if carried out under non-stoichiometric monomer ratios.[92] However, thiol-yne photopolymerization has rarely been exploited for functional particle-based platforms. DuPrez et al.[93-94] first applied this concept for synthesis of thiol or alkyne-functionalized microbeads (diameters ≈ 400 μm) *via* microfluidics using stoichiometric excess of pentaerythritol tetra(3-mercaptopropionate) (PETMP) or 1,7-octadiyne, and explored the microbeads as resin supports for solid phase synthesis. Aside from DuPrez's microbead work, we are currently unaware of any methodologies reported in literature that exploit thiol-yne photopolymerization for direct synthesis of functional polymer nanoparticles.

Herein, we report thiol-yne photopolymerization in miniemulsion as a simple, rapid, and one-pot synthetic approach to polythioether nanoparticles with tuneable particle size and clickable functionality. We demonstrate the synthesis of nanoparticles with mean particle diameters ranging from 45 nm to 200 nm through simple modifications to the miniemulsion formulation and processing parameters. Facile access to thiol or alkyne functional nanoparticles, and subsequent postpolymerization modifications of these functional moieties using thiol-Michael, thiol-yne, and CuAAC click reactions are reported.

3.3 Experimental

3.3.1 Materials

Hexadecane, 4-p-methoxy phenol, sodium dodecyl sulfate (SDS), 1,7-octadyne, 1-hexyne, 2,2-dimethoxy-2-phenylacetophenone (DMPA), tetrahydrofuran (THF), 7-

mercapto-4-methylcoumarin, sulforhodamine B, silver nitrate (AgNO₃), sodium

borohydride (NaBH4, ≥96% purity), dodecanethiol (DDT, ≥98% purity), ethanol (EtOH,

ACS reagent grade), toluene and butyl acetate (Sigma-Aldrich), pentaerythritol tetra(3-

mercaptopropionate) (PETMP, BrunoBock), 1-hydroxycyclohexyl phenyl ketone

(Irgacure 184, CIBA), 7-methoxy-4-methylcoumarin (TCI, Tokyo, Japan) and Texas

Red® C2 maleimide (Invitrogen) Click-iT® EdU Imaging Kit with Alexa Fluor® 488

azide (Life Technologies™) were obtained at the highest purity available and used

without further purification unless otherwise specified. Trimethylolpropane Tripropargyl

Ether (TMPTPE) was prepared according to a previously reported method.[95]

3.3.2 General Sample Preparation

Each sample was prepared in a 20 mL scintillation vial with a total volume 10

mL. The organic stock solution shown in Table 3.1 was added into the vial containing a

stock solution of SDS and deionized water. The samples were then placed into an ice bath

and sonicated using a Q-700A-110 probe ultrasonicator at 20 % amplitude for 20

minutes.

Table 3.1 General formulation of organic stock solution for thiol-yne

photopolymerization in miniemulsion.

Organic Fraction	Mass (g)	Wt. %
Hexadecane	0.5 (2.2 mmol)	7.32
1,7 Octadiyne	0.5 (4.7 mmol)	7.32
PETMP	2.3 (4.7 mmol)	33.67
Irgacure 184	0.1 (0.49 mmol)	1.46
4-p-methoxy phenol	0.03 (0.24 mmol)	0.44
n-butyl acetate	3.4 (29 mmol)	49.78

The miniemulsions were then cured using an Omnicure S1000-1B with a 100W mercury lamp (λ_{max}=365 nm, 320-500 nm filter) and an intensity of 185 mW/cm^2 for 10 minutes unless noted otherwise. All samples were made in triplicate to ensure reproducible data. To optimize the formulation for small nanoparticles, the organic fraction was varied with a constant SDS concentration of 20 mM.

3.3.3 Preparation of nanoparticles with excess thiol and excess alkyne

Nanoparticles with excess thiol were prepared using a 3.2:1 thiol to alkyne stoichiometry, for example, PETMP (3.68 g, 7.531 mmol) and 1,7-octadiyne (0.50 g, 4.7 mmol). The remaining constituents in the organic formulation from Table 1 were held constant. 250 µL of organic solution was pipetted into 9.75 mL of 20 mM SDS in DI water. The sample was then ultrasonicated for 20 minutes at 10% amplitude and cured under UV light for 10 minutes. Nanoparticles containing excess alkyne were synthesized similarly using a 1.51:1 alkyne to thiol ratio, i.e. 1,7-octadiyne (0.758 g, 7.14 mmol) and PETMP (2.30 g, 4.71 mmol).

3.3.4 Fluorescent tagging of excess thiol nanoparticles

From the nanoparticle suspension (10 mL) with excess thiol prepared in 1.3, 2 mL were removed and placed into a 20 mL scintillation vial wrapped in aluminum foil with a stir bar. A stock solution of Texas Red® C2 maleimide was made by the addition of 10 µL of Texas Red® C2 maleimide to 100 µL of DMSO. 50 µL of the Texas Red® C2 maleimide stock solution was added to the nanoparticles and stirred overnight. The nanoparticle were purified by centrifugation (5 minutes at 13,300 rpm, Fisher Scientific™ accuSpin™ Micro 17 centrifuge) to remove unreacted Texas Red® C2 maleimide. The supernatant was removed and the nanoparticle pellet was re-suspended

in 1 mL DI water. The nanoparticle suspension was then suspended in glycerol on a glass slide and a coverslip was affixed and imaged immediately. The resulting slide was analyzed using a Zeiss LSM 510 confocal laser scanning microscopes.

3.3.5 Fluorescent tagging of excess alkyne nanoparticles *via* 7-mercapto-4-methylcoumarin

From the nanoparticle suspension (10 mL) with excess yne prepared in 1.3, 1 mL was removed and centrifuged for 18 min at 13,300 rpm. The supernatant was removed and the nanoparticle pellet was re-suspended in 1 mL of THF. A solution was prepared containing 21 mg of 7-mercapto-4-methylcoumarin, 30 mg of DMPA and 1 mL of THF was added. The solutions were combined and exposed to UV light for 5 minutes to induce the radical thiol-ene reaction. The solution was centrifuged for 10 minutes, supernatant removed, the pellet re-suspended in THF. The coumarin-functionalized nanoparticle were then cast onto a glass slide with a drop of glycerol and a coverslip for analysis by confocal laser scanning microscopy.

3.3.6 Fluorescent tagging of excess alkyne nanoparticles *via* Alexa Fluor® 488 azide

From the nanoparticle suspension (10 mL) with excess yne prepared in 1.3, 2 mL were removed and placed into a 20 mL scintillation vial wrapped in aluminum foil with a stir bar. The 1X Click-iT® EdU buffer was prepared with 1.0 mL of dH_2O to the Click-iT® EdU vial. To the Alexa Fluor® 488 vial, 100 µL of Click-iT® reaction buffer, 800 µL of $CuSO_4$ solution, and 100 µL of the prepared 1X Click-iT® reaction buffer was added. From this, 500 µL of the reaction cocktail was added to the nanoparticle suspension and allowed to react overnight. The solution was then centrifuged (10 minutes at 13,300 rpm, Fisher Scientific™ accuSpin™ Micro 17 centrifuge), supernatant

removed, nanoparticles resuspended in 1 mL of H_2O and then added to a slide with glycerol. A coverslip was placed on top and was immediately imaged using a Zeiss LSM 510 confocal laser scanning microscope.

3.3.7 Preparation of hydrophobically modified silver nanoparticle

Dodecanthiol capped AgNPs were prepared using a modified procedure.[96] Briefly, a 2.25 mM stock solution of $AgNO_3$ was prepared with 19.11 mg $AgNO_3$ in 50 mL of EtOH. A second 69.4 mM solution of $NaBH_4$ was prepared with 0.2625 g in 100 mL of EtOH. Into a 20 mL scintillation vial, 14 mL of $NaBH_4$ stock with 25.7 µL of DDT with a magnetic stirbar. The solution was stirred and in one continuous addition, 4 mL of $AgNO_3$ stock was added, upon which the solution immediately turned yellow and gradually turned dark brown. The solution was centrifuged at 8500 rpm for 12 minutes, supernatant removed, 20 mL EtOH added three times. The final solution was resuspended in varying amounts of either toluene or butyl acetate to adjust the concentration of AgNPs.

3.3.8 Preparation of composite Ag nanoparticles

Each sample was prepared by mixing 250 µL of the 2:1 SH:yne octadiyne formulation with 50 µL of AgNPs (3% wt AgNP solution in butyl acetate). The solution was pipetted up and down to ensure mixing, upon which 250 µL was dispersed in a solution of SDS and deionized water. The samples were placed into an ice bath and were sonicated using a Q-700A-110 probe ultrasonicator at 20 % amplitude for 20 minutes. The miniemulsions were then cured using an Omnicure S1000-1B with a 100W mercury lamp (λ_{max}=365 nm, 320-500 nm filter) and an intensity of 185 mW/cm^2 for 10 minutes.

3.3.9 Characterization

The size and distribution of the nanoparticles were measured by dynamic light scattering (DLS) using a Microtrac Nanotrac Ultra NPA150. Transmission electron micrographs (Digital Imaging with Gatan Model 785 ES1000W Erlangshen CCD Camera) were taken with a Zeiss 900 TEM operating at 50keV and a JEOL JEM-2100 TEM operating at 200 keV. Samples were applied to 200 mesh copper grids (3.05 mm, 200 lines/inch square mesh, EMS Cat. #G200-Cu) coated with Formvar (5% polyvinyl formal resin). UV-vis measurements were performed on a Perkin-Elmer Lambda 6 UV/Vis spectrophotometer with quartz cuvettes. Atomic force microscopy was performed using a Bruker Icon in tapping mode. The samples were imaged with T300R-25 probes (Bruker AFM Probes) with a spring constant of 40 Nm-1. The samples then stained using OsO4. ^{1}H NMR was recorded on a Varian Mercury Plus 300 MHz NMR in D_2O. Samples for DSC analysis were prepared by placing 5–8 mg of freeze-dried cured nanoparticles into an aluminum hermetic DSC pan. Thermal history was erased before running DSC traces as samples were cooled to -50 ℃ and heated to 100 ℃ at 5 ℃/min. Samples were then cooled to -50 ℃ at 10 ℃/min and then heated at a rate of 5 ℃/min to 200 ℃. All DSC tests were run on a TA Instruments Q200 differential scanning calorimeter.

3.4 Results and Discussion

As shown in Scheme 3.1, thiol-alkyne miniemulsions were prepared from combinations of pentaerythritol tetra(3-mercaptopropionate) with three different alkyne monomers, including 1-hexyne, 1,7-octadiyne, and trimethylolpropane tripropargyl ether (TMPTPE) to provide polythioether nanoparticles with a range of thermal properties. Hexadecane, Irgacure 184® (1-hydroxycyclohexyl phenyl ketone), 4-methoxyphenol, and

butyl acetate (BA) served as the hydrophobe, photoinitiator, radical inhibitor, and organic

diluent, respectively.   The organic-soluble constituents were dispersed into the aqueous

continuous phase containing sodium dodecylsulfate (SDS) as a surfactant using ultrasonic

emulsification.   Exposure of these thiol-yne miniemulsions to UV light resulted in

complete conversion of the thiol and alkyne functional groups, as indicated by the absence

of peaks at 2567 cm^{-1} and 3285 cm^{-1} in FTIR (Fig. S1).
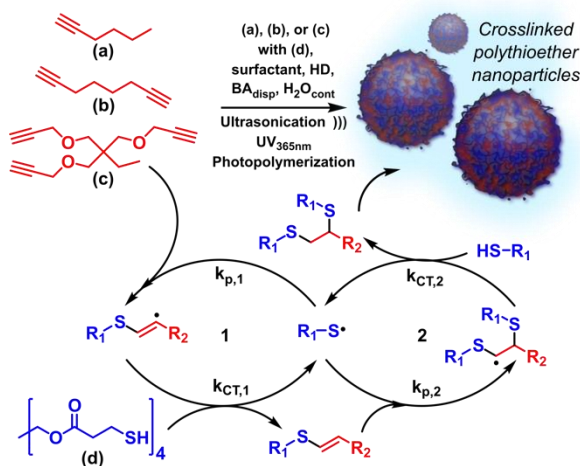
Scheme 3.1 (a-d) Various multifunctional alkynes and thiols used to generate
polythioether nanoparticles via thiol-alkyne photopolymerization in miniemulsion.
Thiol-yne involves sequential addition and hydrogen abstraction steps of primary alkynes
(1) and subsequent vinyl sulfides (2) to generate crosslinked nanoparticles.

The size of the dispersed monomer droplets, and consequently the size of the

polymer nanoparticles obtained following photopolymerization, depends on a number of

parameters including surfactant concentration, monomer weight fraction, and total

ultrasonic energy input. These parameters were explored thoroughly in our recent thiol-

ene miniemulsion work; here, we report thiol-yne nanoparticle synthesis under optimized

conditions. Figure 1 shows how nanoparticle size depends on the monomer phase weight

fraction in a miniemulsion formulation containing a fixed amount of surfactant (20 mM

SDS). Hexyne, octadiyne, and TMPTPE, when paired with PETMP, all exhibited a minimum particle size of 40 – 75 nm between 2 and 3 wt.% monomer phase – a result that can be attributed to an optimum surface coverage of SDS necessary to stabilize the equilibrium droplet size under these specific conditions. An increase in monomer phase loading depletes SDS coverage enabling droplet coalescence, whereas a decrease in monomer phase loading provides excess SDS that can facilitate Ostwald ripening *via* the diffusion of organic soluble constituents from smaller droplets, across the aqueous phase, into larger droplets. Both of these conditions result in larger nanoparticles, as shown by the u-shaped data in Figure 1a. Nonetheless, low polydispersity values were observed across the monomer loading range, from 0.260 for 2.5 wt.% to 0.467 for 5 wt.%, as illustrated by the DLS distribution curves in Figure 1b.
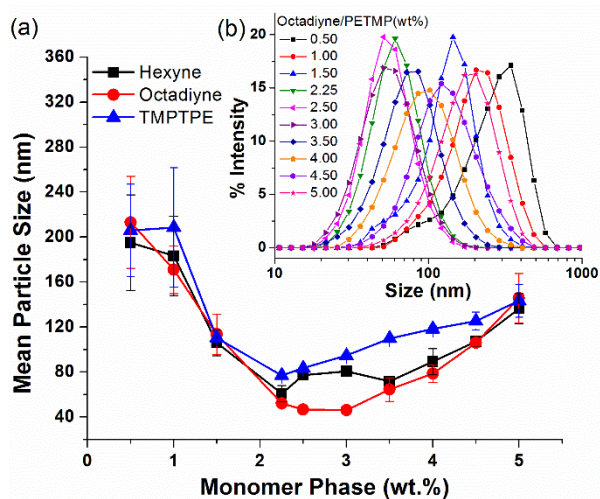
Figure 3.1 (a) Effect of weight fraction of the organic monomer phase on the results particle size and distribution. (b) Inset shows nanoparticle size distribution curves obtained by dynamic light scattering.

The thermal properties of the nanoparticles were analysed by differential scanning calorimetry (DSC). As shown in Fig. S2, hexyne-PETMP nanoparticles exhibited the lowest glass transition temperature (T_g) at -32.5 °C – a result attributed to a low crosslink

density obtained from the monofunctional alkyne. As expected, increasing the functionality of the alkyne to difunctional or trifunctional by employing either 1,7-octadiyne or TMPTPE, respectively, provided nanoparticles with higher T_g. The 1,7-octadiyne based nanoparticles showed a T_g at 45.7 °C, while TMPTPE based nanoparticles showed a T_g at 47.3 °C (Fig. S2). These results are consistent with an expected increase in T_g with an increase in network crosslink density at higher alkyne functionality.

Particle morphology was characterized using atomic force microscopy (AFM) and transmission electron microscopy (TEM). All samples showed particle sizes in good agreement with data obtained by dynamic light scattering. For the hexyne-PETMP monomer pair (Fig. 2a), the particles exhibited an ill-defined spherical morphology with a strong tendency to aggregate upon drying for analysis. We attribute this behaviour to a low crosslink density resulting from the hexyne-PETMP constituents, and consequently a low T_g as confirmed by DSC. The low T_g of these nanoparticles confers tackiness and leads to agglomeration of the particles. However, both the 1,7-octadiyne-PEMTP and TMPTPE-PETMP monomer pairs provide nanoparticles with well-defined spherical morphologies that are stable against aggregation upon drying, and can be re-dispersed into aqueous solution. The stability of these nanoparticles can be attributed to the higher glass transition temperature, as discussed previously.
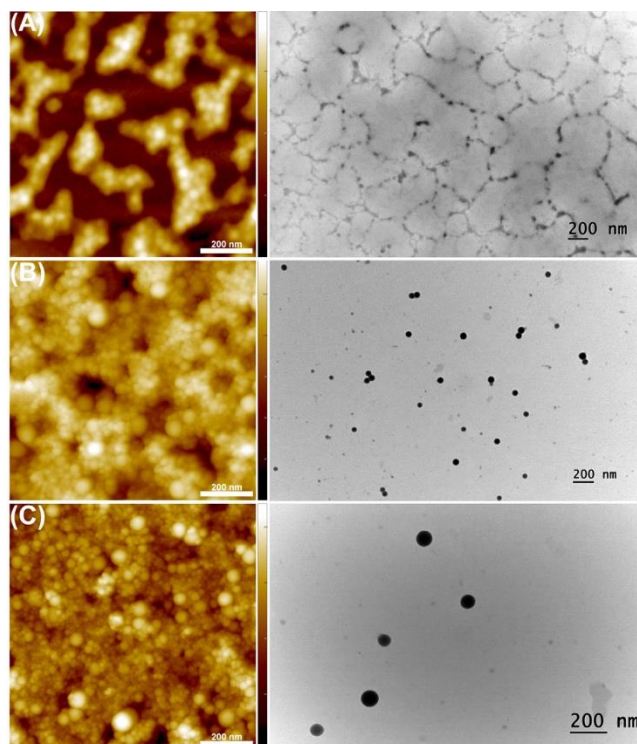
Figure 3.2 AFM and TEM images corresponding to (A) hexyne-PETMP, (B) 1,7-octadiyne-PETMP, and (C) TMPTPE-PETMP particles.

Miniemulsion polymerization offers a versatile approach to synthesize composite inorganic-organic nanoparticles *via* encapsulation inorganic materials to endow properties such as magnetism, antimicrobial activity, and fluorescence.[71, 97-99] However, surprisingly few examples have been reported that exploit the rapid nature of photopolymerization to prepare hybrid nanoparticles.[100] Here, we demonstrate thiol-yne photopolymerization as a rapid two-step synthetic approach to prepare silver/polythioether nanoparticles. First, hydrophobically modified AgNPs were prepared *via* sodium borohydride reduction of silver citrate in the presence of dodecanethiol yielding 9 ± 3 nm AgNPs with a $\lambda_{max} = 435$ nm (Fig. S3 and S4).[96] After purification, the AgNPs were dispersed in BA and combined with the thiol-alkyne monomer formulation. The reaction mixture was then ultrasonicated in the presence of water and SDS, and

polymerized with ultraviolet light for 20 min to yield composite Ag/polythioether

nanoparticles. Typical thermal polymerization routes require 4 – 24 h reaction time.[98-99]

TEM analysis revealed well-defined core-shell particle morphologies with AgNPs strictly

confined within the core of the polythioether nanoparticles (Fig. 3a). Image analysis

carried out on a population of nanoparticles imaged at 50 keV revealed an average

composite diameter of 127 ± 8 nm, an average 68 ± 6 nm AgNP core, and a clearly

defined polythioether shell of ~ 30 nm. TEM images collected at 200 keV showed the

inorganic core was comprised of individual AgNPs (Fig. 3b). It is noteworthy that

relatively few "empty" polythioether nanoparticles (i.e. devoid of AgNPs in the core) or

unencapsulated AgNPs were observed in the TEM images surveyed – an observation

indicative of a high encapsulation efficiency that minimizes the need for subsequent

purification protocols.
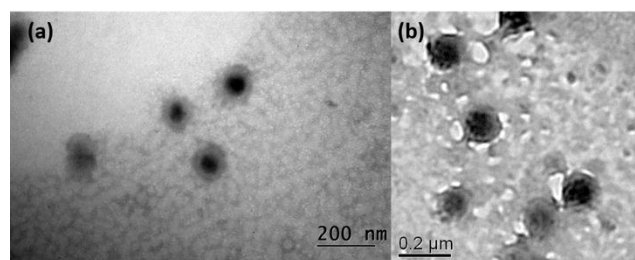
Figure 3.3 Representative TEM micrographs of composite polythioether–silver
nanoparticles collected at (a) 50keV and (b) 200 keV, showing clusters of 9 nm AgNPs
encapsulated within 1,7-octadiyne-PETMP nanoparticles.

        To take full advantage of the step polyaddition nature of thiol-yne

photopolymerization, different stoichiometries of thiol (SH) and alkyne were reacted

within the miniemulsions to prepare thiol or alkyne functionalized polymer nanoparticles.

The ratios of SH to alkyne were adjusted from 1.5:1 and 3.2:1, and the resulting

nanoparticles were analysed *via* FTIR (Fig. S1). Nanoparticles prepared from the

monomer feed with excess SH (3.2:1 SH:yne) showed the presence of residual thiol

functionality at 2567 cm^{-1}. Conversely, nanoparticles resulting from the monomer feed

with excess yne (1.5:1, SH:yne) showed a strong alkyne absorption at 3285 cm^{-1}. The

preservation of the excess thiol and alkyne functionality provided a convenient strategy

for postpolymerization modification of the nanoparticle surface using various click

reactions. As illustrated in Scheme 2, thiol-yne, thiol-Michael, and CuAAC reactions

were employed to ligate a series of fluorescent dyes to the nanoparticle surface. To the

thiol-functionalized nanoparticles (3.2:1 SH:yne), Texas Red maleimide was attached

using a thiol-Michael click reaction (Scheme 2a). Following purification by repetitive

centrifugation/wash steps, nanoparticles with red fluorescence were confirmed by

confocal microscopy (λ_{em} 615 nm, Fig. 4a).
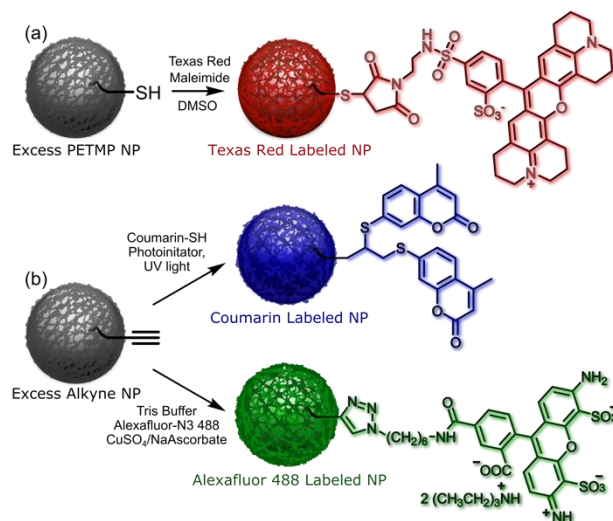
Scheme 3.2 (a) Thiol-functional polythioether nanoparticles prepared with excess
PETMP and postmodified *via* thiol-Michael with Texas Red maleimide. (b) Alkyne-
functional polythioether nanoparticles prepared with excess 1,7-octadiyne postmodified
with 7-mercapto-4-methylcoumarin *via* thiol-yne or with Alexa Fluor® 488 azide *via*
CuAAC.

The alkyne-functionalized nanoparticles were tagged with fluorescent dyes *via* two routes. First, 7-mercapto-4-methylcoumarin was immobilized using a photoinitiated thiol-yne reaction in the presence of 2,2-dimethoxy-2-phenylacetophenone to afford nanoparticles that fluoresce blue (λ_{em} 385 nm), as shown by confocal microscopy in Fig. 4b. Lastly, the CuAAC click reaction between Alexa Fluor® 488 azide and the alkyne-functionalized nanoparticles resulted in fluorescently tagged nanoparticles with green emission (λ_{em} 385 nm, Fig. 4c). Control experiments were also carried out under the same conditions using non-reactive dyes to show physisorption plays no role in immobilization of the fluorescent tags (Fig. S5). This two-step process of generating functional nanoparticles and subsequent functionalization through high efficiency reactions simplifies current multi-synthetic processes while also expanding the library of functional groups that can react with these particles.
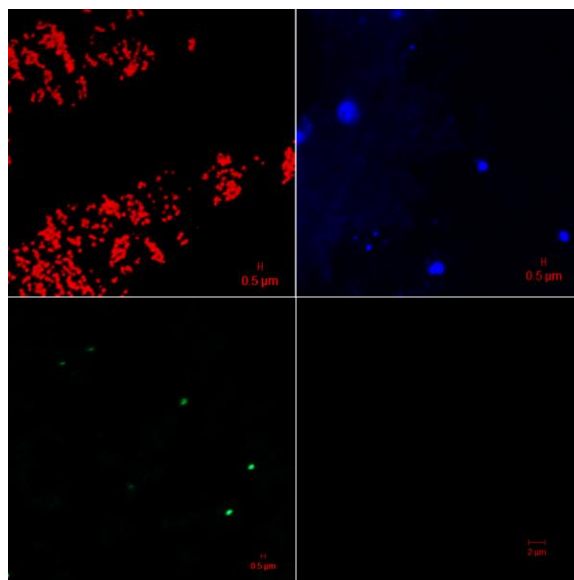
Figure 3.4 Fluorescence microscopy of (a) thiol-functional nanoparticles postmodified with Texas Red maleimide using a thiol-Michael reaction, (b) alkyne-functional nanoparticles postmodified by photoinitiated thiol-yne with 7-mercapto-4-methylcoumarin, and (c) alkyne-functional nanoparticles postmodified by CuAAC with Alexa Fluor® 488 azide. (d) shows exemplary control experiment with non-reactive dyes.

3.5 Conclusions

In conclusion, we have demonstrated the versatility of thiol-alkyne photopolymerization in miniemulsion for the preparation of polythioether nanoparticles. Simple off-stoichiometric monomer feed ratios provided access to functional nanoparticles that express thiol and alkyne moieties at the nanoparticle surface – and these moieties are readily available for postpolymerization modification using various click chemistries. We also demonstrated thiol-yne photopolymerization in miniemulsion as a means to synthesize hybrid silver/polythioether nanoparticles with defined core-shell morphologies; this approach provides hybrid nanoparticles in a fraction of time (20 min) as compared with previously reported thermally-initiated routes (4-24 h). We anticipate that thiol-yne miniemulsions

will provide facile access to a functional and hybrid nanoparticle platform with antimicrobial, delivery, and imaging applications.

CHAPTER IV – FUNCTIONAL MICROCAPSULES VIA THIOL-ENE

PHOTOPOLYMERIZATION IN DROPLET-BASED MICROFLUIDICS

4.1 Abstract

Thiol-ene chemistry was exploited in droplet-based microfluidics to fabricate advanced microcapsules with tunable encapsulation, degradation, and thermal properties. In addition, by utilizing the thiol-ene photopolymerization with tunable crosslink density, we demonstrate the importance of monomer conversion on the retention of omniphilic cargo in double emulsion templated microcapsules. Furthermore, we highlight the rapid cure kinetics afforded by thiol-ene chemistry in a continuous flow photopatterning device for hemispherical microparticle production.

4.2 Introduction

Microcapsules hold great potential for applications involving the encapsulation, delivery, and release of actives in the fields of agriculture,[101] home care,[102] drug delivery,[103] and cosmetics,[104] with some commercial applications already in place. A variety of techniques, such as interfacial polymerization, complex coacervation, sol-gel encapsulation, and spray-drying have been used for the preparation of functional microcapsules.[105] However, the size, shell thickness, and composition of the microcapsules obtained from these techniques vary significantly, limiting the usage of

capsule technologies in many practical (or advanced) applications. Droplet-based microfluidics can overcome limitations associated with variability during microcapsule production by the precise control of multi-phasic flows, leading to highly monodisperse multiple emulsion drops with fine-tunable size, morphologies, and compositions of each compartment; these emulsion drops have been utilized as templates to prepare functional microcapsules in which the chemical compositions of polymeric shells, shell thicknesses, and volume ratios of encapsulant to membrane can be fine-tuned.[106] Traditionally, the polymeric shells in these emulsion-templated microcapsules[107-108] are obtained by dissolving a polymer in a volatile solvent and allowing for solidification,[109] through dewetting of a cosolvent to form polymersome shells from amphiphilic polymers,[110] or direct photopolymerization of monomers.[111] Capsule shells fabricated from solvent approaches typically result in a non-homogeneous structure during solidification; this leads to the undesired formation of small defects, and consequently, to loss of encapsulated active. By contrast, defect-free shell structures can be achieved by photopolymerization of monomers.[112] While a wide variety of materials have been examined for microparticle fabrication *via* photopolymerization, (i.e. methacrylates, acrylates, and crosslinkable poly(dimethyl siloxane) (PDMS)), many have intrinsic drawbacks. Methacrylates and acrylates suffer from inhibition of the polymerization by oxygen,[113] polymerization induced stress development,[114] incomplete reaction during curing,[65, 115] and most importantly, the formation of highly heterogeneous polymer networks.[116] PDMS is capable of efficient photopolymerization but exhibits poor mechanical properties and poor solvent resistance leading to premature leakage of small actives that are highly diffusive.[117] Thus, there remains an unmet need for a new tunable

material platform for emulsion-based microcapsules that is photocurable, insensitive to oxygen, inexpensive, and modular in nature; this platform should possess tunable thermal-mechanical and chemical functionality, with simple processing conditions, in order to expand the range of possible applications.

Thiol-ene photopolymerization – a robust, radical-mediated step polyaddition process – offers a promising route for synthesis of microcapsules possessing the aforementioned properties;[118-119] however, previous reports of thiol-ene in microfluidics have primarily focused on the synthesis of solid microparticles.[94] Multifunctional thiol and alkene monomers – a large number of which are commercially available – offer unparalleled control of thermal-mechanical properties, crosslink density, and incorporation of orthogonal chemistries while providing rapid polymerization kinetics without the oxygen inhibition typically associated with other radical based polymerizations.[118] Additionally, the onset of gelation during polymerization occurs at high conversion facilitating low polymerization induced shrinkage and uniform network architecture.[120]

In this paper, we describe a microfluidic approach for fabricating functional microcapsules via thiol-ene photopolymerization that show enhanced retention of an encapsulated model small active (fluorescein) that was previously shown to be highly permeable.[121] By inserting degradable anhydride monomers into the thiol-ene backbone, we demonstrate tailored release kinetics from a homogenous degradable network, which reflects the recent Microbead-Free Waters Act of 2015,[122] where all non-degradable plastic particles less than 5 mm are to be banned from sale in the United States.[122] We also show that thiol-ene microcapsules can be oxidized to enhance the thermal-

61

mechanical properties. Furthermore, we highlight the rapid cure kinetics afforded by thiol-ene chemistry in a continuous flow photopatterning device for hemispherical microparticle production.

4.3 Experimental

4.3.1 Materials

Thiol-ene monomers used for the microcapsule shells and microparticles, trimethylolpropane tris(3-mercaptopropionate) (TMPTMP, Sigma-Aldrich, MW = 398.56 g mol^{-1}), tri(ethylene glycol) divinyl ether (TEGDVE, Sigma-Aldrich, MW = 202.25 g mol^{-1}), triallyl-1,3,5-triazine-2,4,6-(1H,3H,5H)-trione (TTT, Sigma-Aldrich, MW = 249.27 g mol^{-1}) and 4-pentenoic anhydride (PA, Sigma-Aldrich, MW = 182.22 g mol^{-1}) were used as received without further purification. Poly(vinyl alcohol) (PVA, Mw = 13 - 23 000 g mol^{-1}, 87-89% hydrolyzed), photoinitiator (2-hydroxy-2-methylpropiophenone), n-octadecyltrimethoxy silane, 1,3-Dihydro-1,3,3-trimethylspiro[2H-indole-2,3'-[3H]naphth[2,1-b][1,4]oxazine] (Photorome I), fluorescein (green fluorescent dye), and sulforhodamine B (red fluorescent dye) were purchased from Sigma-Aldrich and 2-[methoxy(polyethyleneoxy)propyl] trimethoxy silane was purchased from Gelest. Distilled water (>18.2 MΩ•m, Millipore) (DI water) were used for all experiments.

4.3.2 Characterization Methods.

A Bruker Ascend 600 MHz (TopSpin 3.5) spectrometer was used to record ^{1}H/^{13}C NMR spectra with either chloroform-d or acetonitrile-d_3. High resolution mass spectroscopy (HRMS) was performed with positive electrospray ionization on a Bruker 12 Tesla APEX-Qe FTICR-MS with an Apollo II ion source. Dynamic mechanical analysis (DMA) was performed using a TA Instruments Q800 dynamic mechanical

analyzer in tension mode equipped with a gas cooling accessory. Samples were clamped, evaluated at a strain of 1 %, and heated from -80 °C to 80 °C at a ramp rate of 3 °C min^{-1}. Kinetic data was obtained using real-time FTIR (RT-FTIR) spectroscopy by determining the conversions of the thiol and ene functional groups. The RT-FTIR studies were conducted using a Nicolet 8700 FTIR spectrometer with a KBr beam splitter and a MCT/A detector with a 320–500 nm filtered ultraviolet light source. Each sample was exposed to a UV light with an intensity of 400 mW cm^{-2}. Series scans were recorded, where spectra were taken approximately 2 scan s^{-1} with a resolution of 4 cm^{-1}. Thiol conversion was monitored via integration of the SH peak between 2500-2620 cm^{-1} while the conversion of the alkene was monitored between 3050-3125 cm^{-1}. Optical density (OD) and fluorescence readings were performed in a BioTek Synergy 2 programmable microplate reader (BioTek Instruments).

4.3.3 Fabrication of a microfluidic device and its operation

Two cylindrical glass capillaries (World precision Instruments) of inner and outer diameters 0.58 mm and 1.00 mm were tapered to a diameter of 40 µm with a micropipette puller (P-97, Sutter Instrument). One of the cylindrical capillaries, the injection capillary, was grinded to final inner diameter of 70 µm. This tapered injection capillary was hydrophobically modified by dipping into n-octadecyltrimethoxy silane for 20 min and subsequently drying with compressed air. The resulting injection capillary was inserted into a square capillary whose inner diameter (1.05 mm) is slightly larger than that of the outer diameter of the injection capillary (1 mm). Next, a small tapered glass capillary was prepared manually by heating and pulling a cylindrical capillary using a gas torch; this capillary was inserted into the injection capillary for the injection of an

aqueous phase that forms the innermost drop of the double emulsions. Finally, the other tapered cylindrical collection capillary was grinded to final inner diameter of 400 µm and was inserted into the square capillary from the other end; we treat this collection capillary with 2-[methoxy(polyethyleneoxy)propyl] trimethoxy silane to make the wall hydrophilic prior to the assembly. During drop generation, the volumetric flow rate was controlled using syringe pumps (Harvard Apparatus). The production of thiol-ene double emulsion drops within the microfluidic devices was recorded using an inverted microscope (Leica) equipped with a high-speed camera (Phantom V9).

4.3.4 Fabrication of microcapsules from double emulsion drops

The thiol-ene monomer comprising the emulsion drops were polymerized by UV exposure (Omnicure S1000) at the exit of the capillary device to produce microcapsules. We note that thiol-ene monomers contain 2.5 wt% of photoinitiator, 2-hydroxy-2-methylpropiophenone. For photo-patterned microparticles, 0.3 wt% of Photorome I was added.

4.3.5 Confocal Microscopy

The optical and fluorescence images of the microcapsules with different monomer conversion of the thiol-ene shell encapsulating both fluorescein (green dye) and sulforhodamine B (red dye) as well as the degradable microcapsules encapsulating sulforhodamine B were taken with a Leica TCS SP5 confocal laser scanning microscope, using a 10X dry objective with NA = 0.3.

4.3.6 Fourier Transform – Infrared spectroscopy (FT-IR)

The data was collected using a Bruker Lumos FTIR microscope with a liquid nitrogen cooled MCT detector using 64 scans in ATR mode with a single bounce Ge ATR crystal.

To avoid any background absorption from PVA, the microcapsule samples were prepared without any surfactant in the innermost aqueous phase and rigorously rinsed with DI water to remove any PVA adsorbed at the exterior of the capsule shell prior to measurement.

4.3.7 Scanning electron microscopy (SEM)

Microcapsules were cut open for cross-sectional imaging and sputter-coated with 2 nm Platinum-Palladium (80:20) prior to imaging. Images were obtained on a Zeiss Ultra Plus Field Emission Scanning Electron Microscope (FESEM) using an acceleration voltage of 3 kV and an InLense detector.

4.4 Results and Discussion

To fabricate thiol-ene double emulsion drops, we use a glass capillary microfluidic device containing two tapered cylindrical glass capillaries – one for the injection, and the other for collection as shown in Figure 1a. Briefly, the tapered capillaries are aligned by insertion within a square capillary whose inner diameter is slightly larger than the outer diameter of the cylindrical capillaries. The injection capillary is treated with n-octadecyltrimethoxy silane to modify the surface hydrophobic and the collection capillary is treated with 2-[methoxy(polyethyleneoxy)propyl] trimethoxy silane to make it hydrophilic. Additionally, a small cylindrical capillary is inserted into the injection capillary for the injection of an aqueous phase that forms the innermost drop of the double emulsions.
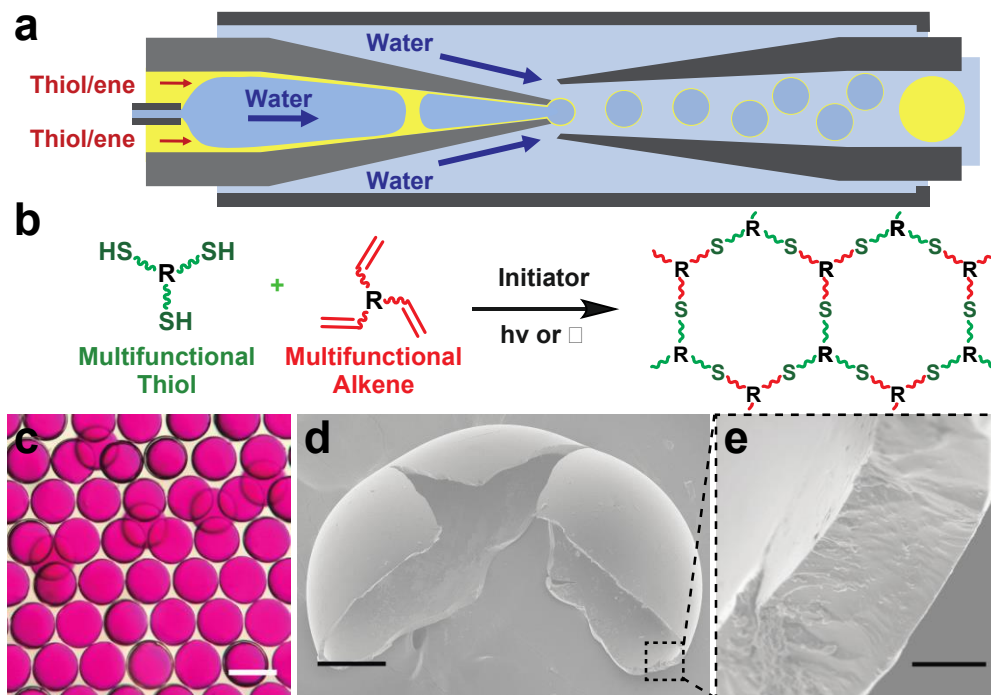
Figure 4.1 Production of thin-shell thiol-ene microcapsules. a) Glass capillary microfluidic device for preparation of thin-shell thiol-ene double emulsion drops. b) General scheme for the production of uniform thiol-ene networks. c) Optical microscope images of monodisperse double emulsion drops produced; flows rates of the innermost aqueous phase (Q_I), middle thiol-ene monomer phase (Q_M) and outer aqueous phase (Q_O) were set at 500, 1000, 10 000 µL h^{-1}, respectively. Scale bar represents 300 µm. d-e) Scanning electron microscope (SEM) images of dried microcapsules composed of TTT:TMPTMP at d) low magnification (scale bar 100 µm) and at e) higher magnification (scale bar 5 µm).

The photocurable thiol-ene resin consisting of the thiol trimethylolpropane tris(3-mercaptopropionate) (TMPTMP) and either tri(ethylene glycol) divinyl ether (TEGDVE), triallyl-1,3,5-triazine-2,4,6-(1H,3H,5H)-trione (TTT), or 4-pentenoic anhydride (PA) pairs shown in Scheme 1, is interjected through the injection capillary. The hydrophobic treatment of the injection capillary facilitates plug-like flow with preferential wetting of the thiol-ene resin around the capillary. We inject an aqueous surfactant solution as the continuous phase through the interstitial space between the square and collection capillaries. The plug-like stream of encapsulated drops from the injection capillary break

66

up into monodisperse double emulsion drops with a thin thiol-ene layer by shearing of the aqueous continuous phase. The resulting drops then flow through the collection capillary and are photocured with UV light (Figure 1b) to yield thin-shell microcapsules as shown in the optical microscope image of Figure 1c. The resulting microcapsules are 300 µm in diameter (Figure 1d) with a shell thickness of approximately 8 µm as shown in the scanning electron microscope images of Figure 1d and 1e. Based on the volume ratio of core to microparticle, the loading capacity of the aqueous encapsulant phase is estimated to be around 85 %.
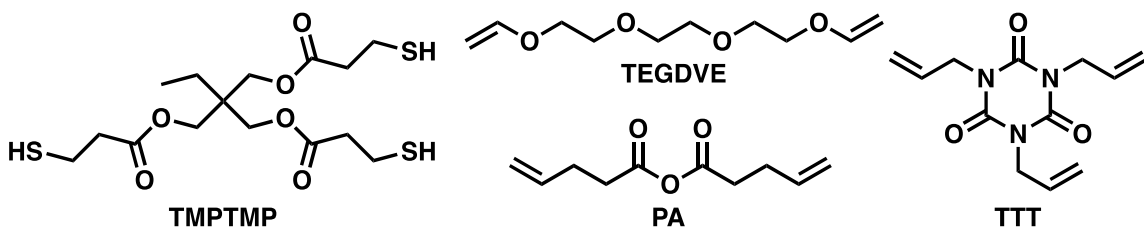
Scheme 4.1 Chemical structures of the monomers employed for thiol-ene microcapsules and microparticles.

The ability to produce a highly impermeable, yet homogenous membrane with thiol-ene photopolymerization offers new opportunities for encapsulation and retention of small molecules in polymer microcapsules. To validate this capability, we prepared double emulsion microcapsules with different monomer conversion of the thiol-ene shell (TTT-TMPTMP, 1;1 SH:ene ratio) while encapsulating both fluorescein (green dye) and sulforhodamine B (red dye) as representative small actives as shown in Figure 2a. These two dyes exhibit different octanol/water partition coefficients (log $P_{oct/wat}$); sulforhodamine B (hydrophilic, log $P_{oct/wat} = -2.02$),[123] and fluorescein (omniphilic, log $P_{oct/wat} = 0.34$).[124] Among these two model molecules, fluorescein was previously shown to completely leak within 24 h from double emulsion microcapsules with

photopolymerizable acrylate shells without the additional reinforcement of fluorocarbon oil within the polymerized shell.[121]
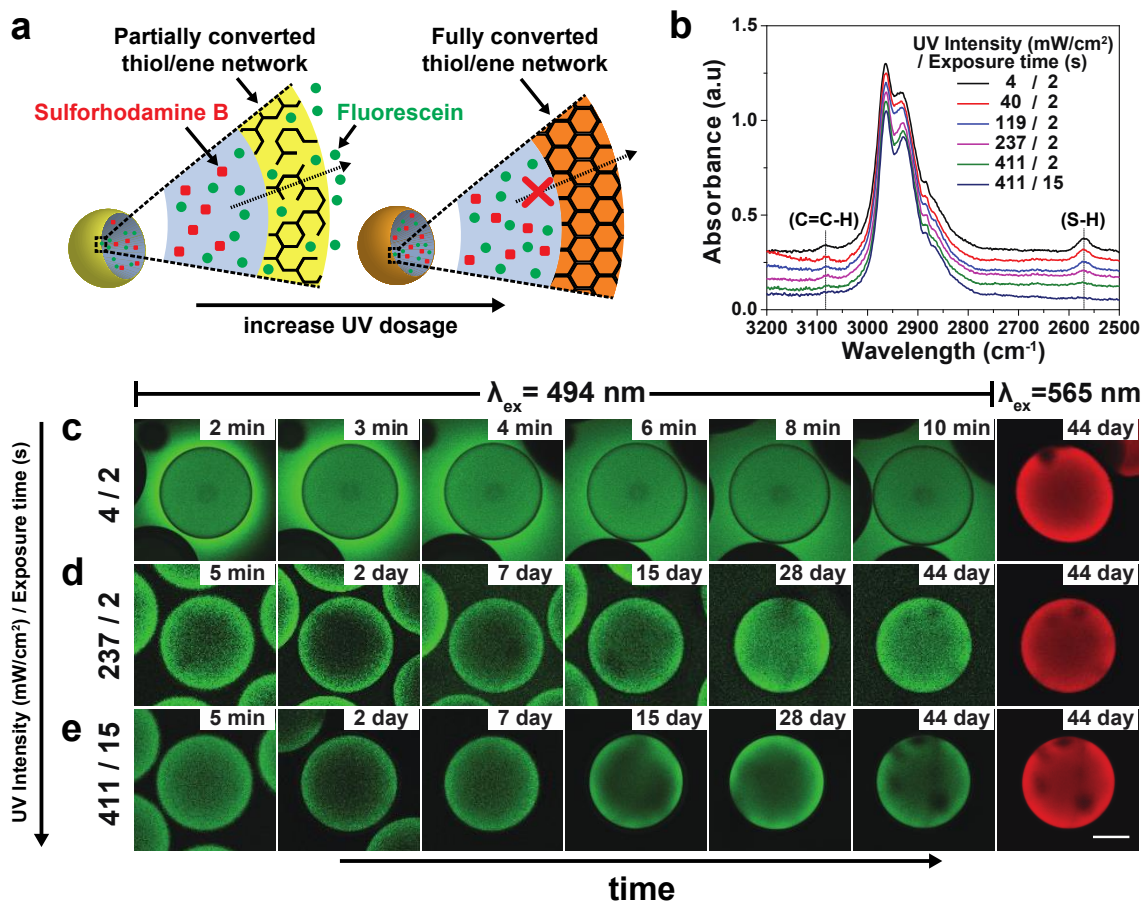
Figure 4.2 The effect of monomer conversion on the retention of small actives in thiol-ene microcapsules. a) IR spectra of the resulting microcapsules after different cure conditions b) Scheme representing partially and fully converted thiol-ene network in microcapsules. c-e) Fluorescence images of microcapsules encapsulating both fluorescein (λ_{ex} = 494) and sulforhodamine B (λ_{ex} = 494) at different curing conditions: c) 4 mW cm^{-2}/ 2 s, d) 237 mW cm^{-2} / 2 s, and e) 411 mW cm^{-2} / 15 s. Scale bar represents 100 µm.

To study the effect of thiol-ene monomer conversion on the retention of these two types of small actives, we prepared sets of microcapsules with different extent of cure by independently varying the UV intensity and the cure time from 4 - 411 mW cm^{-2} and 2 - 15 seconds, respectively. To determine conversion, we use Fourier-transform infrared spectroscopy (FT-IR) to monitor the consumption of thiol at 2570 cm^{-1} and ene at 3085

cm^{-1} under various polymerization conditions as shown in Figure 2b. Microcapsules cured under low intensity (4 mW cm^{-2}) for short durations (2 s) results in ~10% conversion and a partially cured membrane as indicated by the significant residual thiol- and ene- peaks in the IR spectra of Figure 2b. Increasing the cure intensity and curing time results in higher conversion, with 90% conversion of the monomers after curing under 411 mW cm^{-2} for 15 s. By monitoring the leakage of dyes from microcapsules with different cure dosage via confocal laser microscopy over two months, we show that controlling the monomer conversion of the thiol-ene network results in microcapsules with tailored release as shown in the series of fluorescent images of Figure 2c-e and Figure S1. For low UV dosage (4 mW cm^{-2}, 2 s) microcapsules, an immediate release of fluorescein was observed within 10 minutes, while sulforhodamine B was completely retained after 44 days as shown in the fluorescence images of Figure 2c. Fluorescein's log $P_{o/w}$ value of 0.34 signifies that this dye can readily diffuse through both oil and water phase leading to rapid permeation through the incompletely cured membrane. By contrast, ionically charged sulforhodamine B with a log $P_{o/w}$ value of -2.02 is unable to diffuse through the membrane resulting in complete retention within the capsule shell. The long-term retention of sulforhodamine B in microcapsules cured under low UV dosage also indicates that these microcapsules do not have physical defects such as holes, cracks, or voids as both dyes are not simultaneously released. The retention of fluorescein was substantially improved by increasing the UV dosage (237 mW cm^{-2}, 2 s) as shown in Figure 2d, where the onset of fluorescein release occurred between 2-7 days. The leakage still occurs, but at a much slower rate likely due to a higher (~60%) yet incomplete conversion of the thiol-ene monomers as indicated by the IR spectra. Improved retention

of both dyes for up to 44 days was achieved by increasing the UV dosage (411 mW cm^{-2}, 15 s) to ensure high conversion (~90%) of the membrane as shown in Figure 2e. Intensity profiles comparing the dye release between Figure 3d and Figure 3e at 2 and 44 days further show the near complete retention of fluorescein at higher cure intensities (Figure S2). These results indicate that the highly uniform polymer network provided by thiol-ene chemistry enables encapsulation and enhanced retention of omniphilic actives in microcapsules. Notably, fluorocarbon triple emulsions were required to achieve similar retentions; however, these triple emulsions were sensitive to surfactant selection and are environmentally unfriendly.[121]

The thiol-ene based microcapsules also provide the ease of incorporating degradable linkages, such as anhydrides, within a network to fabricate degradable microcapsules. Following the work of Shipp *et al.*,[125] we polymerized 4-pentenoic anhydride (PA) with TMPTMP, as shown in Scheme 1, to fabricate a degradable thiol-ene anhydride membrane. We encapsulated an aqueous solution of Sulforhodamine B due to its inability to permeate through a polymer membrane unless a significant void is formed, which is achieved in this case via surface erosion of the membrane. We monitored the leakage of sulforhodamine B using confocal laser microscopy and observe full retention up to 3 h and subsequent gradual disappearance of the dye from the capsule as shown in the fluorescence and optical images of Figure 3a. These results are in good agreement with literature, as within 15 h, significant degradation of the membrane has occurred leading to release of the encapsulated dye.
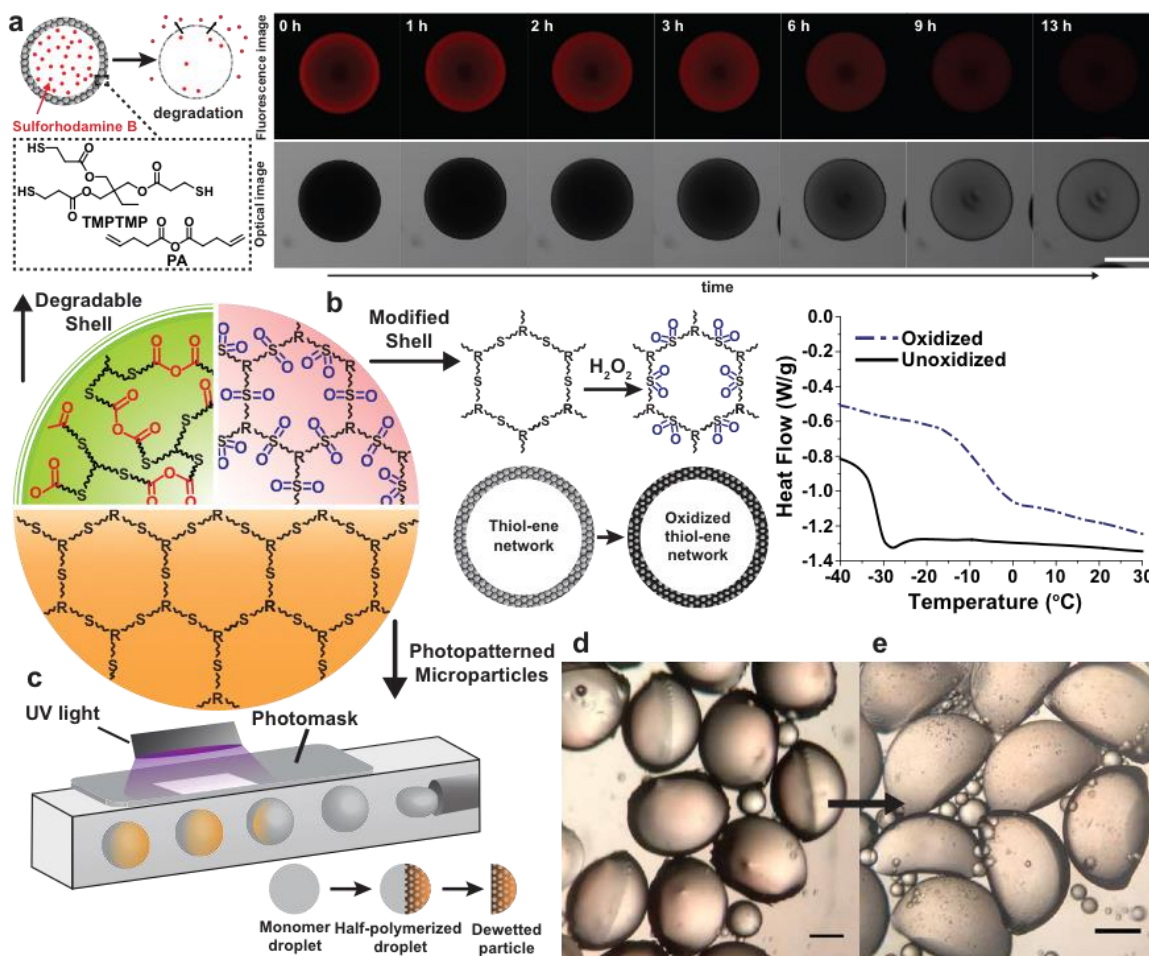
Figure 4.3 a) Monomers used to prepare degradable microcapsules encapsulating aqueous solution of sulforhodamine B (red). The series of fluorescence (top) and optical (bottom) images on the right shows full retention of the dye within the microcapsule up to 3 h in DI water and subsequent gradual release due to surface erosion of the shell. Scale bar represents 50 µm. b) Conversion of thiol-ene (sulfide) network into oxidized thiol-ene (sulfone) networks with hydrogen peroxide treatment. The plot on the right shows the differential scanning calorimetry (DSC) data before and after oxidation. c) Scheme of a continuous photopatternable droplet device and the resulting droplets d) before and e) after dewetting. Scale bars represent 500 µm.

We further explore the utility of thiol-ene network in emulsion templated microcapsules by demonstrating their ability to be post-functionalized through very efficient reactions. We first prepared double-emulsion microcapsules consisting of TEGDVE and TMPTMP to fabricate low glass transition (T_g = -36 °C) temperature microcapsules. Then, we modified the sulfide linkages present in the capsule shell into

71

sulfone linkages with H_2O_2 using the protocol recently highlighted by Podgórski *et al.*[126]

Upon simple incubation of the microcapsules with H_2O_2 for 24 hours, an increase in T_g

from -36 °C to -8 °C was observed as shown in the differential scanning calorimetry plot

of Figure 3b. This oxidation can be applied to networks derived from other thiol-ene

monomer pairs to even increase the glass transition temperature up to 120 °C higher than

the original network.[126] This result indicates that the capsule shell can be post-modified to

achieve microcapsules with tunable thermomechanical properties which may provide

unique opportunities in advanced energy dampening coating technologies.

We also exploit the rapid cure kinetics of thiol-ene based systems by

demonstrating the production of photopatterned microparticles in a continuous process. A

single emulsion droplet generator was outfitted with a steel photomask placed to expose

half the channel width to UV light as shown in Figure 3c. The monomer combination,

TEGDVE:TMPTMP, was used with the addition of a colorless spiropyran, Photorome I,

which undergoes a photoinduced color change upon exposure to UV light. A certain

percentage of Photorome I is irreversibly converted into a colored state which allows for

visual contrast between the polymerized and non-polymerized sections of the

microparticles (Figure A.3). As the droplets pass under the photomask, a color change

was observed in the UV exposed half of the droplet, as shown in the optical image of the

collected droplets in Figure 3d. Collection of the photopatterned microparticles in

deionized water without presence of any surfactants to stabilize the drop allows the non-

polymerized oil portion to dewet and form polymerized hemispherical particles as shown

in the optical image of Figure 3e. This simple demonstration exploits the rapid cure

kinetics of thiol-ene photopolymerization which can yield new asymmetric or three

dimensional structures from emulsion drops. We anticipate that this approach will afford new tools for the polymer and colloid community with applications in particle self-assembly, drug delivery, and diagnostics.

4.5 Conclusion

In summary, thiol-ene chemistry was exploited in droplet based microfluidics to fabricate microcapsules with tunable encapsulation, degradation, and thermal properties. This work demonstrates the importance of monomer conversion on the retention of omniphilic cargo in double emulsion templated microcapsules. The wide range of commercially available thiol-ene monomers enabled easy incorporation of degradable anhydride linkages within the thiol-ene membrane – generating degradable microcapsules. The thiol-ene membrane itself can be oxidized to improve thermal/mechanical properties of the microparticles. Lastly, the rapid cure kinetics show great promise in generating photopolymerizable microparticles with complex geometries via continuous flow photomasking. The strategies of utilizing thiol-ene chemistry in fabrication of advanced microcapsules/particles outlined in this work are general and can be further extended to many biological applications including, tissue engineering, [127] and immobilization of peptides and dyes within gels.[128] Moreover, while allyl and vinyl ethers were primarily discussed in this work, other alkenes such as norbornenes, n-vinyl amides, N-substituted maleimides or acrylates can be used to tune reactivity, release kinetics, and provide new network architectures with different reactive handles for simple post-polymerization modification or sequestration. The rapid cure kinetics, ease of fabrication, and wide range of commercial monomers suggest unprecedented opportunities for designer emulsions with well-defined network architectures.

Table A.1 Typical SDS stock solution formulation to prepare samples with various concentrations of organic phase.

SDS Stock Solution	Mass (g)	Weight %
SDS	0.578 (2.00 mmol)	0.600
DI water	90.0	99.4

Table A.2 Typical SDS stock solution formulation to prepare samples with various concentrations of organic phase.

SDS Stock (mL)	DI Water (µL)	Organic Stock (µL)
9	500	500
9	600	400
9	650	350
9	700	300
9	725	275
9	750	250
9	775	225
9	800	200
9	815	185
9	825	175
9	850	150
9	900	100
9	950	50
9	975	25

Effect of Various Concentrations of SDS

The organic concentration was kept constant at 2.5 % (v/v) while the relative amounts of SDS stock (Table A.3) and DI water were adjusted to maintain 10 mL total volume (Table A.4).

Table A.3 Aqueous formulation to prepare samples at a variety of SDS concentrations.

SDS Stock Solution	Mass (g)	Weight %
SDS	2.38 (8.00 mM)	2.5
DI water	90.0	97.5

Table A.4 Samples preparation for varied SDS concentration with a constant organic stock.

[SDS] (mmol)	SDS Stock (µL)	DI Water (µL)	Organic Stock (µL)
0.80	9000	750	250
0.40	4500	5250	250
0.20	2250	7500	250
0.10	1125	8625	250
0.05	562.5	9187.5	250
0.025	281.25	9468.75	250

Effect of Sonication Time

Samples with 2.5 % of organic and 20 mM of SDS were prepared while the sonication time was varied from 5, 10, 15, 20, 25, 30, 45, 60 minutes.

Effect of Sonication Amplitude (Intensity setting)

Samples with 2.5 % of organic and 20 mM of SDS were prepared by varying amplitude setting from 5, 10, 15, 20, 25 percent.

Effect of inhibitor

Samples with 20 mM of SDS and 2.5 % organic phase were prepared with varying amounts of inhibitor (MEHQ) ranging from 0 to 60 mg. The samples were emulsified at 10 % amplitude for 20 minutes.

Effect of hexadecane

Two different organic phases with and without hexadecane were prepared following Table SI-1. Samples with 20 mM of SDS were prepared using 2.5 % with and without hexadecane. The samples were then placed into an ice bath and sonicated at 10 % amplitude for 20 minutes. The samples then place in the dark for different amount of time ranging from 0, 3, 6, and 72 hours before curing.
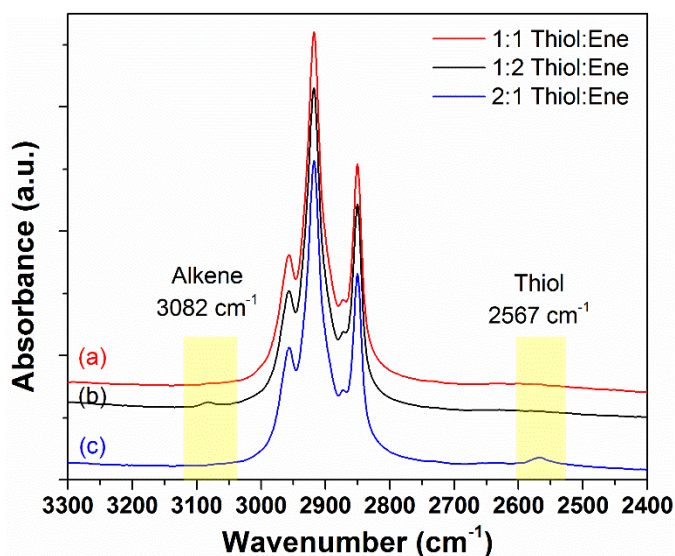
Figure A.1 FTIR spectra of thiol-ene nanoparticles obtained after photopolymerization of miniemulsions containing (a) 1:1 stoichiometric ratios of thiol and alkene functional groups, (b) 1:2 thiol to alkene, and (c) 2:1 thiol to alkene. As expected, the 1:1 samples shows complete conversion of thiol (2567 cm^{-1}) and alkene (3082 cm^{-1}) functional groups.

Figure A.2 Lower magnification TEM image of thiol-ene nanoparticles synthesized at 2.5 wt. % organic fraction.
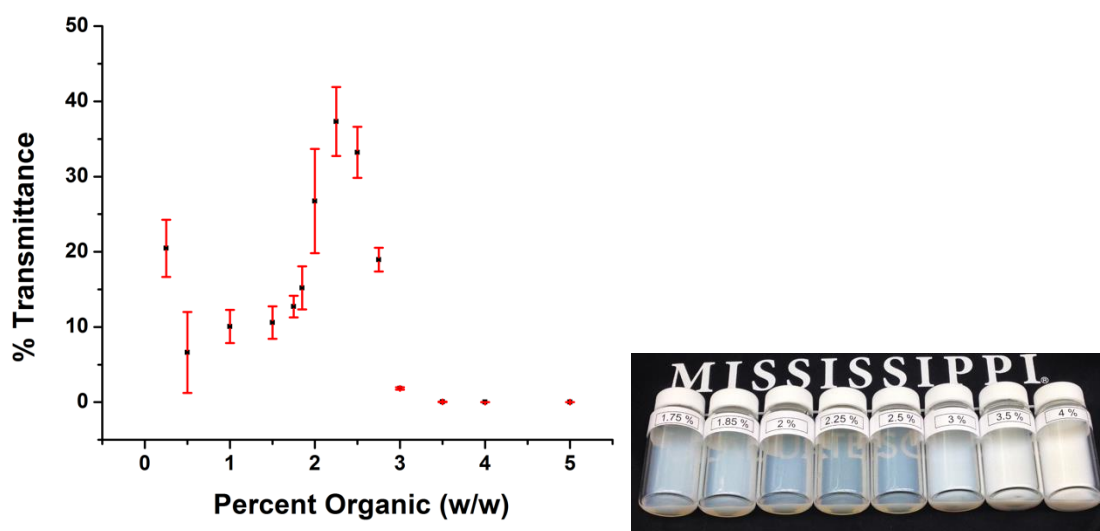
Figure A.3 Percent transmittance of thiol-ene miniemulsions as a function of organic weight fraction in the formulation.
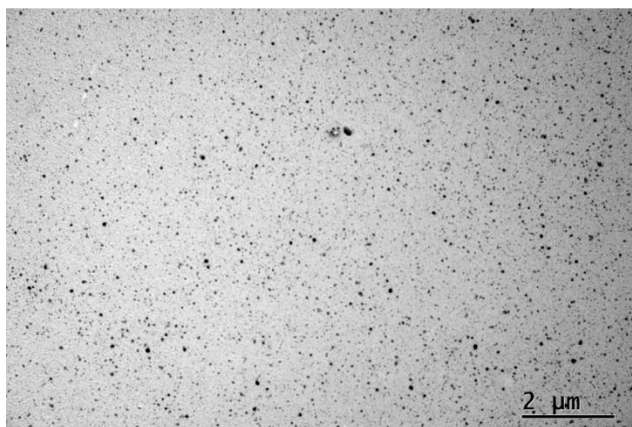
Figure A.4 TEM image of thiol-ene nanoparticles synthesized with stoichiometric excess of thiol groups.
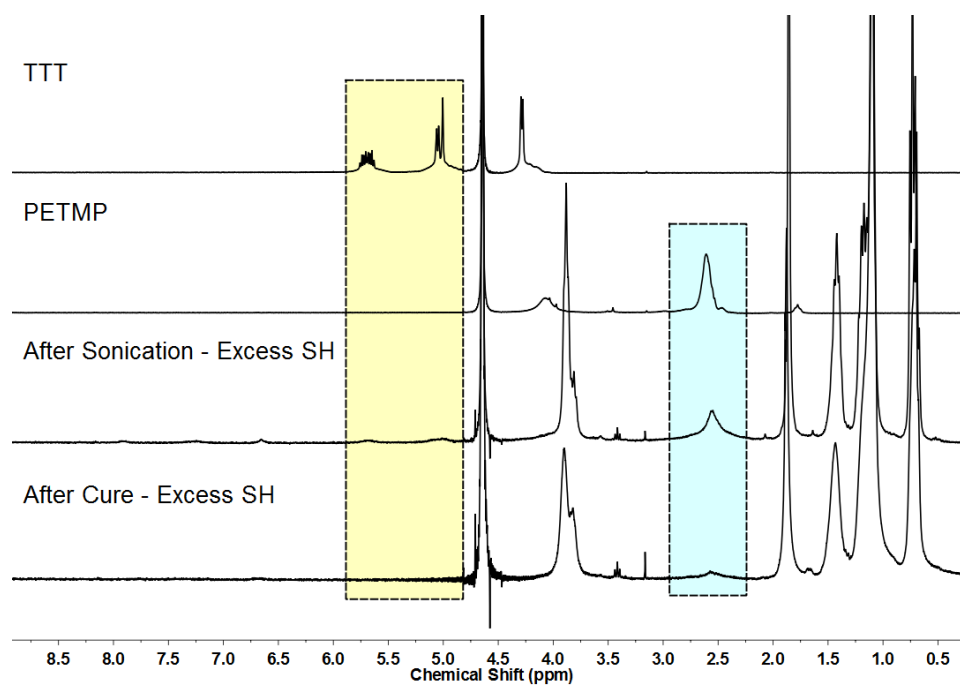
Figure A.5 ^{1}H NMR of TTT and PETMP starting materials, miniemulsion containing excess PETMP (2:1 thiol:ene) prior to UV exposure, and miniemulsion containing excess PETMP after UV exposure. The lower spectrum confirms the presence of thiol ($\sim$ 2.5

ppm) remaining on the nanoparticles, and the complete consumption of the alkene. See

Figure A.1 for complimentary FTIR data.
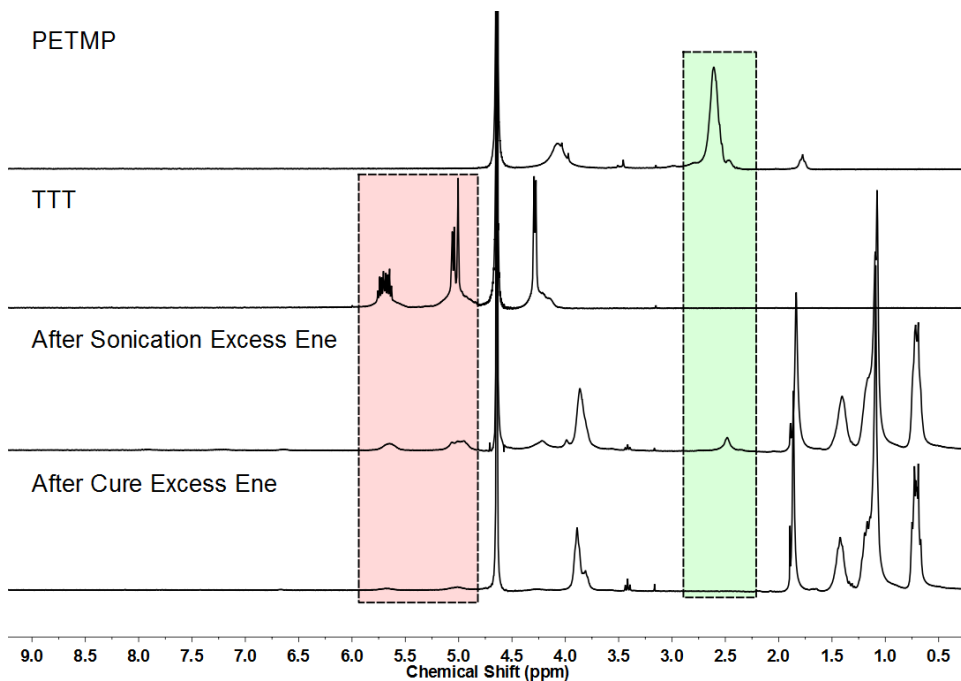
Figure A.6 ^{1}H NMR of TTT and PETMP starting materials, miniemulsion containing

excess TTT (1:2 thiol:ene) prior to UV exposure, and miniemulsion containing excess

TTT after UV exposure. The lower spectrum confirms the presence of alkene (5.0 – 5.8

ppm) remaining on the nanoparticles, and the complete consumption of the thiol at 2.5

ppm. See Figure A.1 for complimentary FTIR data.
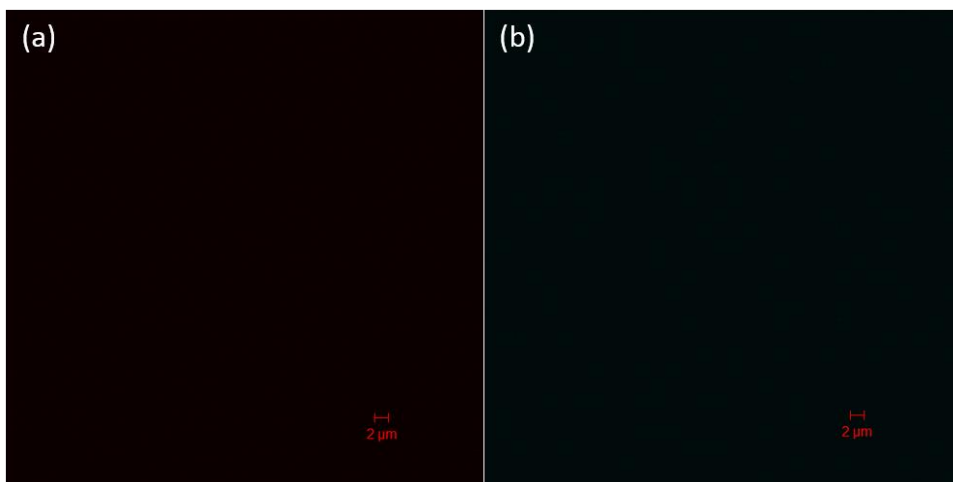
Figure A.7 Confocal fluorescence control experiments for nanoparticle postpolymerization functionalization: (a) Thiol-functionalized nanoparticles (synthesized with excess 2:1 excess thiol:ene) were exposed to sulphorhodamine B (without maleimide) using the same reaction conditions as for Texas Red C2 maleimide. (b) Alkene-functionalized nanoparticles (synthesized with excess 1:2 excess thiol:ene) were exposed to 7-methoxy-4-methylcoumarin (without thiol) using the same reaction conditions as for 7-mercapto-4-methylcoumarin. After washing, the absence of nanoparticles in the fluorescence images in (a) and (b) shows that covalent attachment, rather than physisorption is responsible for nanoparticle fluorescence when employing reactive fluorescent tags.
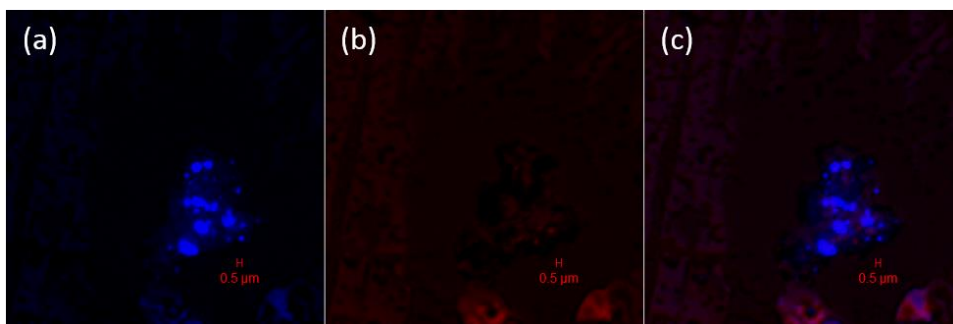
Figure A.8 Control experiments for nanoparticle postpolymerization functionalization: Alkene-functionalized nanoparticles (synthesized with excess 1:2 excess thiol:ene) were reacted with 7-mercapto-4-methylcoumarin in the presence of the non-reactive dye sulphorhodamine B to show that the non-reactive dye is not physisorbing onto the surface of the nanoparticles. (a) Image at excitation (λ_{ex} = 405 nm) for 7-mercapto-4-methylcoumarin, (b) image at excitation (λ_{ex} = 543 nm) for sulphorhodamine B, and (c) composite overlaid image.
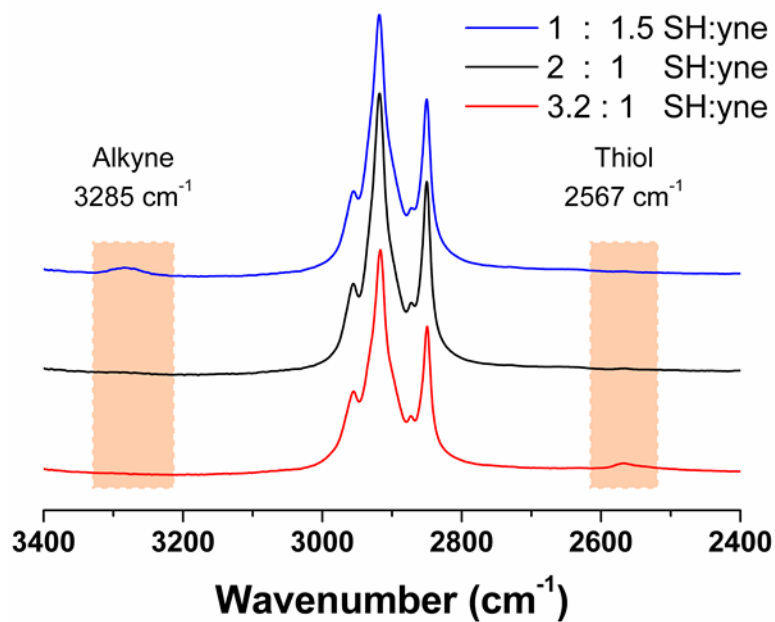
Figure B.1 FT-IR spectra of octadiyne samples prepared at off stoichiometric ratios.
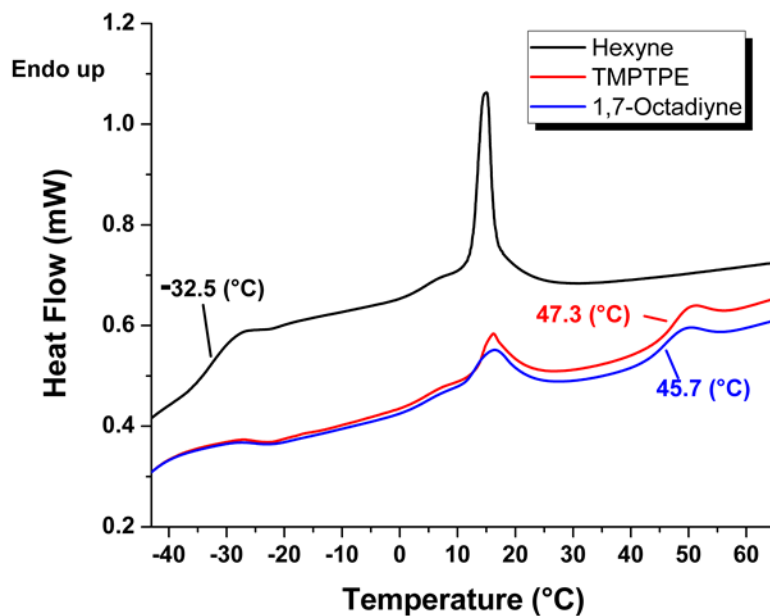
Figure B.2 DSC thermograms of all three alkyne formulations prepared in the absence of hexadecane to eliminate additional peaks. The melting peak from 17-18 °C is attributed to SDS crystallization.[129]
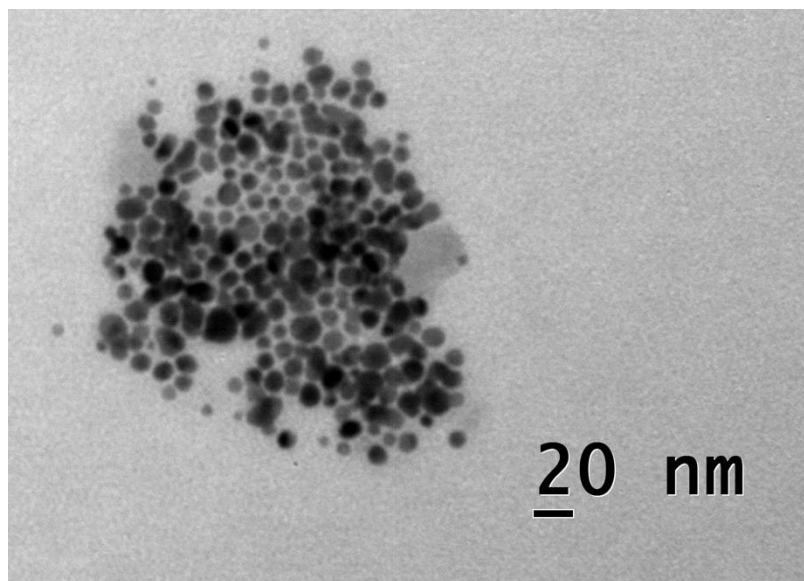
Figure B.3 TEM image of synthesized dodecanethiol capped AgNPs.
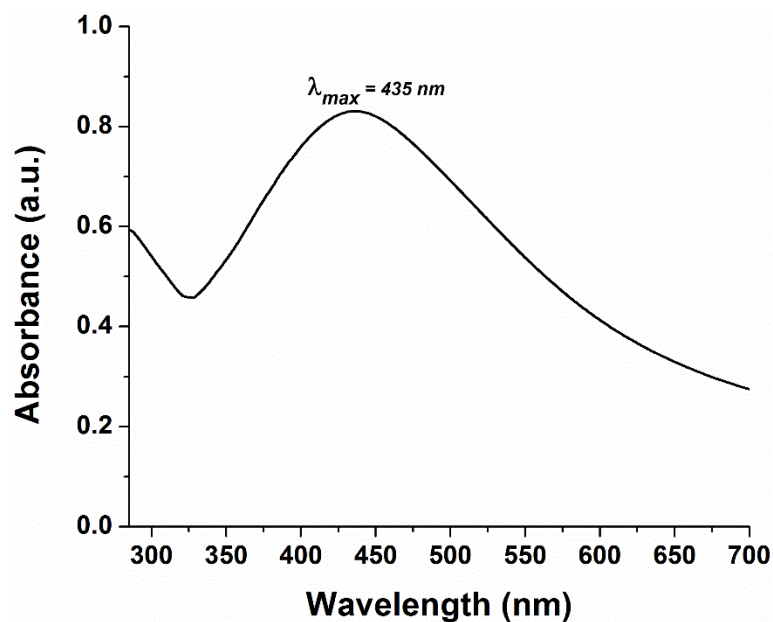
Figure B.4 UV-vis spectra of AgNPs dispersed in toluene.
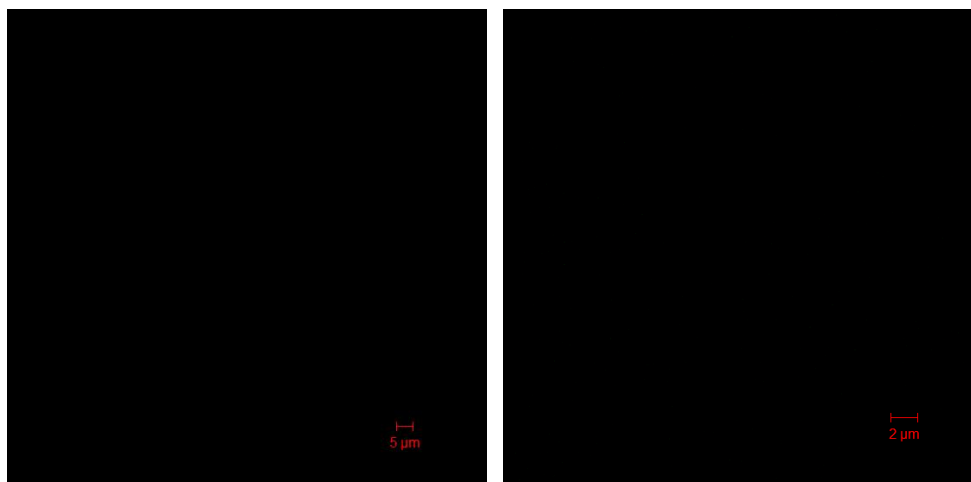
Figure B.5 Control experiments for nanoparticle postpolymerization functionalization: (a) Thiol-functionalized nanoparticles (synthesized with excess 3.2:1 excess thiol:yne) were exposed to sulphorhodamine B (without maleimide) using the same reaction conditions as for Texas Red C2 maleimide. (b) Alkyne-functionalized nanoparticles (synthesized with excess 1.51:1 excess yne:thiol) were exposed to 7-methoxy-4-methylcoumarin (without thiol) using the same reaction conditions as for 7-mercapto-4-methylcoumarin. After washing, the absence of nanoparticles in the fluorescence images in (a) and (b) shows that covalent attachment, rather than physisorption is responsible for nanoparticle fluorescence when employing reactive fluorescent tags.
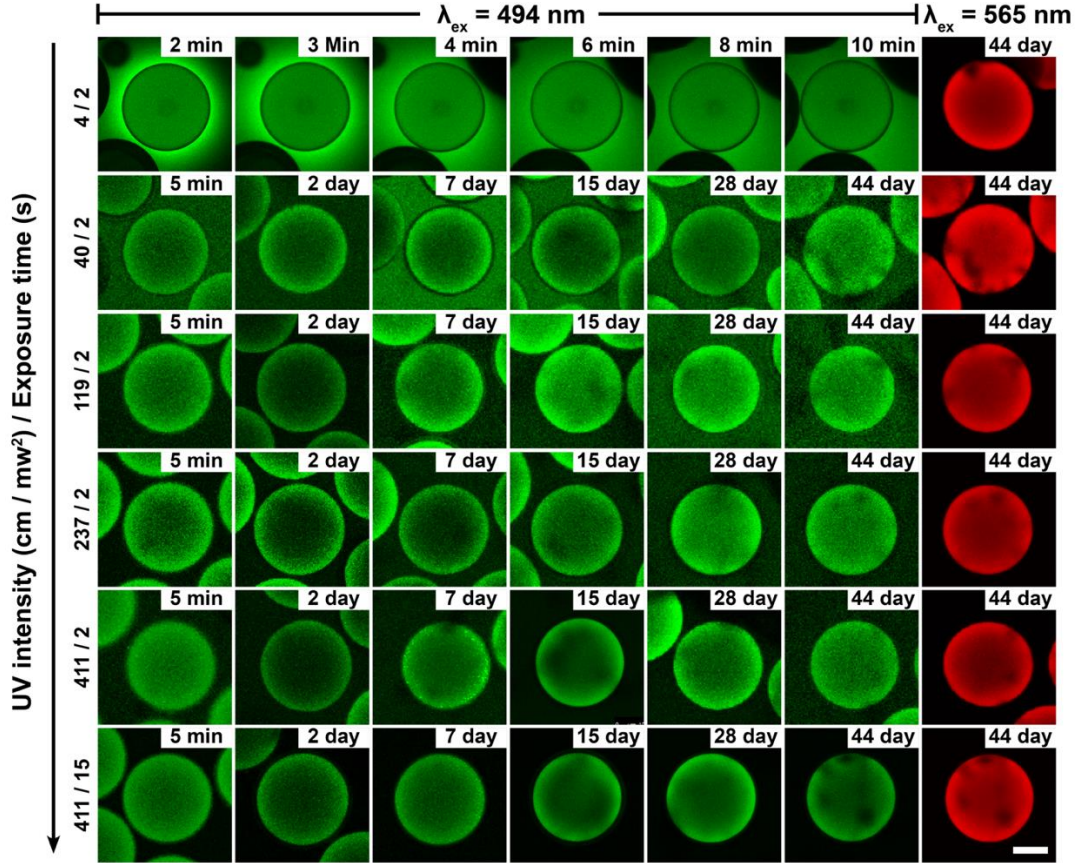
Figure C.1 Full spectrum of release profiles with different curing conditions.
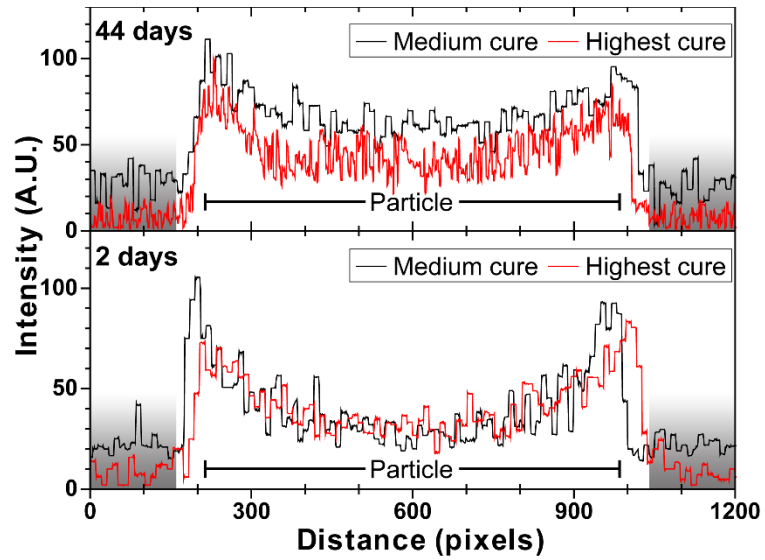
Figure C.2 Intensity profiles of the green fluorescence in the microcapsules shown in Figure 2d – medium cure (237 mW cm^{-2} with 2 s exposure time) and Figure 2e – highest cure (411 mW cm^{-2} with 15 s exposure time). The profiles show greater intensity outside of the particles under medium cure conditions at both 2 and 44 day time points.
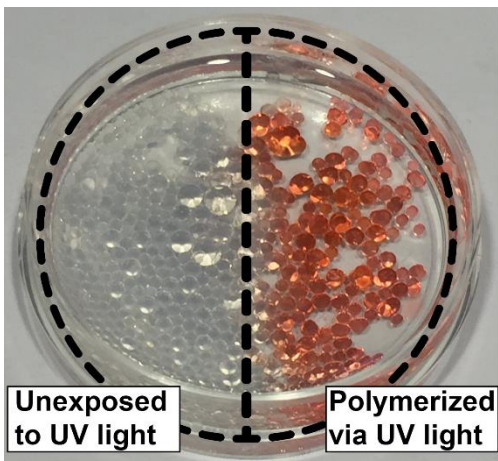
Figure C.3 A photograph showing that a certain percentage of Photorome I is irreversibly converted into a colored state upon exposure to UV.

REFERENCES

1.   Lowe, A. B., Thiol-ene "click" reactions and recent applications in polymer and materials synthesis. *Polymer Chemistry* **2010,** *1* (1), 17-36.

2.   Kade, M. J.; Burke, D. J.; Hawker, C. J., The power of thiol-ene chemistry. *J. Polym. Sci. A Polym. Chem.* **2010,** *48* (4), 743-750.

3.   Hoyle, C. E.; Bowman, C. N., Thiol–ene click chemistry. *Angew. Chem., Int. Ed.* **2010,** *49* (9), 1540-1573.

4.   Lowe, A. B.; Hoyle, C. E.; Bowman, C. N., Thiol-yne click chemistry: A powerful and versatile methodology for materials synthesis. *Journal of Materials Chemistry* **2010,** *20* (23), 4745-4750.

5.   Hoogenboom, R., Thiol–yne chemistry: A powerful tool for creating highly functional materials. *Angew. Chem., Int. Ed.* **2010,** *49* (20), 3415-3417.

6.   Chern, C.-S., *Principles and applications of emulsion polymerization*. John Wiley & Sons: 2008.

7.   Arshady, R., Suspension, emulsion, and dispersion polymerization: A methodological survey. *Colloid & Polymer Science* **1992,** *270* (8), 717-732.

8.   Lovell, P. A.; El-Aasser, M. S., *Emulsion polymerization and emulsion polymers*. Wiley: 1997.

9.   Shah, R. K.; Shum, H. C.; Rowat, A. C.; Lee, D.; Agresti, J. J.; Utada, A. S.; Chu, L.-Y.; Kim, J.-W.; Fernandez-Nieves, A.; Martinez, C. J.; Weitz, D. A., Designer emulsions using microfluidics. *Mater. Today* **2008,** *11* (4), 18-27.

10.   Shah, R. K.; Shum, H. C.; Rowat, A. C.; Lee, D.; Agresti, J. J.; Utada, A. S.; Chu, L.-Y.; Kim, J.-W.; Fernandez-Nieves, A.; Martinez, C. J., Designer emulsions using microfluidics. *Materials Today* **2008,** *11* (4), 18-27.

11.   Antonietti, M.; Landfester, K., Polyreactions in miniemulsions. *Prog. Polym. Sci.* **2002,** *27* (4), 689-757.

12.   Crespy, D.; Landfester, K., Miniemulsion polymerization as a versatile tool for the synthesis of functionalized polymers. *Beilstein J. Org.Chem.* **2010,** *6*, 1132-1148.

13.   Landfester, K.; Tiarks, F.; Hentze, H.-P.; Antonietti, M., Polyaddition in miniemulsions: A new route to polymer dispersions. *Macromol. Chem. Phys.* **2000,** *201* (1), 1-5.

14.   Chiaradia, V.; Valério, A.; Feuser, P. E.; Oliveira, D. d.; Araújo, P. H. H.; Sayer, C., Incorporation of superparamagnetic nanoparticles into poly(urea-urethane) nanoparticles by step growth interfacial polymerization in miniemulsion. *Colloids and Surfaces A: Physicochemical and Engineering Aspects* **2015,** *482* (Supplement C), 596-603.

15.   Tiarks, F.; Landfester, K.; Antonietti, M., One-step preparation of polyurethane dispersions by miniemulsion polyaddition. *J. Polym. Sci. Part A: Polym. Chem.* **2001,** *39* (14), 2520-2524.

16.   Siebert, J. M.; Baier, G.; Musyanovych, A.; Landfester, K., Towards copper-free nanocapsules obtained by orthogonal interfacial "click" polymerization in miniemulsion. *Chem. Commun.* **2012,** *48* (44), 5470-5472.

17.   Roux, R.; Sallet, L.; Alcouffe, P.; Chambert, S.; Sintes-Zydowicz, N.; Fleury, E.; Bernard, J., Facile and Rapid Access to Glyconanocapsules by CuAAC Interfacial Polyaddition in Miniemulsion Conditions. *ACS Macro Lett.* **2012,** *1* (8), 1074-1078.

18.   Tan, J.; Li, C.; Dan, S.; Li, H.; Gu, J.; Zhang, B.; Zhang, H.; Zhang, Q., One-step thiol-isocyanate dispersion polymerization: Preparation of uniform, cross-linked and functional particles. *Chemical Engineering Journal* **2016,** *304*, 461-468.

19.   Kuypers, S.; Pramanik, S. K.; D'Olieslaeger, L.; Reekmans, G.; Peters, M.; D'Haen, J.; Vanderzande, D.; Junkers, T.; Adriaensens, P.; Ethirajan, A., Interfacial thiol–isocyanate reactions for functional nanocarriers: a facile route towards tunable morphologies and hydrophilic payload encapsulation. *Chemical Communications* **2015,** *51* (87), 15858-15861.

20.   Alexandrino, E. M.; Wagner, M.; Landfester, K.; Wurm, F. R., Poly(phosphoester) Colloids by Interfacial Polycondensation in Miniemulsion. *Macromolecular Chemistry and Physics* **2016,** *217* (17), 1941-1947.

21.   Jasinski, F.; Lobry, E.; Tarablsi, B.; Chemtob, A.; Croutxé-Barghorn, C. l.; Le Nouen, D.; Criqui, A., Light-mediated thiol–ene polymerization in miniemulsion: A fast route to semicrystalline polysulfide nanoparticles. *ACS Macro Letters* **2014,** *3* (9), 958-962.

22.   Zou, J.; Hew, C. C.; Themistou, E.; Li, Y.; Chen, C. K.; Alexandridis, P.; Cheng, C., Clicking Well-Defined Biodegradable Nanoparticles and Nanocapsules by UV-Induced Thiol-Ene Cross-Linking in Transparent Miniemulsions. *Advanced Materials* **2011,** *23* (37), 4274-4277.

23.   Amato, D. V.; Amato, D. N.; Flynt, A. S.; Patton, D. L., Functional, sub-100 nm polymer nanoparticles via thiol–ene miniemulsion photopolymerization. *Polymer Chemistry* **2015,** *6* (31), 5625-5632.

24.   Amato, D. N.; Amato, D. V.; Mavrodi, O. V.; Braasch, D. A.; Walley, S. E.; Douglas, J. R.; Mavrodi, D. V.; Patton, D. L., Destruction of Opportunistic Pathogens via Polymer Nanoparticle-Mediated Release of Plant-Based Antimicrobial Payloads. *Advanced healthcare materials* **2016,** *5* (9), 1094-1103.

25.   Amato, D. N.; Amato, D. V.; Narayanan, J.; Donovan, B. R.; Douglas, J. R.; Walley, S. E.; Flynt, A. S.; Patton, D. L., Functional, composite polythioether nanoparticles via thiol–alkyne photopolymerization in miniemulsion. *Chemical Communications* **2015,** *51* (54), 10910-10913.

26.   Hoyle, C. E.; Lee, T.; Roper, T., Thiol-enes: Chemistry of the past with promise for the future. *J. Polym. Sci. Part A: Polym. Chem.* **2004,** *42* (21), 5301-5338.

27.   Hoyle, C. E.; Bowman, C. N., Thiol-ene click chemistry. *Angew. Chem. Int. Ed.* **2010,** *49* (9), 1540-1573.

28.   Hoyle, C. E.; Lowe, A. B.; Bowman, C. N., Thiol-click chemistry: A multifaceted toolbox for small molecule and polymer synthesis. *Chem. Soc. Rev.* **2010,** *39* (4), 1355-1387.

29.   Durham, O. Z.; Krishnan, S.; Shipp, D. A., Polymer Microspheres Prepared by Water-Borne Thiol–Ene Suspension Photopolymerization. *ACS Macro Letters* **2012,** *1* (9), 1134-1137.

30.   Durham, O. Z.; Shipp, D. A., Suspension thiol-ene photopolymerization: Effect of stabilizing agents on particle size and stability. *Polymer* **2014,** *55* (7), 1674-1680.

31. Durham, O. Z.; Norton, H. R.; Shipp, D. A., Functional polymer particles via thiol–ene and thiol–yne suspension "click" polymerization. *RSC Advances* **2015,** *5* (82), 66757-66766.

32. Durham, O. Z.; Shipp, D. A., Suspension "click" polymerizations: thiol-ene polymer particles prepared with natural gum stabilizers. *Colloid and Polymer Science* **2015,** *293* (8), 2385-2394.

33. Barker, E. M.; Buchanan, J. P., Thiol-ene polymer microbeads prepared under high-shear and their successful utility as a heterogeneous photocatalyst via C 60-capping. *Polymer* **2016,** *92*, 66-73.

34. Hoffmann, C.; Chiaula, V.; Yu, L.; Pinelo, M.; Woodley, J. M.; Daugaard, A. E., Simple Preparation of Thiol–Ene Particles in Glycerol and Surface Functionalization by Thiol–Ene Chemistry (TEC) and Surface Chain Transfer Free Radical Polymerization (SCT-FRP). *Macromolecular rapid communications* **2017**.

35. Tan, J.; Li, C.; Zhou, J.; Yin, C.; Zhang, B.; Gu, J.; Zhang, Q., Fast and facile fabrication of porous polymer particles via thiol–ene suspension photopolymerization. *RSC Advances* **2014,** *4* (26), 13334-13339.

36. Alimohammadi, F.; Wang, C.; Durham, O. Z.; Norton, H. R.; Bowman, C. N.; Shipp, D. A., Radical mediated thiol-ene/yne dispersion polymerizations. *Polymer* **2016,** *105*, 180-186.

37. Wang, C.; Zhang, X.; Podgórski, M.; Xi, W.; Shah, P.; Stansbury, J.; Bowman, C. N., Monodispersity/Narrow Polydispersity Cross-Linked Microparticles Prepared by Step-Growth Thiol–Michael Addition Dispersion Polymerizations. *Macromolecules* **2015,** *48* (23), 8461.

38. Wang, C.; Podgorski, M.; Bowman, C. N., Monodisperse functional microspheres from step-growth "click" polymerizations: preparation, functionalization and implementation. *Materials Horizons* **2014,** *1* (5), 535-539.

39. Cox, L. M.; Sun, X.; Wang, C.; Sowan, N.; Killgore, J. P.; Long, R.; Wu, H.-A.; Bowman, C. N.; Ding, Y., Light-Stimulated Permanent Shape Reconfiguration in Cross-Linked Polymer Microparticles. *ACS Applied Materials & Interfaces* **2017,** *9* (16), 14422-14428.

40. Podgórski, M.; Wang, C.; Yuan, Y.; Konetski, D.; Smalyukh, I.; Bowman, C. N., Pristine Polysulfone Networks as a Class of Polysulfide-Derived High-Performance Functional Materials. *Chem. Mater.* **2016,** *28* (14), 5102-5109.

41. Wang, C.; Zieger, M. M.; Schenzel, A.; Wegener, M.; Willenbacher, J.; Barner-Kowollik, C.; Bowman, C. N., Photoinduced Tetrazole-Based Functionalization of Off-Stoichiometric Clickable Microparticles. *Advanced Functional Materials* **2017,** *27* (7).

42. Wang, C.; Chatani, S.; Podgórski, M.; Bowman, C. N., Thiol-Michael addition miniemulsion polymerizations: functional nanoparticles and reactive latex films. *Polymer Chemistry* **2015,** *6* (20), 3758-3763.

43. Jasinski, F.; Rannée, A. s.; Schweitzer, J.; Fischer, D.; Lobry, E.; Croutxé-Barghorn, C. l.; Schmutz, M.; Le Nouen, D.; Criqui, A.; Chemtob, A., Thiol–Ene Linear Step-Growth Photopolymerization in Miniemulsion: Fast Rates, Redox-Responsive Particles, and Semicrystalline Films. *Macromolecules* **2016,** *49* (4), 1143-1153.

44.   Amato, D. V.; Amato, D. N.; Flynt, A. S.; Patton, D. L., Functional, sub-100 nm polymer nanoparticles via thiol-ene miniemulsion photopolymerization. *Polymer Chemistry* **2015,** *6* (31), 5625-5632.

45.   Amato, D. N.; Amato, D. V.; Narayanan, J.; Donovan, B. R.; Douglas, J. R.; Walley, S. E.; Flynt, A. S.; Patton, D. L., Functional, composite polythioether nanoparticles via thiol-alkyne photopolymerization in miniemulsion. *Chemical Communications* **2015,** *51* (54), 10910-10913.

46.   Amato, D. N.; Amato, D. V.; Mavrodi, O. V.; Braasch, D. A.; Walley, S. E.; Douglas, J. R.; Mavrodi, D. V.; Patton, D. L., Destruction of Opportunistic Pathogens via Polymer Nanoparticle-Mediated Release of Plant-Based Antimicrobial Payloads. *Advanced Healthcare Materials* **2016,** *5* (9), 1094-1103.

47.   de Meneses, A. C.; dos Santos, P. C. M.; Machado, T. O.; Sayer, C.; de Oliveira, D.; de Araújo, P. H. H., Poly (thioether-ester) nanoparticles entrapping clove oil for antioxidant activity improvement. *Journal of Polymer Research* **2017,** *24* (11), 202.

48.   Machado, T. O.; Cardoso, P. B.; Feuser, P. E.; Sayer, C.; Araújo, P. H., Thiol-ene miniemulsion polymerization of a biobased monomer for biomedical applications. *Colloids and Surfaces B: Biointerfaces* **2017,** *159*, 509-517.

49.   Cardoso, P. B.; Machado, T. O.; Feuser, P. E.; Sayer, C.; Meier, M. A.; Araújo, P. H., Biocompatible Polymeric Nanoparticles From Castor Oil Derivatives via Thiol-Ene Miniemulsion Polymerization. *European Journal of Lipid Science and Technology*.

50.   Chen, N.; Dempere, L. A.; Tong, Z., Synthesis of pH-Responsive Lignin-Based Nanocapsules for Controlled Release of Hydrophobic Molecules. *ACS Sustainable Chemistry & Engineering* **2016,** *4* (10), 5204-5211.

51.   Lafleur, J. P.; Senkbeil, S.; Novotny, J.; Nys, G.; Bøgelund, N.; Rand, K. D.; Foret, F.; Kutter, J. P., Rapid and simple preparation of thiol–ene emulsion-templated monoliths and their application as enzymatic microreactors. *Lab Chip* **2015,** *15* (10), 2162-2172.

52.   Durham, O. Z.; Chapman, D. V.; Krishnan, S.; Shipp, D. A., Radical Mediated Thiol-Ene Emulsion Polymerizations. *Macromolecules* **2017,** *50* (3), 775-783.

53.   Amato, D. V.; Lee, H.; Werner, J. G.; Weitz, D. A.; Patton, D. L., Functional Microcapsules via Thiol–Ene Photopolymerization in Droplet-Based Microfluidics. *ACS Applied Materials & Interfaces* **2017,** *9* (4), 3288-3293.

54.   Prasath, R. A.; Gokmen, M. T.; Espeel, P.; Du Prez, F. E., Thiol-ene and Thiol-yne Chemistry in Microfluidics: A Straightforward Method Towards Macroporous and Nonporous Functional Polymer Beads. *Polym. Chem.* **2010,** *1* (5), 685.

55.   Windham, A. D.; Lowe, P. M.; Conley, K. W.; Netchaev, A. D.; Buchanan, R. K.; Buchanan, J. P., Controlled thiol-ene polymer microsphere production using a low-frequency acoustic excitation coaxial flow method. *Polymer* **2016,** *94*, 8-13.

56.   Li, C.; Tan, J.; Gu, J.; Qiao, L.; Zhang, B.; Zhang, Q., Rapid and efficient synthesis of isocyanate microcapsules via thiol-ene photopolymerization in Pickering emulsion and its application in self-healing coating. *Composites Science and Technology* **2016,** *123*, 250-258.

57.   Liao, Z.; Xue, D.; Li, H.; Shi, L., Fragrance-Containing Microcapsules Based on Interfacial Thiol-Ene Polymerization. *Journal of Applied Polymer Science* **2016,** *133* (36).

58.   Durham, O. Z.; Poetz, K. L.; Shipp, D. A., Polyanhydride Nanoparticles: Thiol–Ene 'Click'Polymerizations Provide Functionalized and Cross-Linkable Nanoparticles with Tuneable Degradation Times. *Australian Journal of Chemistry* **2017,** *70* (6), 735-742.

59.   Tan, J.; Li, C.; Zhou, J.; Yin, C.; Zhang, B.; Gu, J.; Zhang, Q., Fast and facile fabrication of porous polymer particles via thiol–ene suspension photopolymerization. *RSC Adv.* **2014,** *4* (26), 13334.

60.   Wang, J.; Wang, X.; Yan, G.; Fu, S.; Tang, R., pH-sensitive nanogels with ortho ester linkages prepared via thiol-ene click chemistry for efficient intracellular drug release. *Journal of colloid and interface science* **2017,** *508*, 282-290.

61.   Solans, C.; Izquierdo, P.; Nolla, J.; Azemar, N.; Garcia-Celma, M. J., Nano-emulsions. *Curr. Opin. Colloid Interface Sci.* **2005,** *10* (3), 102-110.

62.   Weiss, J.; Herrmann, N.; McClements, D., Ostwald ripening of hydrocarbon emulsion droplets in surfactant solutions. *Langmuir* **1999,** *15* (20), 6652-6657.

63.   Asua, J. M., Miniemulsion polymerization. *Prog. Polym. Sci.* **2002,** *27* (7), 1283-1346.

64.   Park, T. G., Degradation of poly (D, L-lactic acid) microspheres: effect of molecular weight. *Journal of Controlled Release* **1994,** *30* (2), 161-173.

65.   Simon, G. P.; Allen, P. E. M.; Bennett, D. J.; Williams, D. R. G.; Williams, E. H., Nature of Residual Unsaturation During Cure of Dimethacrylates Examined by CPPEMAS Carbon-13 NMR and Simulation Using a Kinetic Gelation Model. *Macromolecules* **1989,** *22* (9), 3555.

66.   van Berkel, K. Y.; Hawker, C. J., Tailored Composite Polymer-Metal Nanoparticles by Miniemulsion Polymerization and Thiol-ene Functionalization. *Journal of polymer science. Part A, Polymer chemistry* **2010,** *48* (7), 1594-1606.

67.   Lee, H.; Choi, C.-H.; Abbaspourrad, A.; Wesner, C.; Caggioni, M.; Zhu, T.; Nawar, S.; Weitz, D. A., Fluorocarbon Oil Reinforced Triple Emulsion Drops. *Adv. Mater.* **2016,** *28* (38), 8425-8430.

68.   Choi, C.-H.; Lee, H.; Abbaspourrad, A.; Kim, J. H.; Fan, J.; Caggioni, M.; Wesner, C.; Zhu, T.; Weitz, D. A., Triple Emulsion Drops with An Ultrathin Water Layer: High Encapsulation Efficiency and Enhanced Cargo Retention in Microcapsules. *Adv. Mater.* **2016,** *28* (17), 3340-3344.

69.   Rao, J. P.; Geckeler, K. E., Polymer nanoparticles: Preparation techniques and size-control parameters. *Prog. Polym. Sci.* **2011,** *36* (7), 887-913.

70.   Landfester, K., Miniemulsion Polymerization and the Structure of Polymer and Hybrid Nanoparticles. *Angew. Chem. Int. Ed.* **2009,** *48* (25), 4488-4507.

71.   van Berkel, K. Y.; Hawker, C. J., Tailored composite polymer–metal nanoparticles by miniemulsion polymerization and thiol-ene functionalization. *J. Polym. Sci. Part A: Polym. Chem.* **2010,** *48* (7), 1594-1606.

72.   Zou, J.; Hew, C. C.; Themistou, E.; Li, Y.; Chen, C.-K.; Alexandridis, P.; Cheng, C., Clicking Well-Defined Biodegradable Nanoparticles and Nanocapsules by UV-Induced Thiol-Ene Cross-Linking in Transparent Miniemulsions. *Adv. Mater.* **2011,** *23* (37), 4274-4277.

73.   Durham, O. Z.; Krishnan, S.; Shipp, D. A., Polymer Microspheres Prepared by Water-Borne Thiol–Ene Suspension Photopolymerization. *ACS Macro Lett.* **2012,** *1* (9), 1134-1137.

74.   Jasinski, F.; Lobry, E.; Tarablsi, B.; Chemtob, A.; Croutxé-Barghorn, C.; Le Nouen, D.; Criqui, A., Light-Mediated Thiol–Ene Polymerization in Miniemulsion: A Fast Route to Semicrystalline Polysulfide Nanoparticles. *ACS Macro Lett.* **2014,** *3* (9), 958-962.

75.   Wang, C.; Podgórski, M.; Bowman, C. N., Monodisperse functional microspheres from step-growth "click" polymerizations: preparation, functionalization and implementation. *Mater. Horiz.* **2014**.

76.   Brown, J. C.; Pusey, P. N.; Dietz, R., Photon correlation study of polydisperse samples of polystyrene in cyclohexane. *J. Chem. Phys.* **1975,** *62* (3), 1136-1144.

77.   Tadros, T. F.; Lemmens, M.; Levecke, B.; Booten, K., Formulation and Stabilization of Nanoemulsions Using Hydrophobically Modified Inulin (Polyfructose) Polymeric Surfactant. Tadros, T. F., Ed. Wiley-VCH: 2008; Vol. 4, pp 35-50.

78.   Skinner, E. K.; Whiffin, F. M.; Price, G. J., Room temperature sonochemical initiation of thiol-ene reactions. *Chem. Commun.* **2012,** *48* (54), 6800.

79.   Hecht, L. L.; Wagner, C.; Landfester, K.; Schuchmann, H. P., Surfactant concentration regime in miniemulsion polymerization for the formation of MMA nanodroplets by high-pressure homogenization. *Langmuir* **2011,** *27* (6), 2279-2285.

80.   Jenkins, P.; Snowden, M., Depletion flocculation in colloidal dispersions. *Adv. Colloid Interfac.* **1996,** *68* (0), 57-96.

81.   Kiratzis, N.; Faers, M.; Luckham, P. F., Depletion flocculation of particulate systems induced by hydroxyethylcellulose. *Colloids and Surfaces A: Physicochemical and Engineering Aspects* **1999,** *151* (3), 461-471.

82.   Landfester, K.; Bechthold, N.; Tiarks, F.; Antonietti, M., Formulation and Stability Mechanisms of Polymerizable Miniemulsions. *Macromolecules* **1999,** *32* (16), 5222-5228.

83.   Delmas, T.; Piraux, H.; Couffin, A.; Texier, I.; Vinet, F.; Poulin, P.; Cates, M.; Bibette, J., How To Prepare and Stabilize Very Small Nanoemulsions. *Langmuir* **2011,** *27* (5), 1683-1692.

84.   Carlborg, C. F.; Haraldsson, T.; Oberg, K.; Malkoch, M.; van der Wijngaart, W., Beyond PDMS: off-stoichiometry thiol-ene (OSTE) based soft lithography for rapid prototyping of microfluidic devices. *Lab Chip* **2011,** *11* (18), 3136-3147.

85.   Storha, A.; Mun, E. A.; Khutoryanskiy, V. V., Synthesis of thiolated and acrylated nanoparticles using thiol-ene click chemistry: towards novel mucoadhesive materials for drug delivery. *RSC Adv.* **2013,** *3* (30), 12275-12279.

86.   Khot, L. R.; Sankaran, S.; Maja, J. M.; Ehsani, R.; Schuster, E. W., Applications of nanomaterials in agricultural production and crop protection: A review. *Crop Protection* **2012,** *35* (0), 64-70.

87.   Petros, R. A.; DeSimone, J. M., Strategies in the design of nanoparticles for therapeutic applications. *Nat. Rev. Drug Discov.* **2010,** *9* (8), 615-627.

88.   Amato, D. V.; Amato, D. N.; Flynt, A. S.; Patton, D. L., Functional, sub-100 nm polymer nanoparticles via thiol-ene miniemulsion photopolymerization. *Polym. Chem.* **2015**, DOI: 10.1039/C4PY01449A.

89.   Wang, C.; Chatani, S.; Podgorski, M.; Bowman, C. N., Thiol-Michael Addition Miniemulsion Polymerizations: Functional Nanoparticles and Reactive Latex Films. *Polym. Chem.* **2015**, DOI: 10.1039/C5PY00326A.

90.   Chan, J. W.; Zhou, H.; Hoyle, C. E.; Lowe, A. B., Photopolymerization of Thiol-Alkynes: Polysulfide Networks. *Chem. Mater.* **2009,** *21* (8), 1579-1585.

91.   Lowe, A. B.; Hoyle, C. E.; Bowman, C. N., Thiol-yne click chemistry: A powerful and versatile methodology for materials synthesis. *J. Mater. Chem.* **2010,** *20* (23), 4745-4750.

92.   Fairbanks, B. D.; Scott, T. F.; Kloxin, C. J.; Anseth, K. S.; Bowman, C. N., Thiol-Yne Photopolymerizations: Novel Mechanism, Kinetics, and Step-Growth Formation of Highly Cross-Linked Networks. *Macromolecules* **2009,** *42* (1), 211-217.

93.   Gokmen, M. T.; Brassinne, J.; Prasath, R. A.; Du Prez, F. E., Revealing the nature of thio-click reactions on the solid phase. *Chem. Commun.* **2011,** *47* (16), 4652-4654.

94.   Prasath, R. A.; Gokmen, M. T.; Espeel, P.; Du Prez, F. E., Thiol-ene and Thiol-yne Chemistry in Microfluidics: A Straightforward Method Towards Macroporous and Nonporous Functional Polymer Beads. *Polym. Chem.* **2010,** *1* (5), 685-692.

95.   Gorman, I. E.; Willer, R. L.; Kemp, L. K.; Storey, R. F., Development of a triazole-cure resin system for composites: Evaluation of alkyne curatives. *Polymer* **2012,** *53* (13), 2548-2558.

96.   Farrell, Z.; Shelton, C.; Dunn, C.; Green, D., Straightforward, One-Step Synthesis of Alkanethiol-capped Silver Nanoparticles from an Aggregative Model of Growth. *Langmuir* **2013,** *29* (30), 9291-9300.

97.   Erdem, B.; Sudol, E. D.; Dimonie, V. L.; El-Aasser, M. S., Encapsulation of inorganic particles via miniemulsion polymerization. I. Dispersion of titanium dioxide particles in organic media using OLOA 370 as stabilizer. *J. Polym. Sci. Part A: Polym. Chem.* **2000,** *38* (24), 4419-4430.

98.   Ramírez, L. P.; Landfester, K., Magnetic Polystyrene Nanoparticles with a High Magnetite Content Obtained by Miniemulsion Processes. *Macromol. Chem. Phys.* **2003,** *204* (1), 22-31.

99.   van Berkel, K. Y.; Piekarski, A. M.; Kierstead, P. H.; Pressly, E. D.; Ray, P. C.; Hawker, C. J., A Simple Route to Multimodal Composite Nanoparticles. *Macromolecules* **2009,** *42* (5), 1425-1427.

100.   Liu, D.; Jiang, X.; Yin, J., One-Step Interfacial Thiol–Ene Photopolymerization for Metal Nanoparticle-Decorated Microcapsules (MNP@MCs). *Langmuir* **2014,** *30* (24), 7213-7220.

101.   Tsuji, K., Microencapsulation of Pesticides and their Improved Handling Safety. *J. Microencapsul.* **2001,** *18* (2), 137-147.

102.   Nelson, G., Application of microencapsulation in textiles. *Int. J. Pharm.* **2002,** *242* (1-2), 55-62.

103.   Mitragotri, S.; Burke, P. A.; Langer, R., Overcoming the Challenges in Administering Biopharmaceuticals: Formulation and Delivery Strategies. *Nat. Rev. Drug Discovery* **2014,** *13* (9), 655-672.

104.   Prow, T. W.; Grice, J. E.; Lin, L. L.; Faye, R.; Butler, M.; Becker, W.; Wurm, E. M. T.; Yoong, C.; Robertson, T. A.; Soyer, H. P.; Roberts, M. S., Nanoparticles and Microparticles for Skin Drug Delivery. *Adv. Drug Delivery Rev.* **2011,** *63* (6), 470-491.

105.   Gouin, S., Microencapsulation: Industrial Appraisal of Existing Technologies and Trends. *Trends Food Sci.Tech.* **2004,** *15* (7–8), 330-347.

106.   Shah, R. K.; Shum, H. C.; Rowat, A. C.; Lee, D.; Agresti, J. J.; Utada, A. S.; Chu, L.-Y.; Kim, J.-W.; Fernandez-Nieves, A.; Martinez, C. J.; Weitz, D. A., Designer Emulsions Using Microfluidics. *Mater. Today* **2008,** *11* (4), 18-27.

107.   Lee, T. Y.; Choi, T. M.; Shim, T. S.; Frijns, R. A. M.; Kim, S.-H., Microfluidic Production of Multiple Emulsions and Functional Microcapsules. *Lab Chip* **2016,** *16* (18), 3415-3440.

108.   Datta, S. S.; Abbaspourrad, A.; Amstad, E.; Fan, J.; Kim, S.-H.; Romanowsky, M.; Shum, H. C.; Sun, B.; Utada, A. S.; Windbergs, M.; Zhou, S.; Weitz, D. A., 25th Anniversary Article: Double Emulsion Templated Solid Microcapsules: Mechanics And Controlled Release. *Adv. Mater.* **2014,** *26* (14), 2205-2218.

109.   Utada, A. S.; Lorenceau, E.; Link, D. R.; Kaplan, P. D.; Stone, H. A.; Weitz, D. A., Monodisperse Double Emulsions Generated from a Microcapillary Device. *Science* **2005,** *308* (5721), 537.

110.   Thiele, J.; Abate, A. R.; Shum, H. C.; Bachtler, S.; Förster, S.; Weitz, D. A., Fabrication of Polymersomes using Double-Emulsion Templates in Glass-Coated Stamped Microfluidic Devices. *Small* **2010,** *6* (16), 1723-1727.

111.   Kim, S.-H.; Weitz, D. A., One-Step Emulsification of Multiple Concentric Shells with Capillary Microfluidic Devices. *Angew. Chem. Int. Ed.* **2011,** *50* (37), 8731-8734.

112.   de Jong, J.; Lammertink, R. G. H.; Wessling, M., Membranes and Microfluidics: A Review. *Lab Chip* **2006,** *6* (9), 1125.

113.   Lee, T. Y.; Guymon, C. A.; Jönsson, E. S.; Hoyle, C. E., The Effect of Monomer Structure on Oxygen Inhibition of (Meth)acrylates Photopolymerization. *Polymer* **2004,** *45* (18), 6155-6162.

114.   Stansbury, J. W.; Trujillo-Lemon, M.; Lu, H.; Ding, X.; Lin, Y.; Ge, J., Conversion-Dependent Shrinkage Stress and Strain in Dental Resins and Composites. *Dent. Mater.* **2005,** *21* (1), 56-67.

115.   Lovell, L. G.; Lu, H.; Elliott, J. E.; Stansbury, J. W.; Bowman, C. N., The Effect of Cure Rate on the Mechanical Properties of Dental Resins. *Dent. Mater.* **2001,** *17* (6), 504-511.

116.   Kannurpatti, A. R.; Anseth, J. W.; Bowman, C. N., A Study of the Evolution of Mechanical Properties and Structural Heterogeneity of Polymer Networks Formed by Photopolymerizations of Multifunctional (Meth)acrylates. *Polymer* **1998,** *39* (12), 2507-2513.

117.   Shim, J.-u.; Patil, S. N.; Hodgkinson, J. T.; Bowden, S. D.; Spring, D. R.; Welch, M.; Huck, W. T. S.; Hollfelder, F.; Abell, C., Controlling the Contents of Microdroplets by Exploiting the Permeability of PDMS. *Lab Chip* **2011,** *11* (6), 1132-1137.

118.   Hoyle, C. E.; Bowman, C. N., Thiol–Ene Click Chemistry. *Angew. Chem. Int. Ed.* **2010,** *49* (9), 1540-1573.

119.   Hoyle, C. E.; Lee, T. Y.; Roper, T., Thiol–Enes: Chemistry of the Past with Promise for the Future. *J. Polym. Sci., Part A: Polym. Chem.* **2004,** *42* (21), 5301-5338.

120.   Lee, T. Y.; Carioscia, J.; Smith, Z.; Bowman, C. N., Thiol-Allyl Ether-Methacrylate Ternary Systems. Evolution Mechanism of Polymerization-Induced Shrinkage Stress and Mechanical Properties. *Macromolecules* **2007,** *40* (5), 1473-1479.

121.   Lee, H.; Choi, C.-H.; Abbaspourrad, A.; Wesner, C.; Caggioni, M.; Zhu, T.; Nawar, S.; Weitz, D. A., Fluorocarbon Oil Reinforced Triple Emulsion Drops. *Adv. Mater.* **2016,** *28* (38), 8425-8430.

122.   Microbead-Free Waters Act
of 2015. In *H.R.1321*, Public Law 114-114, 2015.

123.   Kasnavia, T.; Vu, D.; Sabatini, D. A., Fluorescent Dye and Media Properties Affecting Sorption and Tracer Selection. *Ground Water* **1999,** *37* (3), 376-381.

124.   Oba, Y.; Poulson, S. R., Octanol-Water Partition Coefficients vs. pH for Fluorescent Dye Tracers (Fluorescein, Eosin Y), and Implications for Hydrologic Tracer Tests. *Geochem. J.* **2012,** *46* (6), 517-520.

125.   Shipp, D. A.; McQuinn, C. W.; Rutherglen, B. G.; McBath, R. A., Elastomeric and Degradable Polyanhydride Network Polymers by Step-Growth Thiol-ene Photopolymerization. *Chem. Commun.* **2009,** (42), 6415-6417.

126.   Podgórski, M.; Wang, C.; Yuan, Y.; Konetski, D.; Smalyukh, I.; Bowman, C. N., Pristine Polysulfone Networks as a Class of Polysulfide-Derived High-Performance Functional Materials. *Chem. Mater.* **2016,** *28* (14), 5102-5109.

127.   Khademhosseini, A.; Langer, R., Microengineered Hydrogels for Tissue Engineering. *Biomaterials* **2007,** *28* (34), 5087-5092.

128.   Gupta, N.; Lin, B. F.; Campos, L. M.; Dimitriou, M. D.; Hikita, S. T.; Treat, N. D.; Tirrell, M. V.; Clegg, D. O.; Kramer, E. J.; Hawker, C. J., A Versatile Approach to High-Throughput Microarrays Using Thiol-Ene Chemistry. *Nat. Chem.* **2010,** *2* (2), 138-145.

129.   Szeląg, H.; Szumała, P., Effect of alkyl sulfate on the phase behavior of microemulsions stabilized with monoacylglycerols. *Journal of Surfactants and Detergents* **2011,** *14* (2), 245-255.